Universidad de Valladolid

ESCUELA DE INGENIERÍAS INDUSTRIALES

UNIVERSITY OF VALLADOLID

SCHOOL OF INDUSTRIAL ENGINEERS

Master in Chemical Engineering

MASTER THESIS

Intensification potential of hollow fiber membrane contactors for CO_2 physical absorption using methanol as solvent

Author:

Álvarez Escalante, Iván

Supervisors:

Rode, Sabine

Belaissaoui, Bouchra

ENSIC

Nancy, January 2021

TFM REALIZADO EN PROGRAMA DE INTERCAMBIO

TÍTULO: Intensification potential of hollow fiber membrane contactors for CO_2 physical absorption using methanol as solvent

ALUMNO: Iván Álvarez Escalante

FECHA: 29-01-2021

CENTRO: École nationale supérieure des industries chimiques

UNIVERSIDAD: Université de Lorraine

TUTORAS: Sabine Rode y Bouchra Belaissaoui

INTENSIFICATION POTENTIAL OF HOLLOW FIBER MEMBRANE CONTACTORS FOR CO_2 PHYSICAL ABSORPTION USING METHANOL AS SOLVENT

Student:

Ivan ALVAREZ ESCALANTE

Supervisors:

Sabine RODE

Bouchra BELAISSAOUI

January 2021

ABSTRACT:

Integrated Gasification Combined Cycle (IGCC) produces syngas through the gasification of carbonaceous fuels. Removing CO_2 for storage from the hydrogen gas is a key step in the process for the IGCC power plant for both the power generation and mitigation of greenhouse gas emissions. Rectisol^{TM} is a commercial process which is applied to syngas physical absorption using methanol as solvent and packed contactor technology.

This study investigates the intensification potential of using dense layer hollow fiber membrane contactors (HFMC) instead of packed contactors (PC), which have additional design constraints due to flooding. Moreover, it has been considered pressure drop restrictions in the HFMC design.

The research is based on previous simulation work with Aspen HYSYS taken out under different operating conditions of inlet temperature, inlet pressure and inlet CO_2 concentration.

It was obtained an intensification potential such that the volume of the contactor could be reduced as minimum 100 times if PC are substituted by HFM. In addition, a parametric study revealed that for HFMC contactor, the volume is not notably affected by methanol inlet temperature, whereas for PC is reduced at higher liquid inlet temperatures. Moreover, it is decreased at higher inlet pressures and at higher concentrations of CO_2 in the gas inlet.

KEYWORDS: Syngas purification**,** intensification**,** physical absorption**,** hollow fiber membrane contactor, methanol

ACKNOWLEDGMENTS

In the first place, I would like to express my gratitude to my supervisors, Professor Sabine Rode and Assistant Professor Bouchra Belaissaoui, for their guidance and patience during my research project. I am extremely grateful for their friendly meetings and for their personal support.

Next, I would like to thank to Dayra, this work would not have been possible without her unconditional support.

And to my parents, for their love and encouragement, without them I would never have enjoyed so many opportunities.

NOMENCLATURE

Latin symbols

Symbol	Definition	Units
A	Cross section area	m^2
a	Specific area	$m^2_{solid}\ m^{-3}_{contactor}$
a_{LG}	Gas-liquid interfacial area.	$m^2_{\ interface\ gas\text{-}liquid}\ m^{-3}_{contactor}$
B	Pore geometry efficiency	dimensionless
C	Concentration	mole m^{-3}
D	Diffusion coefficient	$m^2\ s^{-1}$
d	Diameter	m
E_a	Permeation activation energy	J mol^{-1}
F_{LG}	Flow factor	dimensionless
F_p	Packing factor of the packed column	dimensionless
F_{MC}	Function to integrate in the membrane contactor	m^6 $kmole^{-1}$
F_{PC}	Function to integrate in the packed column	m^4 $kmole^{-1}$
Fr	Froude number	dimensionless
g	Constant of acceleration due to gravity	m s^{-2}
G	Gas molar flow through the cross section	mole s^{-1}
H	Henry constant of component	Pa
HET	Height of a theoretical stage	m
HUT	Height of a transfer unit	m
k	Individual mass transfer coefficient	m s^{-1}
K	Global mass transfer coefficient	m s^{-1}
L	Liquid molar flow through the cross section	mole s^{-1}
M_{mol}	Molar mass of component	g mol^{-1}
m	Partition coefficient gas-liquid	$m^3_{\ gas}\ m^{-3}_{\ liquid}$
N	Molar flow in the interphase	mole m^{-2} s^{-1}
NET	Number of theoretical stages	dimensionless
NUT	Number of transfer units	dimensionless
P	Pressure	Pa
R	Mass transfer resistance	s m^{-1}
R_{LG}	Ratio liquid-gas	m^3 liquid m^{-3} gas
R_g	Universal gases constant	J K^{-1} $mole^{-1}$
Re	Reynolds number	dimensionless
r	Radius	m
Sh	Sherwood number	dimensionless
T	Temperature	K
u	Superficial velocity	m s^{-1}
v	Interstitial velocity	m s^{-1}
V	Total volume of the contactor	m^3
$\dot{V}$	Volumetric flow	m^3 s^{-1}
V_{mol}	Molar volume	cm^3 $mole^{-1}$
We	Webber number	dimensionless
Y	Dimensionless capacity	dimensionless
x	Molar fraction in the liquid phase	mol $mole^{-1}$
y	Molar fraction in the gas phase.	mol $mole^{-1}$
z	Axial coordinate	m
z*	Normalized axial coordinate	dimensionless
Z	Total length of the contactor	m

Greek symbols

Symbol	Definition	Units
ΔH^0_{abs}	Heat of absorption at standard conditions	J $mole^{-1}$
ΔH^0_{dis}	Heat of dissolution at standard conditions	J $mole^{-1}$
δ	Thickness	m
ε	Porosity	dimensionless
η	Recovery of a compound in the contactor	dimensionless
θ	Contact angle between liquid absorbent and the membrane surface	dimensionless
κ	Kozeny equation constant	dimensionless
λ	Extraction ratio	dimensionless
μ	Viscosity	Pa s
P	Permeability	mole m^{-1} s^{-1} Pa^{-1}
P_0	Pre-exponential factor in permeability equation	mole m^{-1} s^{-1} Pa^{-1}
σ_c	Wettability of the used material in the packed column	kg s^{-2}
σ	Surface tension of phase	N m^{-1}
τ	Tortuosity of the membrane	dimensionless
ν	Diffusion volume	cm^3 $mole^{-1}$
ρ	Density	kg m^3
Φ	Association factor	dimensionless
φ	Fiber volume fraction	dimensionless
ω	Acentric factor	dimensionless

Subscripts and superscripts

Symbol	Definition
A	Carbon dioxide
abs	Relative to the absorption process
ax	Relative to the axial direction
*	Relative to normalized length
B	Methanol or Hydrogen
crit	Critical
d	Dense layer
dis	Relative to the dissolution
eq	Related to equilibrium state
ext	External
flood	Relative to flooding
G	Relative to the gas phase
lm	Logarithmic mean
L	Relative to the liquid phase
nom	Nominal
i	Relative to a component
if	Relative to the interface gas-liquid
int	Internal
in	Relative to an inlet stream of the contactor
j	Relative to a phase (gas or liquid)
k	Relative to an equilibrium stage
MC	Relative to the hollow fiber membrane contactor
out	Relative to an outlet stream
ov	Overall

Subscripts and superscripts (cont.)

Symbol	Definition
p	Microporous support
PC	Relative to the Packed column
red	Reduced

Abbreviations

Abbreviation	Definition
ACM	Aspen Custom Modeler
bmim TCM	1-Ethyl-3-methylimidazolium tricyanomethanide
bmim BF_4	1-butyl-3-methylimidazolium tetrafluoroborate
CCS	Carbon Capture and Storage
CPA	Cubic-Plus-Association
DEPG	Dimethyl Ether of Polyethylene Glycol (Selexol^{TM})
ENSIC	École nationale supérieure des industries chimiques
HFMC	Hollow fiber membrane contactor
IGCC	Integrated Gasification Combined Cycle
LRGP	Laboratoire Réactions et Génie des Procédés
MEA	Monoethanolamine.
NASA	The National Aeronautics and Space Administration
NMP	N-Methyl-2- Pyrrolidone, Purisol
PC	Packed contactor
PEG-300	Polyethyleneglycol-300
PSRK	Predictive Soave–Redlich–Kwong
RMT	Relative Membrane Thickness
SRK	Soave-Redlich-Kwong
TEG	Triethylene glycol.
UNIFAC	UNIQUAC Functional-group Activity Coefficients

LIST OF FIGURES

LIST OF TABLES

CONTENTS

1. INTRODUCTION

1.1. Motivation

The earth's atmosphere is a combination of gases which supports life in a delicate balance. Carbon dioxide and other greenhouse gases help regulate temperature by absorbing infra-red thermal radiation generated by the sun and preventing it from passing back into outer space.

Humans effect on climate has been the most significant cause of detected warming since the middle of 20th century, in fact global average surface temperature augmented 0.85 degC between 1880 and 2012 (Figure 1), even in other regions of the world have suffered even an increase of 1.5 degC in at least one season. This temperature growth leads to a significant change in human life and in the natural systems, like extreme weather, an increase in sea level and biodiversity damage. Definitely, human activities have become the main source of change in the Earth, taking out our planet from its delicate equilibrium (Allen *et al*., 2018).

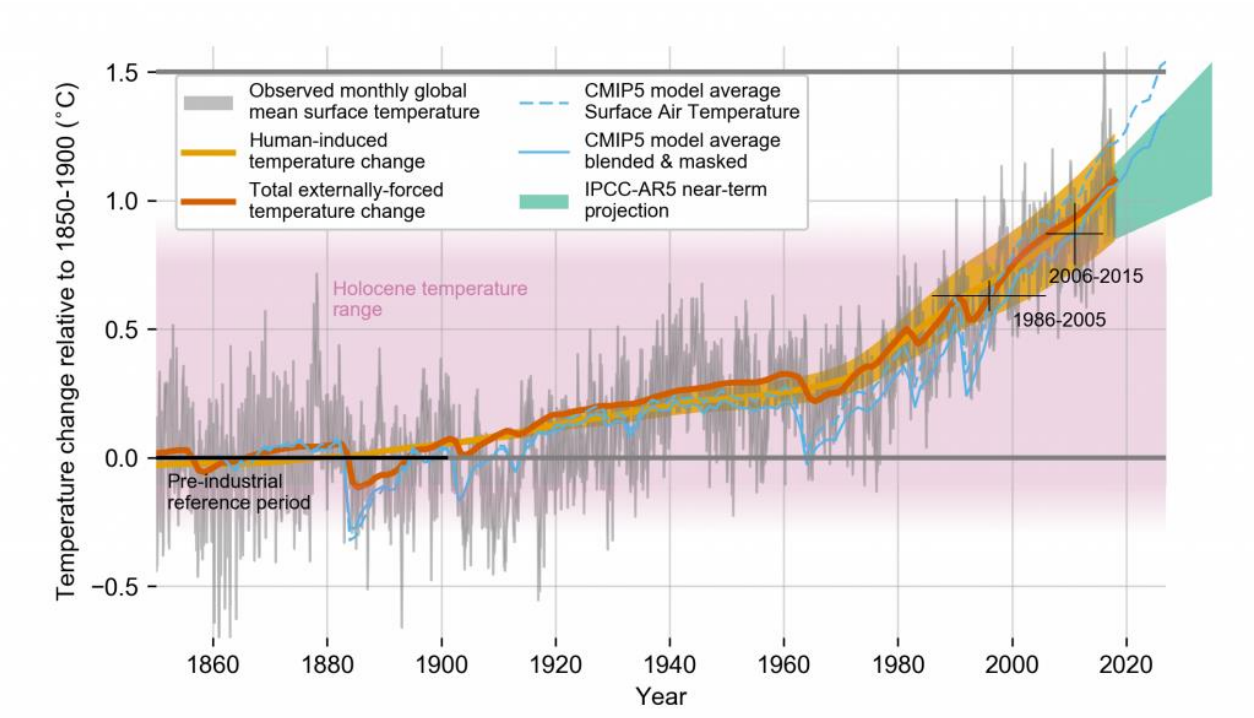

Figure 1. Evolution of global mean surface temperature over the period of instrumental observations (Allen et al., 2018)

Carbon dioxide is a remarkable greenhouse gas and it is emitted by human activities like deforestation and burning fossil fuels as well as natural processes such as organism's respiration and volcanos. In Figure 2 it can be observed that over the last 170 years, concentration of CO_2 has increased by 47% above pre-industrial levels of 1850 (NASA, 2020), as it can be checked in Figure 2.

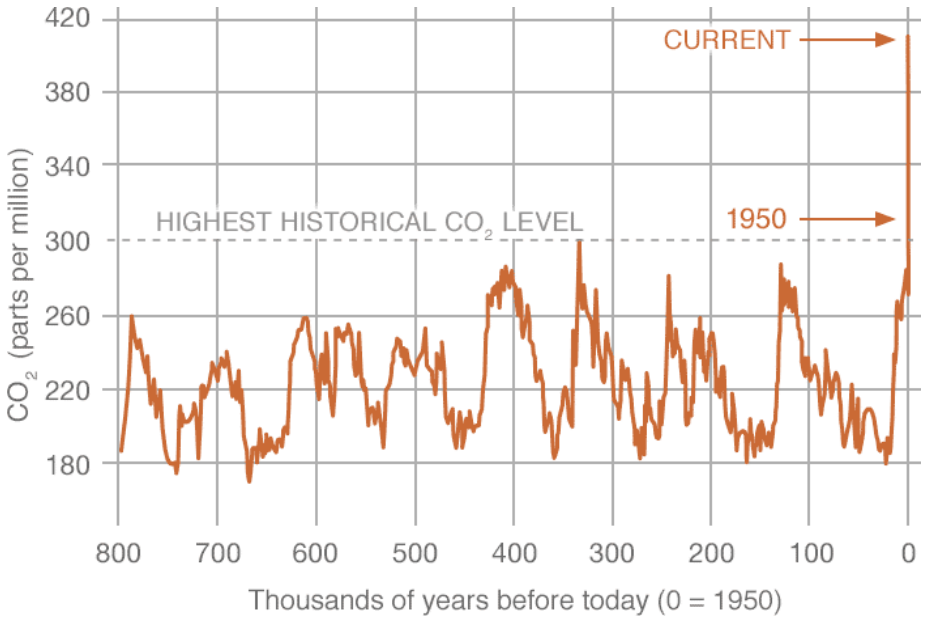

Figure 2. Carbon dioxide historic indirect measurements by reconstruction from ice cores and Mauna Loa CO_2 record (NASA, 2020)

According to IPCC (2014), if there are not supplementary efforts to reduce global greenhouse emissions, they will grow up much more rapidly due to increase of human population and its activities. Scenarios without extra mitigation would lead the earth to a surface temperature increase from 3.7 to 4.8 degC in 2100, taking as reference the preindustrial levels.

Thus, it is crucial to reduce the emissions of CO_2 and other greenhouse gases. It is observed in Figure 3 that the main source of CO_2 in the world are electricity and heat production, with coal, natural gas, and oil as the main fuels, consequently it will be critical to apply carbon capture technologies in that sectors. Carbon Capture and Storage (CCS) is a promising technology to reduce the impact of continued hydrocarbon energy production. CCS firstly isolates the carbon dioxide emissions then stores them in deep geological formations to prevent them escaping back into the atmosphere (Lockwood, 2017).

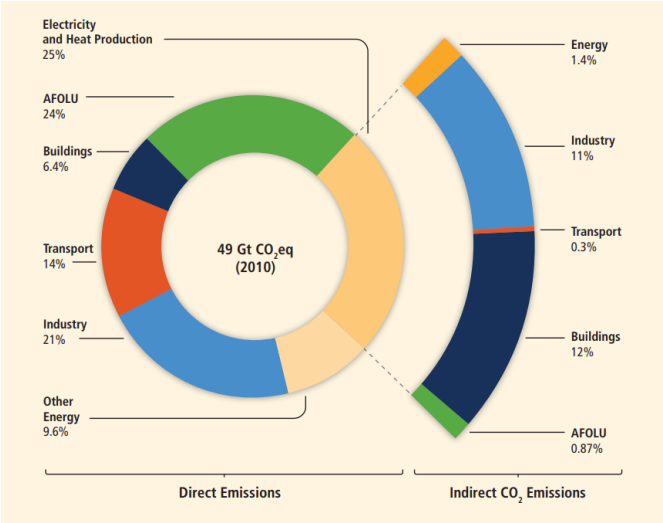

Figure 3. Global greenhouse gas emissions by economic sector (IPCC, 2014)

Post-combustion carbon capture is a well-established and commonly employed CCS technology (Dennis *et al.*, 2014); however, it poses environmental and energy related problems such as significant energy penalties from carbon dioxide compression and amine scrubbing. Oxy-fuel combustion is another promising technology, however with it is limited to pilot-scale operations, no full-scale operations and costly air separation unit (ASU), it remains an under researched area (Theo *et al.*, 2016).

Pre-combustion carbon capture within an integrated gasification combined cycle (IGCC) separates hydrogen from the fuel before the energy generation step by firstly gasifying the fuel to produce a syngas, which after a water gas shift reaction, comprises of predominantly hydrogen and carbon dioxide (30-40% CO2) at high temperature (190-210 degC) and pressure (20-70bar) with trace impurities (Scholes *et al.*, 2010). Currently the process requires a high energy consumption (Shen Yang *et al.*, 2016) with the most energy intensive step of the process being the water gas shift reaction (responsible for 44% of the total efficiency), however the removal of carbon dioxide prior to the hydrogen being suitable as a fuel still contributes a large proportion of the energy usage (21% of the total efficiency). (Belaissaoui and Favre, 2018). This is the area of focus for this research.

Currently the prominent method for carbon dioxide removal within an IGCC is by a packed column absorber (Sun and Smith, 2013). Previous studies for post-combustion carbon capture have demonstrated the intensification benefits of using membrane contactors as a promising alternative to packed columns (Rode *et al.*, 2012) due to their larger interfacial surface area (5000 to 20 000 m^{-1}) and decreased diffusion distances due to submillimeter hydraulic diameters in comparison to a packed column (500 m^{-1}) (Favre and Svendsen, 2012). The membrane separates physically the gas and the liquid streams, thus preventing liquid entrainment or flooding which can cause operational constraints for the packed bed (Villeneuve *et al.*, 2018b). Being able to demonstrate the intensification benefits of membrane contactors has a wide-reaching implication within the

energy sector, where compact, lightweight equipment can have dramatic consequences such as in offshore environments

However, their benefits might be balanced by an increased mass transfer resistance due to the presence of the membrane itself and the possible occurrence of porous membrane wetting (Belaissaoui and Favre, 2018).

1.2.Previous work

1.2.1. Physical, transfer and thermodynamic properties of gas and liquid mixtures of hydrogen, carbon dioxide and methanol in view of the modelling of physical absorption processes

In this work, carried out by Alice Nanyonjo, an ENSIC intern, the physical properties of a H_2 – CO_2 gas mixture, a CO2 – methanol liquid mixture and the liquid-vapor equilibrium of a CO2 – methanol system were studied as applied to physical absorption of CO_2 in methanol at high pressure (20 – 50 bars) and low temperatures (-60, -40°C). Calculations were made at both 1 bar and 30 bars in a temperature range of -60 – 25°C and a H_2 – CO_2 gas mixture containing 39% CO_2, pure methanol being the solvent. The first objective was to validate the estimation of the diffusion coefficient and the dynamic viscosity of the components of different fluids for them to be used directly from a simple procedure in Aspen Custom Modeler (ACM) instead of having to rewrite the correlations in a membrane contactor model, as would be the case in Matlab®. The second was to choose a thermodynamic model that described the liquid – vapor equilibrium of the CO_2 – methanol system.

Different correlations were used to estimate the physical properties and the deviation from those made by Aspen were calculated. For the diffusion coefficient of hydrogen and carbon dioxide into methanol, a 4% average deviation was observed. For H_2 diffusing into CO_2, a 5% average deviation was observed while for methanol diffusing into the H_2 – CO_2 gas mixture, an average 20% deviation was observed. These deviations remain acceptable. For the gas dynamic viscosity, an average 10% deviation was noted for pure H_2. 1.3% was noted for pure CO_2 and 20% methanol for the original gas mole fraction. Moreover, as the mole fraction of CO_2 in the gas reduces, the deviation increases but this is because of the choice of the mixing rules used. For the liquid dynamic viscosity, no deviation was noted for pure components and the CO_2 – MeOH binary solution. whose CO_2 mole fraction was varied from 0.1 to 0.3. In fact, Aspen neglected the binary interactions between the two components.

In literature, experimental data of the VLE of CO_2 – MeOH was compiled and compared to estimations made by 4 models: CPA (Cubic-Plus-Association), SRK (Soave-Redlich-Kwong), PSRK (Predictive Soave–Redlich–Kwong) and UNIFAC (UNIQUAC Functional-group Activity Coefficients) with Henry's Law. CPA was found to best characterize the VLE of the system.

1.2.2. Evaluation of membrane contactors for CO_2 capture from syngas mixtures using physical absorbents: simulation study

This thesis completed by Ewan Mckechnie, another ENSIC intern, looked for to continue previous research completed into the intensification potential of dense hollow fiber membrane contactors, compared to the industry favored packed contactor for carbon dioxide absorption. Using Aspen HYSYS®, a parametric study was completed to understand the optimal operating conditions for physical absorption of carbon dioxide into methanol as well as an investigation into the fluid dynamics within the column to allow further work to be completed into the intensification potential of hollow fiber membrane contactors.

The parametric study looked at optimizing the conditions for absorption to occur as well as developing a database of information as to which the intensification potential could be determined over. The fluid dynamics investigation determined the likelihood of flooding and the operability of the equipment. Flooding can happen at any point within the column and to give a comparable metric, the gas inlet velocity was used. It was found that there was minimal variation in limiting gas inlet velocity within the column.

1.3.Literature review

A few number of articles about the process of CO_2 physical absorption in hollow fiber membrane contactors have been developed in the literature. It is remarkable that not all the articles used methanol as solvent; two of them applied Polyethylene Glycol (PEG) variants, like PEG-300 (Kartohardjono *et al.*, 2017) or Dimethyl Ether of Polyethylene Glycol (DEPG), also known as Selexol™ (Belaissaoui and Favre, 2018). Other articles have selected ionic liquids as physical solvents, like Butyl-3-methlyimidazolium tricyanomethanide (bmim TCM) (Usman *et al.*, 2018) or Pahlavanzadeh *et al*. (2020), in which it has been utilized 1-butyl-3-methylimidazolium tetrafluoroborate (bmim BF_4). However, only two articles have used methanol as solvent, Mahdavian *et al*. (2011) and Scholes *et al*. (2013).

In relation with the inlet gas, most of the processes are about CO_2 removal from syngas, assuming that syngas components are CO_2 and H_2, with the CO_2 molar fraction in syngas around 0.4 (Scholes *et al*., 2013) (Usman *et al.*, 2018) (Belaissaoui and Favre, 2018). Moreover, for some processes the gas inlet contains a mixture of CH_4 and CO_2, for example Mahdavian *et al*. (2011) and Kartohardjono *et al.* (2017) and other include a mixture of air and CO_2. However, it is important that the CO_2 molar fraction is around 0.4 for all the processes found in the literature.

Concerning the pressure conditions, most of the papers are high pressure processes like the process of this report. In found articles the operating pressure goes from 20 bar (Usman *et al.*, 2018), 26 bar (Scholes *et al.*, 2013) and 36 bar in the case of Belaissaoui and Favre. (2018). However, for Pahlavanzadeh *et al*. (2020) the operating pressure is atmospheric as maximum for an absorption of CO_2 from air. Mahdavian *et al*. (2011) and Kartohardjono *et al.* (2017) do not even specify the operating pressure.

Regarding the temperature of the processes, in the articles which involve methanol as solvent the temperature goes from 0 to 30 degC (Mahdavian *et al.*, 2011). In general, it can be stated that the temperature of the literature processes is within the operating temperature interval of this report, except for Scholes *et al.* (2013) and Kartohardjono *et al.* (2017), in which the temperature has not been specified.

Concerning the volumetric flow of the liquid, for most of the articles the liquid volumetric flow is not within the industrial domain (Mahdavian *et al.*, 2011) (Kartohardjono *et al.*, 2017) (Pahlavanzadeh *et al.*, 2020), as occurs in this report. However, Usman *et al.* (2018) and Belaissaoui and Favre (2018) have solvent volumetric flow close to industrial conditions. Scholes *et al.* (2013) does not specify the volumetric flows.

In relation to the geometrical parameters used in the literature, the ratio $\delta_M/r_{M\text{-}ext}$ is between 0.27 and 0.55 for all the papers; concerning the internal diameter of the membrane, its value oscillates between 235 and 607 µm, excluding Scholes *et al.* (2013), in which the authors have not specified the geometrical parameters of the membrane. Regarding the length of the membrane contactor, it fluctuates from 0.065 m for small contactors to 1-1.5 m, which is a typical length of industrial membrane contactors.

Table 1 presents the geometrical parameters and operational domain of the papers found in the literature.

Table 1. Overview of operational parameters in HFMC CO_2 physical absorption studies reported in the literature: A) Mahdavian et al. (2011), B) Scholes et al. (2013), C) Kartohardjono et al. (2017), D) Usman et al. (2018), E) Belaissaoui et al. (2018), F) Pahlavanzadeh et al. (2020)

Ref.	Operational conditions									Membrane		
	η_{CO2} %	Gas	Solvent	T degC	P bar	$V_{L,in}$ m^3/h	$V_{G,in}$ m^3/h	$V_{L,in}$ $V_{G,in}^{-1}$ (-)	$yco_{2,G}$ (-)	$\delta_M/r_{M\text{-}ext}$ (-)	$d_{M\text{-}int}$ µm	Z m
A	~90-97	CH_4 CO_2	Methanol	0 20 30	NS	0.018 0.036	0.06	0.3 0.6	Not clear[b]	0.33	607	0.30
B	90	CO_2 H_2	Methanol	NS	26	NS	Not clear[c]	NS	0.40	NS	NS	NS
C	Not clear[a]	CH_4 CO_2	5%wt PEG-300	NS	NS	0.006 0.036	NS	NS	0.36	0.55	235	0.25
D	90	CO_2 H_2	bmim TCM	50	20	1337	1.49E+06	9E-04	0.45	0.51	430	1.50
E	94.6	CO_2 H_2	Selexol™	35	36	9.16	116.9	0.078	0.38	0.29	370	1.00
F	~45-80	Air CO_2	Ionic liquid Water	30	0-1	0.0012 0.012	0.0024	0.5 5	0.35	0.27	275	0.065

NS: Not specified.

[a] Incorrect CO_2 recovery formula

[b] 8 mol m^{-3}

[c] 642.4 tonnes h^{-1}

1.4.Background theory

1.4.1. Carbon dioxide capture and storage

Carbon capture and storage (CSS) is a process which involve the separation of CO_2 from industrial and energy sources, transport to a storage location and finally long-term isolation in geological formations in the ocean or used in other processes, thus it is not emitted to the atmosphere. Extensive application of CCS technology could be capable of reducing mitigation costs and enhance adaptability in emissions reductions (IPCC, 2005).

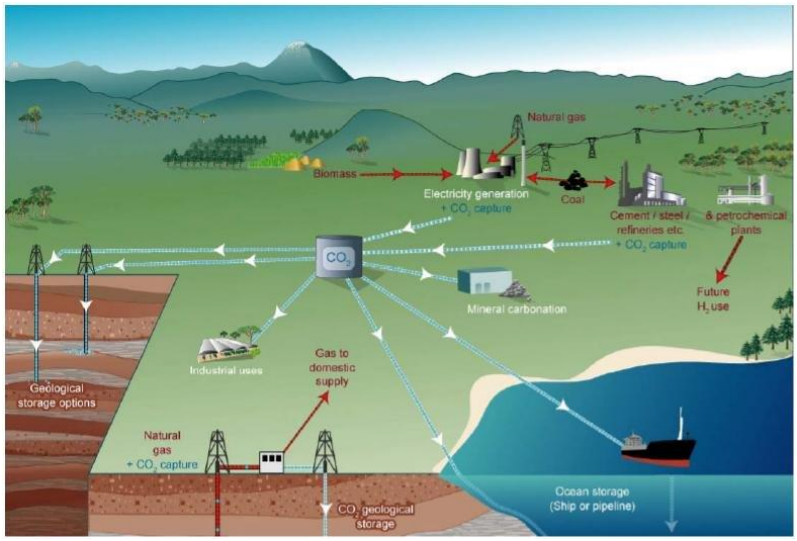

Figure 4. Diagram of possible CCS systems (IPCC, 2005)

The reductions of emissions to the atmosphere with this system is restricted by the fraction of carbon dioxide captured, since an increase of CO_2 production implies a worse efficiency of power plants or industrial processes because of the energy needed to capture CO_2, as well as leakages in transport and in long-term storage.

In the case of a power plant with CCS system, it is estimated a CO_2 emissions reduction of 80-90% compared to a plant without CCS (IPCC, 2005). In Figure 5 it can be observed that there is an increase of CO_2 production in plants with CCS, this is due to the extra energy required to capture, transport and storage, so it is essential to understand the process along its life cycle.

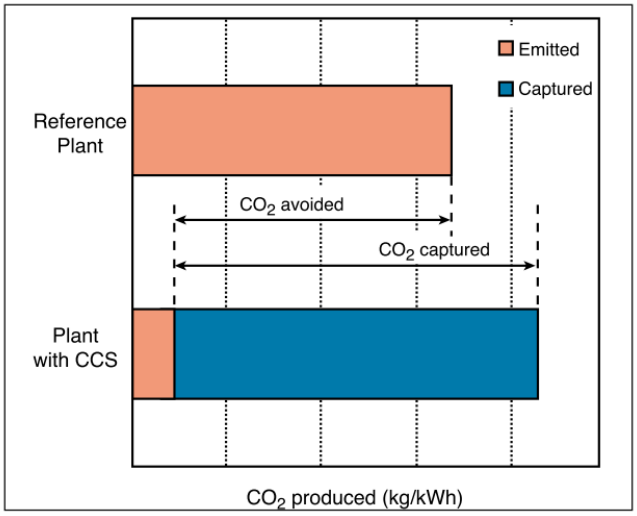

Figure 5. CO_2 capture and storage from power plants (IPCC, 2005)

Thus, carbon capture and storage technology could decrease the global greenhouse emissions of fossil fuel power plants, it is a truly promising strategy, but it has not yet used at large scale and in commercial fossil plants (IPCC, 2014).

Other choices of mitigating climate change could be improving the efficiency of the processes, use less carbon-based fuels and to utilize more nuclear power as well as renewable energies (IPCC, 2005).

1.4.2. Integrated Gasification Combined Cycle

Integrated Gasification Combined Cycle (IGCC) produces synthesis gas (syngas) through the gasification of carbonaceous fuels. Removing carbon dioxide for storage from the hydrogen gas is a key step in the process for the IGCC power plant for both the power generation and mitigation of greenhouse gas emissions. Conventionally, packed columns are used to absorb carbon dioxide from the syngas through pressurized physical solvents such as methanol or Dimethyl Ether of Polyethylene Glycol (DEPG) (Selexol^{TM}). In IGCC pre-combustion carbon capture, syngas is treated to capture CO_2 before to combustion, in order to mitigate the emissions of greenhouse gases (Belaissaoui and Favre, 2018).

In Figure 6 it is observed a scheme of the IGCC process with pre-combustion carbon capture, in which block of interest is the one of CO_2 removal.

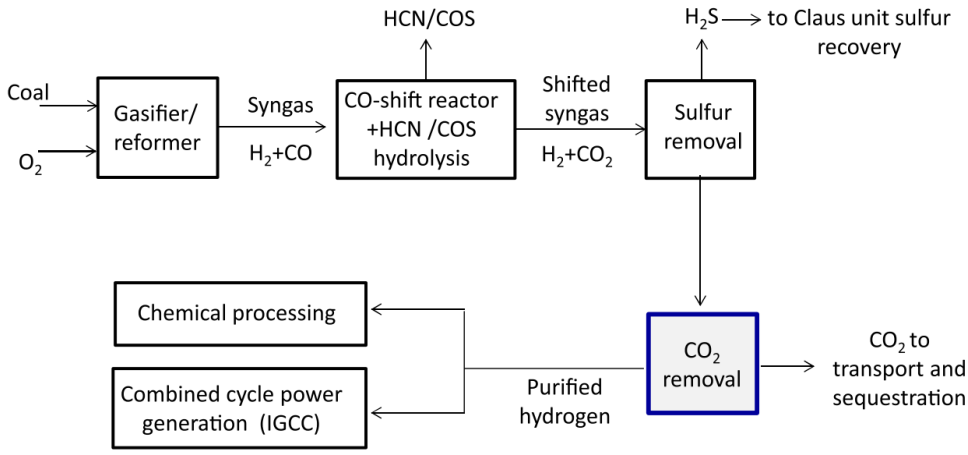

Figure 6. Typical IGCC and pre-combustion carbon capture scheme (Belaissaoui and Favre, 2018)

1.4.3. Rectisol™ process

Rectisol™ is a commercial process developed in the 1950s and it is applied mainly to syngas purification using methanol as solvent, this process comprises physical and chemical absorptions as well as membrane separation, hence it is valuable to do research about membrane intensification potential in this technology (Sun and Smith, 2013). In Figure 7 it can be observed a blocks diagram of Rectisol™ process.

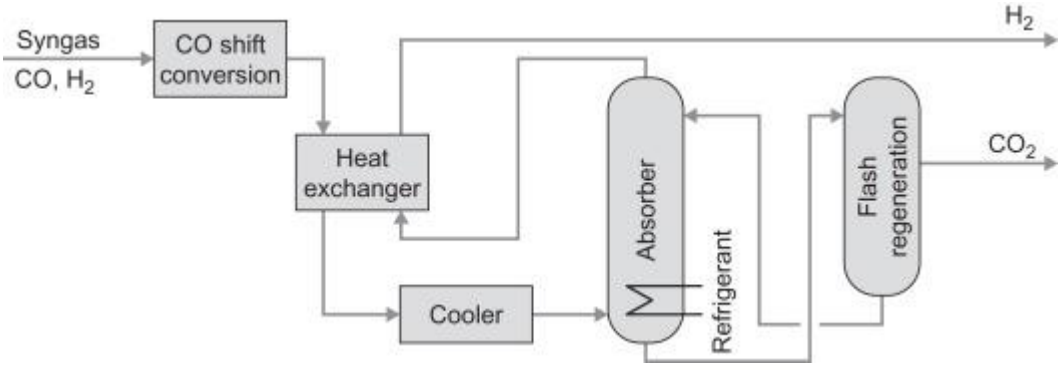

Figure 7. Rectisol™ process for CO_2 removal (Rackley, 2017a)

Physical absorption processes are more economically efficient at higher pressures and lower temperatures. Moreover, methanol absorption power for CO_2 is greater than other solvents like water or N-Methyl-2- Pyrrolidone, Purisol (NMP). This solubility characteristic implies less solvent flowrate and regeneration. Thus, it is important to know the relative solubility of CO_2 in methanol compared to H_2, in the following table it is checked that CO_2 solubility is around 435 times H_2 solubility in methanol at -40 degC (Sun and Smith, 2013).

Table 2. Relative solubility in methanol at -40 degC (Sun and Smith, 2013)

Component	H_2S	COS	CO_2	CH_4	CO	N_2	H_2
Relative solubility	5.9	3.6	1	0.027	0.012	0.0058	0.0023

1.4.4. Absorption using a physical solvent

Carbon dioxide can be captured from syngas mixture mainly by two ways: chemical absorption, where there is a reaction between the liquid solvent and the solute, and physical absorption, which is based on change temperature and pressure in order to favor the absorption. This report will be focused on physical absorption.

Thus, regarding physical absorption, the velocity at which a solute in a gas mixture can be dissolved in a certain liquid solvent depends on the deviation from equilibrium. Assuming an ideal gas, vapor-liquid equilibrium can be defined by Henry's law, which states that the partial pressure of a specie P_i is directly proportional to its liquid-phase mole fraction x_i (Smith, Van Ness and Abbott, 2001).

$$y_i P = H_i x_i \qquad [1]$$

Where H_i is the Henry constant and can be obtained experimentally.

Moreover, Henry's law also can be expressed as a volumetric parameter by a partition coefficient m_i, which is a function of composition, temperature and pressure of the system.

$$m_i = \frac{C_{iL}}{C_{iG}} \qquad [2]$$

In the following graph it is shown a simulation of the variation of the partition coefficient of CO_2 with the temperature in order to obtain a comparison of Aspen HYSYS® estimation to literature references (Nanyonjo. 2020). It is important to remark that this partition coefficient is only valid for diluted systems (in this case $x_{CO2}<0.3$).

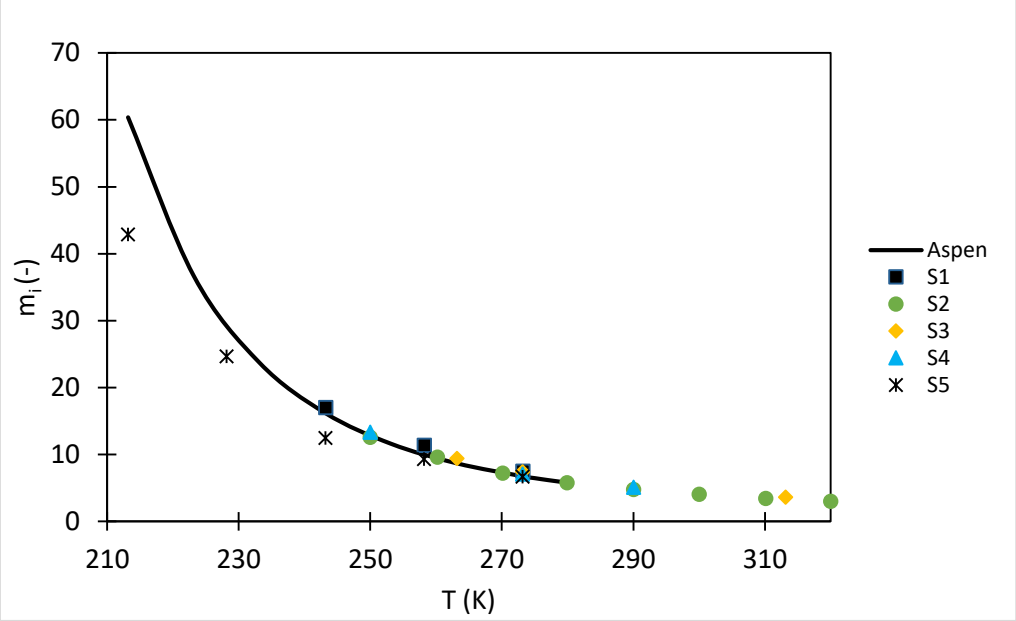

Figure 8. Partition coefficient vs Temperature compared to literature references (Nanyonjo, 2020)

Another important parameter in this process is the heat of absorption, which can have an influence on the gas solubility and the diffusion coefficients. It is well-known that if there is not chemical reaction the heat of absorption is equal to the heat of dissolution (equation 3).

$$\Delta H^0_{abs} = \Delta H^0_{dis} \qquad [3]$$

In addition, heat of absorption can be expressed as the enthalpy change from a VLE data using the standard Clausius equation (Jonassen *et al.*, 2014).

$$\left[\frac{\partial \ln P_i}{\partial (1/T)}\right]_{P,x} = \frac{\Delta H^0_{abs}}{R_g} \qquad [4]$$

Low temperatures and high pressures help the carbon dioxide to be better absorbed without requiring a chemical reaction, as it can be observed in Figure 9. Consequently, physical absorption is ideal to apply to pre-combustion carbon capture, since it is industrially favored, due to its conditions of temperature and pressure (Nanyonjo, 2020).

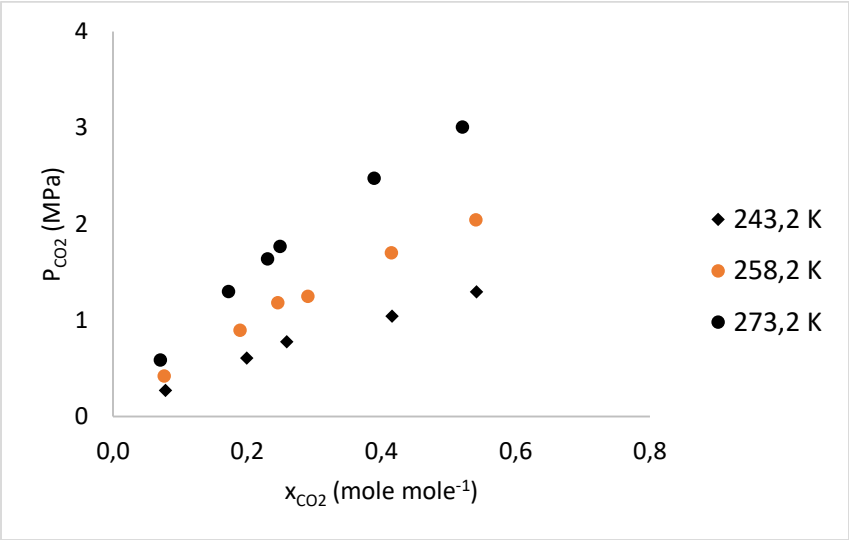

Figure 9. Solubility of CO_2 in methanol at low temperatures (Nanyonjo, 2020)

1.4.5. Packed contactor. Overview

A packed contactor (PC), or packed bed, consists of a cylindrical tower with a gas inlet and outlet, as well as a liquid inlet and outlet. The column is hollow and filled with a packing material which can be structured or unstructured depending on the application, the packing increases the contact area between the two phases, allowing for a higher rate of absorption

The packed column is the industrially favored chemical processing method for both chemical and physical absorption (Sun and Smith, 2013).

Concerning the flow direction, counter-current flow has been selected because that flow implies a greater volume of CO_2 to be extracted compared to similar systems with co-current flow. Figure 10 shows a typical counter-current packed column.

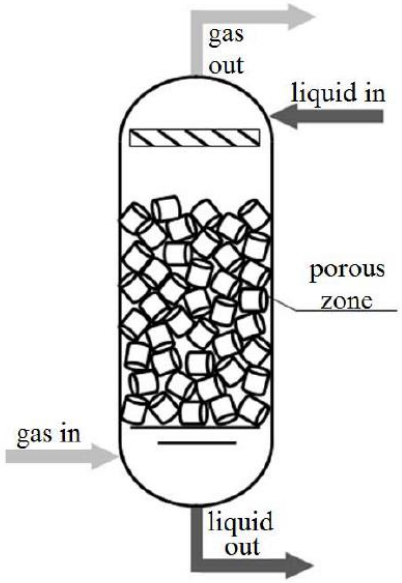

Figure 10. Countercurrent packed column (Asendrych et al., 2013)

The liquid inlet (often pure) is introduced at the top of the tower, whereas the solute (in this case CO_2) is contained in a gas which enters at the bottom of the column (McCabe, 2007). Regarding the packing, there are two possibilities in function of geometry: random packing and structured packing.

An important limitation of packing columns is that the gas velocity must be lower than the flooding velocity, nevertheless when flooding is almost reached most of the packing area is wetted, which implies a higher contact area. Moreover, increasing the gas velocity leads to a growth in the tower diameter and it also exists a pressure drop limitation due to energy costs. Consequently, it is difficult to design this type of towers due to flooding restrictions and requires to be conservative on it, which can involve less efficiency (McCabe, 2007).

1.4.6. Hollow fiber membrane contactor. Overview

The concern in membrane contactors has been increased in the last years, since it has been published a large number of papers on this domain. Membranes can be applied to perform an important number of unit operations, but the concept of the application of membranes to a gas-liquid system in order to perform a mass transfer process was firstly proposed in 1960, and it involves the transport of species in the gas to be absorbed in the liquid (absorption), and vice versa, which would be desorption.

The application of membrane contactors is of interest of chemical, petrochemical, pharmaceutical, and galvanic industries, also for product recovery with water and gas treatment (Kumar *et al.*, 2015). However, nowadays, most of the research about membrane contactors is focused on applications in carbon dioxide capture by absorption in chemical solvents (Chabanon *et al*., 2014).

The most important difference with respect to other membranes processes, such as microfiltration, ultrafiltration, nanofiltration, reverse osmosis and pervaporation is that in this case the membrane does not have to be selective towards some components, the key is that it only offers an interface, therefore the mass transfer does not happen because of the membrane, it occurs because of the diffusion of components from one phase to the other (Hoek and Tarabara, 2013).

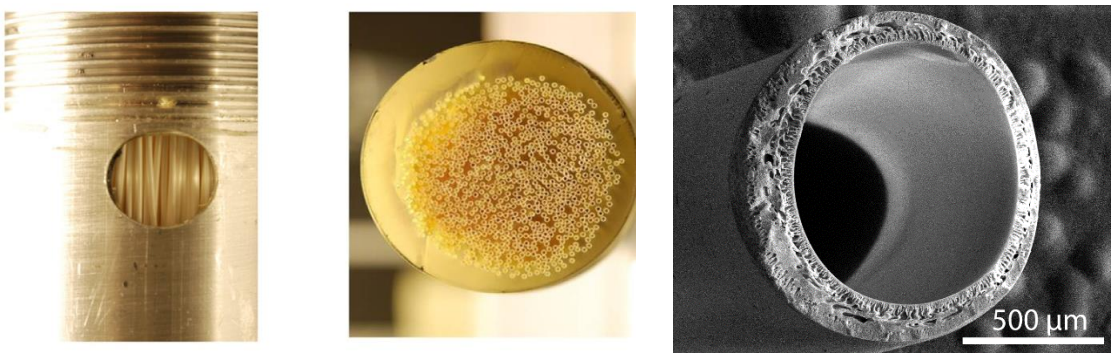

Figure 11. Hollow fiber membrane module and SEM cross section of an hollow fiber (Belaissaoui et al., 2016).

Packed columns, as it was stated previously, are a classic absorption technology based on the direct contact between both phases. However, a new hopeful option are membrane contactors, where the volume of the absorption unit is decreased due to a higher gas-liquid interfacial area (5000-20 000 m^{-1}) compared to an industrial packing (500 m^{-1}), even though having a membrane implies a larger mass transfer resistance. Consequently, membrane contactors have the potential of being one of the most important options related to gas-liquid absorption processes (Belaissaoui *et al.*, 2016).

Furthermore, a significant consideration is that a membrane has an important flooding protection effect for carbon dioxide absorption in chemical solvents, since the membrane divides the two phases (Belaissaoui *et al.*, 2016) (Villeneuve *et al.*, 2018a).

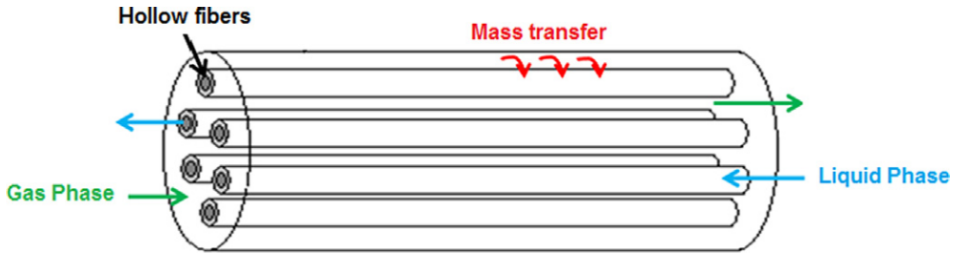

Figure 12. Representation of a hollow fiber membrane contactor for the gas-liquid absorption (Chabanon et al., *2014).*

In Table 3, it is summarized the main advantages and disadvantages of hollow fiber membrane contactors, compared to packed contactors.

Table 3. Hollow fiber membrane contactor (HFMC) advantages and disadvantages compared to packed column (PC)

Advantages	Disadvantages

- Increased interfacial area per unit volume
- Larger operating range for liquid and gas velocities because:
  ○ No flooding due to physical separation of the gas and liquid.
  ○ No foaming
  ○ Pressure profiles of gas and liquid are independent.
- Significantly lighter than packed beds.
- Flow is not driven by gravity.
	- Higher mass transfer resistance because of membrane dense layer.
	- Regarding to the microporous support:
	  ○ Membrane wetting due to liquid breakthrough.
	  ○ Gas bubbling.
	  ○ Capillary condensation.
	- Membrane degradation due to high pressure difference through the membrane.

Finally, the major challenges for membranes contactors currently are the following:

- Membrane wetting. It is the most important limitation of membranes contactors application to industry, since if wetting increases mass transfer resistance and consequently can lead to degenerate the absorption capacity. For a liquid absorber it can be studied by a parameter called LEP, liquid entry pressure, or breakthrough pressure (Zhao *et al.,* 2016). This parameter is expressed with Laplace-Young equation:

$$\mathrm{LEP} = \frac{4\mathrm{B}\,\sigma\cos\theta}{\mathrm{d_{max}}} \qquad [5]$$

  Nevertheless, this issue can be avoided by using a membrane based on a thin dense layer coated on a microporous support (Nguyen *et al.*, 2011).

- Membrane degradation. Chemical degradation due to attack to the membrane by chemical solvents, also thermal degradation of the membrane due to the material bad thermal stability (Zhao *et al.*, 2016).

- Large-scale operation. There are still challenges with using membrane contactors on the industrial scale. Currently the technology has only been used on the pilot plant scale for pre- and post-combustion carbon capture using chemical absorption (Scholes *et al.*, 2014). During the research for this project, no industrial scale membrane contactors could be found in operation using physical absorption, this could lead to unforeseen operational issues during scale up and hesitation from industry to adopt the technology in the near future.

- Long term operation. In a pre-combustion carbon capture setting, the membrane contactor is exposed to higher pressures than would be seen in other industrial uses, this could lead

to deformations in the membrane, increasing the potential for membrane wetting through the modified pore shape, increased average pore size and decreased contact angle (Li *et al.*, 2013). Compaction and plasticization can also occur under high pre-combustion gas pressure conditions, depleting the membrane transport performances. Deformations on the membrane can also lead to increased mass transfer through membrane aging as the microporous layer loses its original structure (Khaisri *et al.*, 2011).

1.5. Thesis aims

This master thesis is a continuation of previous work carried out by the Processes, Reactors, Intensification, Membranes, Optimization (PRIMO), department of the Reactions and Chemical Engineering Laboratory (in French *Laboratoire Réactions et Génie des Procédés*), and aims to:

- Obtain the axial profiles of important variables for both contactors.
- Design of the packed contactor.
- Design of the hollow fiber membrane contactor.
- Study of the pressure in the hollow fiber membrane contactor with the aim of having a good distribution of the fluids.
- Evaluate the intensification potential of hollow fiber membrane contactors.
- Perform a parametric analysis varying the liquid inlet temperature, the inlet pressure and the gas inlet composition of CO_2.

2. SIMULATION AND OPERATIONAL DOMAIN

2.1. Features of the simulation

Aspen HYSYS®, which is one of the top leading and well-known chemical processes simulator. HYSYS is applied in chemical industry to perform steady state simulations, dynamic simulations and also to model, optimize and design processes. It was developed by a Canadian company, Hyprotech, established by researchers from the University of Calgary (Aspentech, 2020).

The simulations, carried out by Mckechnie (2020) and by the author of this report, involved an Aspen HYSYS® standard absorber column with the following features:

- Cubic Plus Association (CPA) property package.
- Staged absorption column.
- Stage 1 represents the top of the column (liquid inlet).
- Stage 10 represents the bottom of the column (gas inlet).
- Counter current flow.
- Constant pressure along the column.

In the following figure is shown a screenshot of the Aspen HYSYS® absorber column used to carry out the simulations:

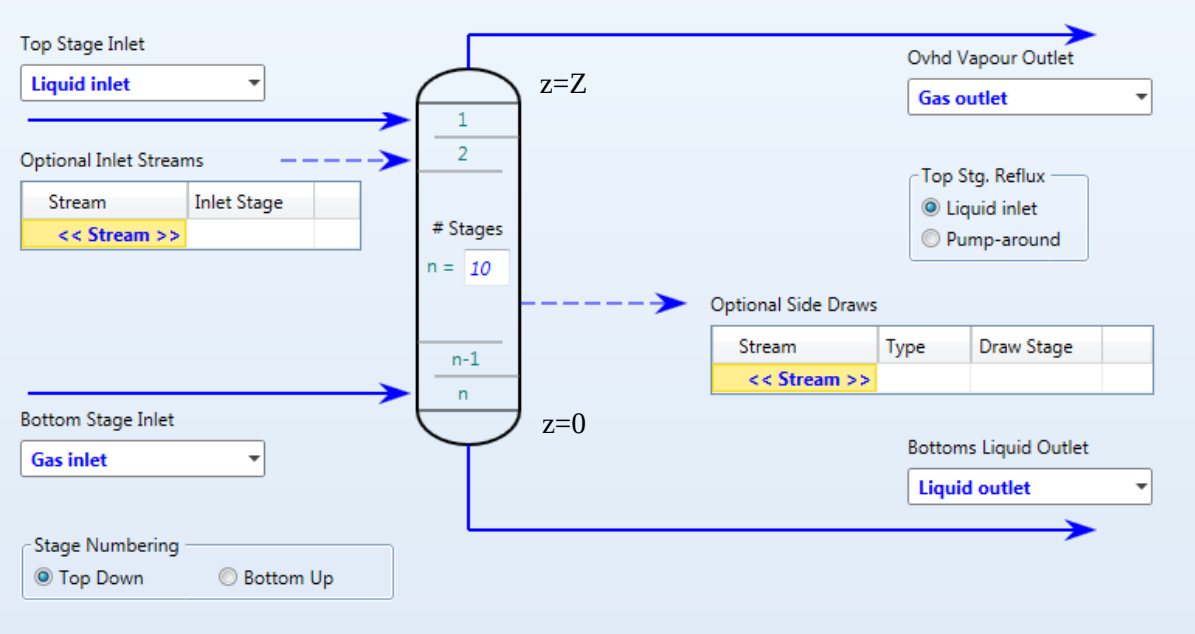

Figure 13. Screenshot of the absorber column in Aspen HYSYS®

2.2. Selection of the thermodynamic package

Cubic-Plus-Association (CPA) equation of state was chosen, based on association theory, it is a combination of the well-known Soave-Redlich-Kwong (SRK) EoS and Wertheim's association term. The publication of that equation was completed in 1996, after that, it has been applied to diverse equilibrium systems with a remarkable success (Kontogeorgis *et al.*, 2006).

The reason why it has been selected CPA EoS is because, according to Aspen simulations, it is the property method which best describes the VLE of carbon dioxide-methanol system in relation to experimental data, better than Soave-Redlich-Kwong (SRK), Predictive Soave–Redlich–Kwong (PSRK) and UNIFAC, models which have been used for this system previously in the literature (Nanyonjo, 2020).

Certainly, Figure 14 supports the affirmation that CPA is the most accurate model, with the VLE of experimental curve for a system CO_2-methanol. In that figure is represented a comparison with experimental data of the models employed to simulate the VLE of CO_2-methanol (Poling *et al.*, 2006), where y_{CO2} and x_{CO2} are the molar fraction of CO_2 in the vapor and in the liquid, respectively.

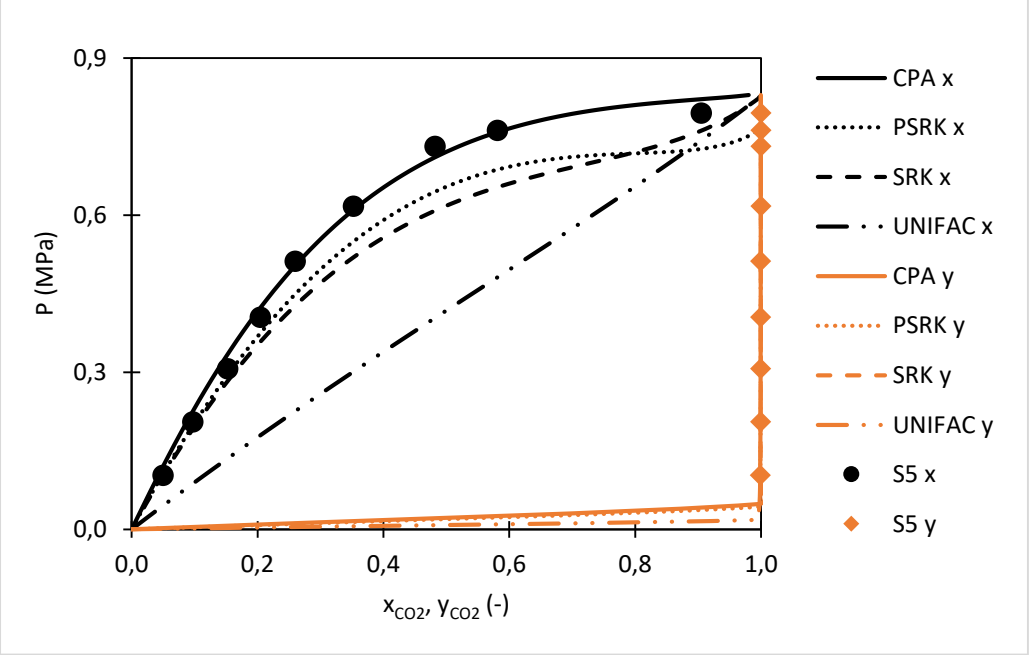

Figure 14. VLE of CO_2-methanol system at -40degC (Nanyonjo, 2020).

Finally, in Table 4 below gives a summary of the conclusions, concerning the accuracy of Aspen HYSYS® at estimating some physical properties.

Table 4. Summary of average deviations of physical properties estimated by Aspen, taking as reference values calculated by correlations (Nanyonjo, 2020)

Physical property	Symbol	Average deviation
Diffusion coefficient of H_2 into Methanol	$D_{H2,MeOH}$	4,00%
Diffusion coefficient of H_2 into CO_2	$D_{H2,CO2}$	5,00%
Diffusion coefficient of methanol into H_2-CO_2 mixture	$D_{MeOH,\ H2+CO2}$	20,00%
Dynamic viscosity of pure H_2	μ_{H2}	10,00%
Dynamic viscosity of pure CO_2	μ_{CO2}	1,30%

2.3. Operational domain

Simulations were performed varying the CO_2 composition of the inlet gas, operating pressure, temperature of the liquid inlet and temperature of the gas inlet. In Table 5 can be observed the operational parameters of the baseline case. It is important to remark that liquid inlet molar flow was adjusted until reaching 95% of CO_2 recovery.

Table 5. Baseline operating parameters on Aspen HYSYS® simulation

Operating conditions	Value	Units
Number of stages	10	dimensionless
Gas molar inlet flowrate, $N_{G,in}$	1.00	kmole h^{-1}
Liquid inlet composition, $x_{CO2,in}$	0.997 (MeOH)	
	0.003 (CO_2)	mole $mole^{-1}$
Carbon dioxide recovery, η_{CO2}	95±1	%
Liquid inlet molar flowr, $N_{L,in}$	1.68	kmole h^{-1}
Inlet pressure, $P_{G,in}$=$P_{L,in}$	40.00	bar
Liquid inlet temperature, $T_{L,in}$	-50.00	degC
Gas inlet temperature, $T_{G,in}$	-20.00	degC
Gas inlet CO_2 composition, $y_{CO2,in}$	0.40	mole $mole^{-1}$

Where CO_2 recovery was calculated with the following equation:

$$\eta_{CO2} = \frac{N_{CO2,G,in} - N_{CO2,G,out}}{N_{CO2,G,in}} \qquad [6]$$

In this report, first of all it is going to be studied the simulation 1, which is the baseline case. The parameters changed for the rest of simulations are presented in Table 6.

Table 6. Parameters varied in the simulated points with Aspen HYSYS®

Variable	Values	Units
Inlet pressure, $P_{G,in}$=$P_{L,in}$	20, 40, 50	bar
Liquid inlet temperature, $T_{L,in}$	-30, -20, -10, 0, 10, 20	degC
Gas inlet temperature, $T_{G,in}$	-30, -20, -10, 0, 10 , 20, 30	degC
Gas inlet CO_2 composition , $y_{CO2,in}$	0.3 and 0.4	mole $mole^{-1}$

2.3. Simulation outputs

In the following figures, it is presented the profiles along the column given by Aspen HYSYS® for the baseline case input parameters of Table 5. These profiles illustrate that the properties and flows change along the column, in addition, there is a pinch point in stage 9 (Figure 17), where the driving force is minimum and the temperature has a peak.

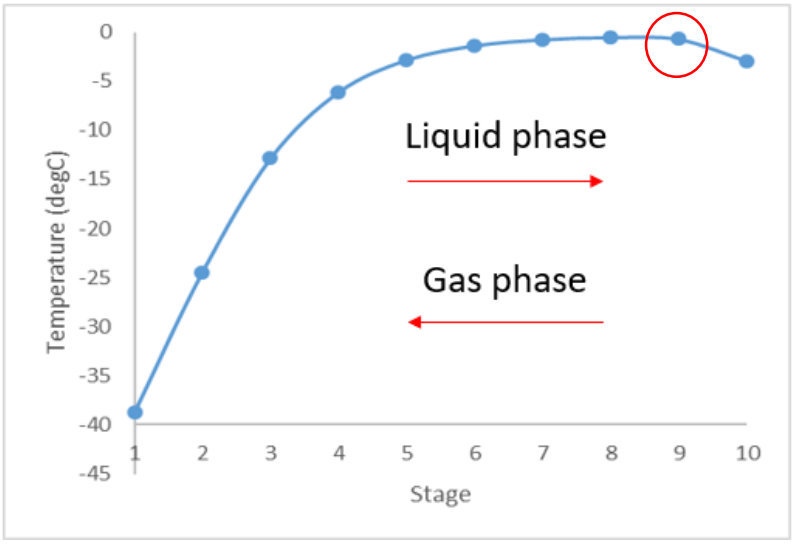

Figure 15. Temperature as a function of the stage in the Aspen HYSYS absorption column (baseline case)

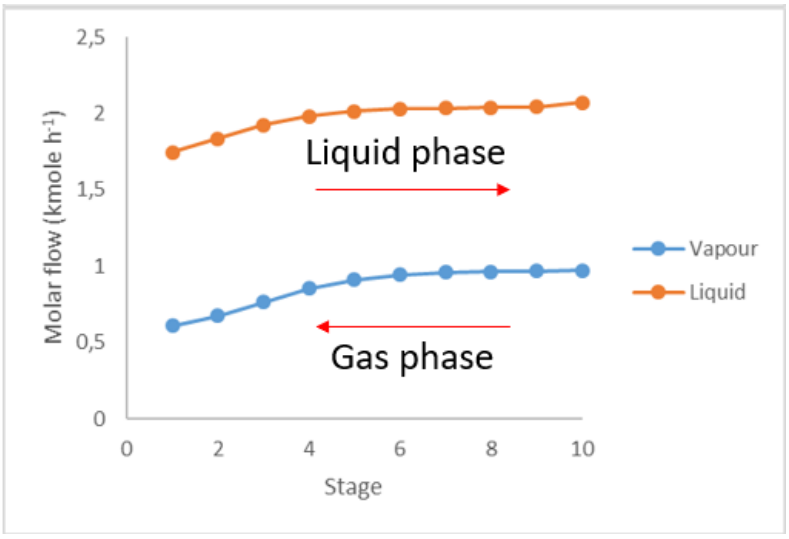

Figure 16. Molar flows of the liquid and the gas phase as a function of the stage in the Aspen HYSYS absorption column (baseline case)

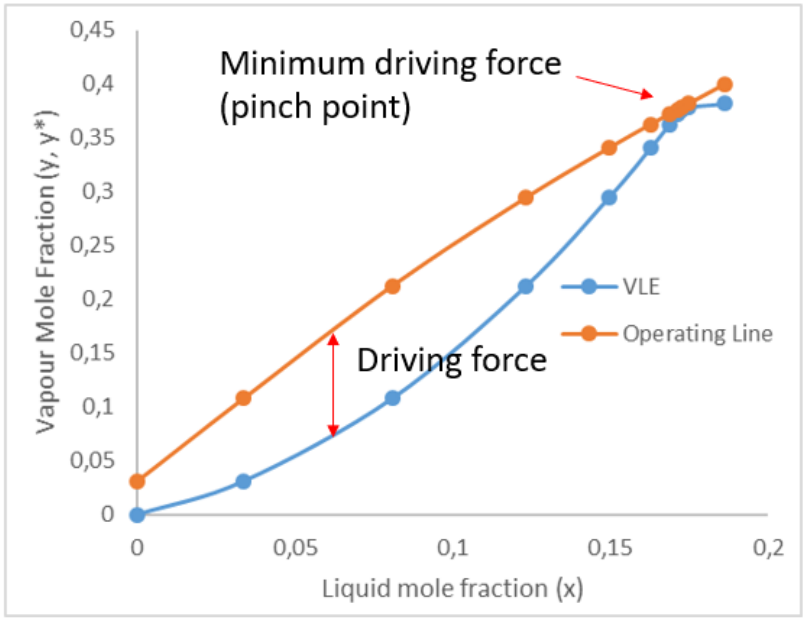

Figure 17. Equilibrium and operating curve in the Aspen HYSYS absorption column (baseline case)

3. DESIGN BASIS AND MODELING APPROACH

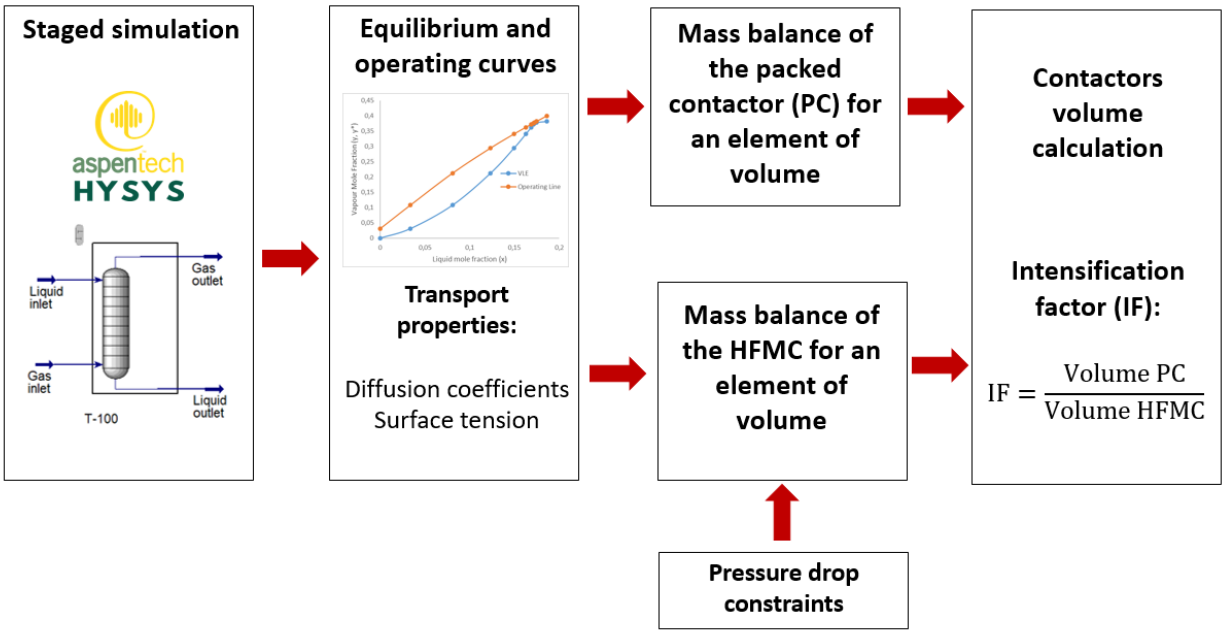

Figure 18. Scheme of the simulation and modeling methodology

In the scheme of Figure 18 is presented the steps followed in this work in order to obtain the intensification potential of hollow fiber membrane technology. In this section will be explained the third step, the mass balance of an element of volume of a contactor.

3.1.Design basis

3.1.1. Mass balance of a contactor

The mass balance in contactor of specie i in the gas phase is presented in the following equation, considering the axial diffusion negligible.

$$u_g \frac{dC_{iG}}{dz} + K_{iG}\, a_{LG} \left(C_{iG} - \frac{C_{iL}}{m_i} \right) = 0 \qquad [7]$$

It is remarkable that the mass balance of Equation 7 can be rearranged in order to integrate the differential equation and calculate the length of a certain contactor (Rode, 2019).

Thus, if the rearranged differential equation is integrated, it is obtained the following expression:

$$Z = \int_0^z dz = \int_{C_{iG,in}}^{C_{iG,out}} \frac{u_G}{a_{LG} \cdot K_{iG}} \cdot \frac{dC_{iG}}{C_{iG} - \frac{C_{iL}}{m_i}} = \int_{C_{iG,in}}^{C_{iG,out}} F\, dC_{iG} \qquad [8]$$

Where:

$$F = \frac{u_G}{a_{LG} \cdot K_{iG}} \cdot \frac{1}{C_{iG} - \frac{C_{iL}}{m_i}} \qquad [9]$$

In order to compute the volume of a contactor, it must multiply the length of the contactor by its cross-section area (Equation 10).

$$V = A \cdot Z = \int_0^z A \, dz = \int_{C_{iG,in}}^{C_{iG,out}} \frac{\dot{V}_G}{a_{LG} \cdot K_{iG}} \cdot \frac{dC_{iG}}{C_{iG} - \frac{C_{iL}}{m_i}} \qquad [10]$$

It should be noted that for our system F is stiff function in a certain range of C_{iG}, so it will be harder to integrate numerically because it should be considered different fitting functions and its precision would not be appropriate. Consequently, the first option selected was to evaluate the inverse of this function and integrate it by parts by a numerical method.

There are two key differences between finding the length of the packed contactor and the length membrane contactor; the global mass transfer coefficient, K_{iG} and also a_{LG} which differs depending on the technology as this favours the membrane contactor due to it being more compact. The global mass transfer coefficient has an increased resistance to mass transfer for the membrane contactor and is calculated differently to account for the geometry of the membrane contactor in comparison to the packed contactor.

Finally, it is important to underline that the design of the volume of the HFMC has some restrictions, mainly related to pressure drop and technology available, that constraints will be exposed at the point 4 of this report.

3.1.2. Design of a contactor by numerical integration

3.1.2.1. Integration by Tchebychev method

There is an integration rule adequate the integration of the F function, although usually is applied to cooling towers, it is the Tchebychev method (Perry, 2008) (Rode, 2020), this rule is suitable because it only requires to estimate the function in four points and evaluates the inverse, so it will not introduce many errors, which is an advantage compared to other methods, like trapezoidal rule. In equation 11 is presented Tchebychev approximation for a function $F(C_{iG})$ between two points.

$$Z = \int_{C_{iG,in}}^{C_{iG,out}} F(C_{iG}) \, dC_{iG} \approx \frac{C_{iG,in} - C_{iG,out}}{4} (F_1 + F_2 + F_3 + F_4) \qquad [11]$$

Where:

$$F_1 = \frac{1}{F\left(C_{iG,in} + 0{,}1(C_{iG,in} - C_{iG,out})\right)} \qquad [12]$$

$$F_2 = \frac{1}{F\left(C_{iG,in} + 0{,}4(C_{iG,in} - C_{iG,out})\right)} \quad [13]$$

$$F_3 = \frac{1}{F\left(C_{iG,out} - 0{,}4\,(C_{iG,in} - C_{iG,out})\right)} \quad [14]$$

$$F_4 = \frac{1}{F\left(C_{iG,out} - 0{,}1\,(C_{iG,in} - C_{iG,out})\right)} \quad [15]$$

3.1.2.2.Integration by Wolfram Alpha®

Wolfram Alpha® is a computational knowledge engine created by Wolfram Research, it consists of a massive store of expert-level knowledge and algorithms to response questions automatically. This language can calculate definite integrals of one or more variables and do a graphic representation of the solution, provided that a fitting function is available for the curve to be integrated (Wolfram Research, 2020).

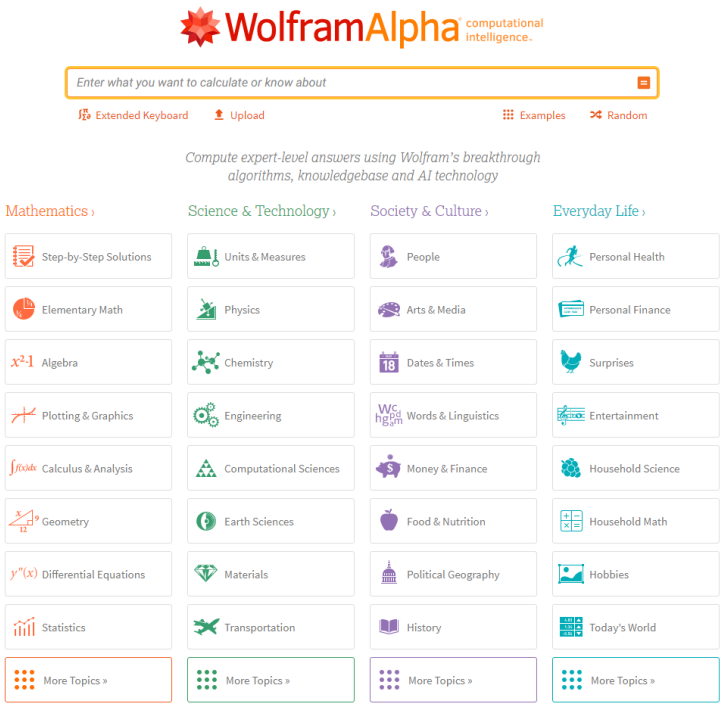

Figure 19. Screenshot of Wolfram Alpha®

Furthermore, this language can be applied to a varied areas of knowledge such as physics, chemistry, engineering, money and finance, etc. In addition, the syntax is very easy and intuitive, for example, for the definite integral of function f(x) between x=a and x=b it would be as follows: *integrate f(x) from x=a and x=b*.

To finish, it is important that the integration of the fitting functions was performed analytically, however the results precision depends on the precision of the polynomial fitting.

3.1.3. Design of a contactor by HUT_{OG} method

On the one hand, it can be defined the local height of a unit transfer of a contactor taking as reference the gas phase (HUT_{OG}) by the following equation, for a certain axial coordinate of the contactor (Rode, 2020):

$$\mathrm{HUT_{OG}} = \frac{\mathrm{u_G}}{\mathrm{K_{AG}\, a_{LG}}} \qquad [16]$$

In case that K_{AG} does not depend on the superficial velocity, Equation 16 can be expressed also as the product of A and HUT_{OG}:

$$\mathrm{A \cdot HUT_{OG}} = \frac{\dot{\mathrm{V}}_\mathrm{G}}{\mathrm{K_{AG}\, a_{LG}}} \qquad [17]$$

For the membrane contactor the interfacial area, a_{LG}, is constant, as it has been stated previously, however for the packed column is variable.

On the other hand, other important parameters are HET, which is defined as the height of a theoretical stage, and NET, the number of theoretical stages. If Z is the total length of the contactor, HET is given by the following expression:

$$\mathrm{HET} = \frac{\mathrm{Z}}{\mathrm{NET}} \qquad [18]$$

To simplify the calculation of Z and V of the contactors can be used the Colburn's relation, which is applied to linear equilibrium and operating curves, it gives a relationship between HET and HUT_{OG} (Rode, 2019).

$$\frac{\mathrm{NUT_{OG}}}{\mathrm{NET}} = \frac{\mathrm{HET}}{\mathrm{HUT_{OG}}} = \frac{\ln \lambda_\mathrm{i}}{\lambda_\mathrm{i} - 1} \qquad [19]$$

Where λ_i is the extraction ratio and it is defined in equation 20, for a certain local axial coordinate of the contactor and for a component i:

$$\lambda_\mathrm{i} = \frac{\dot{\mathrm{V}}_\mathrm{G}}{\dot{\mathrm{V}}_\mathrm{L}\, \mathrm{m_i}} \qquad [20]$$

Nevertheless, in this case the curves are not linear, thus in order to check if the mentioned condition is achieved along the axial coordinate, it is going to be defined the average λ_i along the contactor:

$$\bar{\lambda} = \frac{1}{\mathrm{N}} \sum_{\mathrm{n=1}}^{\mathrm{N}} \lambda_n \qquad [21]$$

Therefore, if $0{,}8 < \bar{\lambda} < 1{,}25$, equation 19 can be simplified (Rode, 2019) and the assumption of equation 22 can be made. This situation usually is reached in systems with a very high capture of CO_2 within typical industrial conditions, as the case studied.

$$\mathrm{HET} \cong \mathrm{HUT_{OG}} \rightarrow \mathrm{Z} \cong \mathrm{HUT_{OG}} \cdot \mathrm{NET} \qquad [22]$$

Consequently, it is admitted implementing a discrete sum of every transfer unit in order to calculate Z and V, for the packed column and the membrane, respectively. Nonetheless, it is important to remark that it is the sum of average $\mathrm{HUT_{OG}}$ of every transfer unit, which is equivalent to the following expressions for Z and V:

$$\mathrm{Z} = \frac{\mathrm{HUT_{OG_1}}}{2} + \sum_{k=2}^{10} \mathrm{HUT_{OG_k}} + \frac{\mathrm{HUT_{OG_{11}}}}{2} \qquad [23]$$

$$\mathrm{V} = \frac{\mathrm{A} \cdot \mathrm{HUT_{OG_1}}}{2} + \sum_{k=2}^{10} \left(\mathrm{A} \cdot \mathrm{HUT_{OG_k}}\right) + \frac{\mathrm{A} \cdot \mathrm{HUT_{OG_{11}}}}{2} \qquad [24]$$

3.1.4. Calculation of the axial coordinate

In order to represent properties along the column as a function of the axial coordinate without knowing previously the value of the length, it is defined the normalized axial coordinate, z*, as following:

$$\mathrm{z^*} = \frac{\mathrm{z}}{\mathrm{Z}} \rightarrow \mathrm{dz} = \mathrm{Z} \cdot \mathrm{dz^*} \qquad [25]$$

If we consider axial coordinate as a set of discrete values, it is obtained the following equation in order to compute z*, depending on whether it known the length (equation 26) or the volume of the contactor (equation 27).

$$\mathrm{z_k}^* = \mathrm{z_{k-1}}^* + \frac{\overline{\mathrm{HUT}}_{\mathrm{OG_{k,k-1}}}}{\mathrm{Z}} \qquad [26]$$

$$\mathrm{z_k}^* = \mathrm{z_{k-1}}^* + \frac{\mathrm{A} \cdot \overline{\mathrm{HUT}}_{\mathrm{OG_{k,k-1}}}}{\mathrm{V}} \qquad [27]$$

Where $\mathrm{z_0}^* = 0$ and:

$$\overline{\mathrm{HUT}}_{\mathrm{OG_{k,k-1}}} = \frac{\mathrm{HUT_{OG_k}} + \mathrm{HUT_{OG_{k-1}}}}{2} \qquad [28]$$

$$\mathrm{A} \cdot \overline{\mathrm{HUT}}_{\mathrm{OG_{k,k-1}}} = \frac{\mathrm{A} \cdot \mathrm{HUT_{OG_k}} + \mathrm{A} \cdot \mathrm{HUT_{OG_{k-1}}}}{2} \qquad [29]$$

In Figure 20 is presented a scheme of the mentioned calculation.

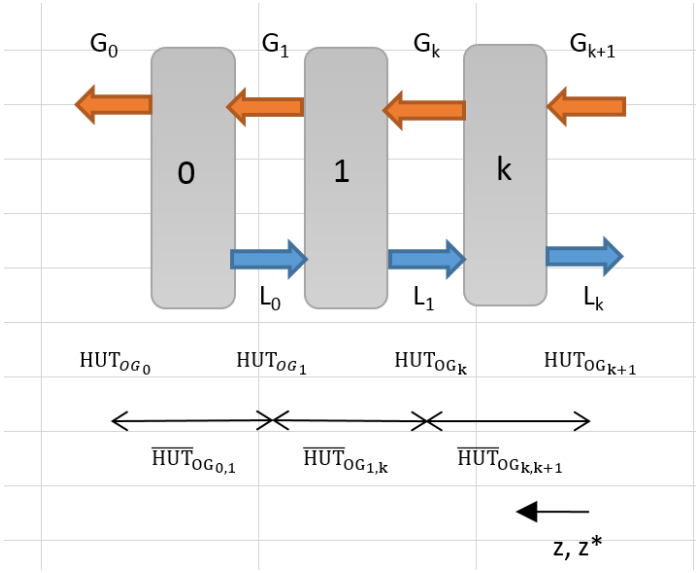

Figure 20. Scheme of the axial coordinate calculation

3.2.Model features

It was supposed a one-dimensional model, since it is not essential to simulate a two-dimensional model: a 1-D adiabatic model works with a suitable precision in order to simulate membrane contactors in industrial conditions, according to Albarracin *et al*. (2016).

Consequently, it was applied a steady-state adiabatic (i.e. no heat losses) one dimensional model to simulate the absorption the carbon dioxide in methanol.

In Table 7, it is detailed the model assumptions, depending on the contactor, in order to perform the simulation and the calculations.

Table 7. Model features

Domain	**Technology**	**Feature**
Fluids	Packed contactor and hollow fiber membrane contactor	- Gas phase consists of a mixture of CO_2 and H_2 - Liquid phase contains methanol and traces of CO_2
Thermal conditions	Packed contactor and hollow fiber membrane contactor	- Gas-liquid flow is not isothermal.
Flow conditions	Packed contactor	- Counter-current operation - Steady state in both phases
	Hollow fiber membrane contactor	- Counter-current operation - Steady state in both phases - 1-D model - Plug flow with axial dispersion negligible

Table 8. Model feature (cont.)

Domain	Technology	Feature
Transfer phenomena	Packed contactor and hollow fiber membrane contactor	- Adiabatic model - The influence of pressure drop in mass transfer is negligible.
Thermodynamics	Packed contactor and hollow fiber membrane contactor	- Ideal gas

3.3. Packed contactor technology

3.3.1. Geometrical parameters

In Table 8 is presented the geometrical parameters of the packed contactor. It has been selected a common industrial packing, metal Pall rings.

Table 9. Geometrical parameters of the packed contactor

Packed column (Metal Pall rings)[1]	Information	Units
Specific area of the packing, a	205	m^{-1}
Packing factor, F_p	183	-
Packing nominal diameter, d_{nom}	0,0254	m

[1] Rode (2019)

3.3.2. Fluid dynamics

It is essential to identify the fluid dynamics of a packed contactor since flooding depends on it. Indeed, fluid dynamics is a function of the geometry of the packing, the physical-chemical characteristics of the fluid and the molar flows (Rode, 2019).

For the hollow fiber membrane contactor, it is not necessary to make this fluid dynamics analysis since there are not restrictions in relation to flooding, so we have an additional degree of freedom given by the geometry of the membrane.

However, in the case of the packed contactor, to analyze the fluid dynamics is essential in order to forecast flooding. There are some parameters which help to predict it, such as the flow factor (F_{LG}) and the dimensionless capacity (Y). According to Rode (2019), Y can be interpreted as Froude number squared corrected by a viscosity term.

$$F_{LG} = \frac{\dot{V}_L}{\dot{V}_G}\sqrt{\frac{\rho_G}{\rho_L}} \qquad [30]$$

$$Y = \left(\frac{\dot{V}_G}{A}\right)^2 \frac{\rho_G}{\rho_L}\frac{F_P}{g}\left(\frac{\mu_L}{\mu_{water,20degC}}\right)^{0,2} \qquad [31]$$

Where, $\mu_{water,20degC}$ is the viscosity of water at 20 degC and F_p is tabulated depending on the packing (see annex 8.1). It is necessary to remark that F_{LG} is not only defined for packed contactor, it can be applied also to the hollow fiber membrane contactor.

Moreover, dimensionless capacity at which flooding happens (Y_{flood}) is given by the following expression:

$$Y_{flood} = \exp\left(0{,}1117 - 4{,}012\ {F_{LG}}^{0,25}\right) \qquad [32]$$

Now, it is possible to determine the limiting area at which flooding occurs, rearranging Equation 31:

$$\frac{A_{flood}}{{F_P}^{0,5}} = \left[\dot{V}_G{}^2\ \frac{\rho_G}{\rho_L}\ \frac{1}{g}\ \frac{1}{Y_{flood}}\ \left(\frac{\mu_L}{\mu_{water,20degC}}\right)^{0,2}\right]^{0,5} \qquad [33]$$

A very common criterion in order to design a packed contactor is to take the inlet gas velocity as 70% of the flooding velocity in the critical section, which equivalent to choose 142,86% of flooding section, A_{flood}, which corresponds to the lowest value of flooding velocity along the 10 stages (the most constraining value).

$$u_{flood} = 70\% \cdot\ u_{G,in} \rightarrow \frac{\dot{V}_{G,in}}{A_{flood}} = 70\% \left(\frac{\dot{V}_{G,in}}{A}\right) \rightarrow A = 142{,}86\% \cdot A_{flood} \qquad [34]$$

3.3.3. Global mass transfer in the packed contactor

In order to integrate of the mass balance and to calculate the height of a transfer unit, it is essential to estimate the global mass transfer coefficient, which depends on the mass transfer in each phase. Even though, the equations which allow to calculate the mass transfer in the packed contactor have a complicated form and are full of inaccuracy (±20%) (Rode, 2019), they are the simplest way to estimate the mass transfer in the contactor.

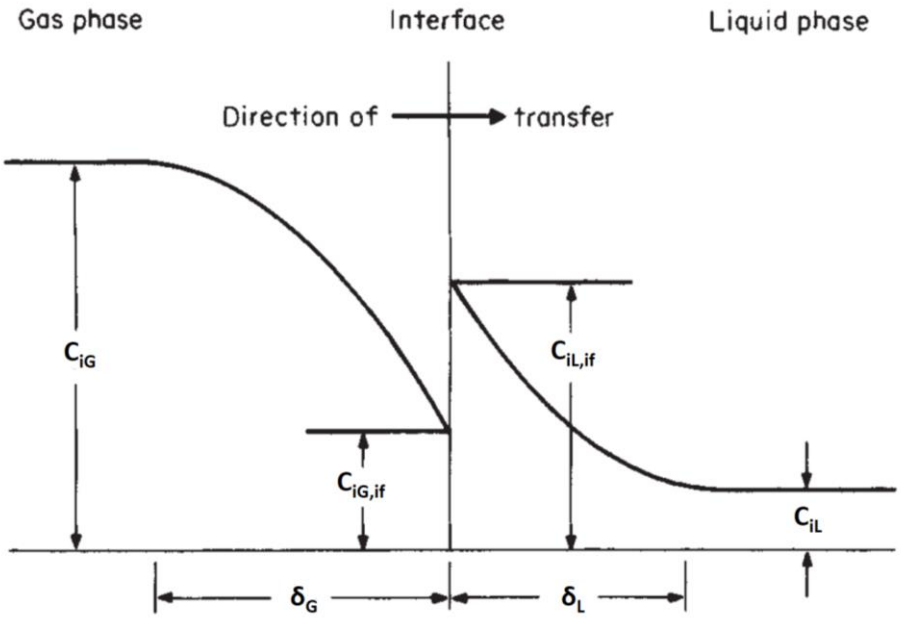

Figure 21. Concentration gradients near a gas-liquid interface.

First, from the mass conservation law in a steady state system, it is obtained Equation 35 (Henley and Seader, 2000) (Perry, 2008), valid only if the section is not varying.

$$N_i = N_{i,G} = k_{iG}\left(C_{iG} - C_{iG,if}\right) = N_{i,L} = k_{iL}\left(C_{iL,if} - C_{iL}\right) \qquad [35]$$

Secondly, N_i also can be defined as a function of global mass transfer coefficients:

$$N_i = K_{iG}(C_{iG} - {C_{iG}}^{eq}) = K_{iL}({C_{iL}}^{eq} - C_{iL}) \qquad [36]$$

These equations can be rearranged to obtain the following formulas:

$$\frac{1}{N_i} = \frac{1}{N_{i,G}} \rightarrow \frac{1}{K_{iG}\left(C_{iG} - {C_{iG}}^{eq}\right)} = \frac{1}{k_{iG}\left(C_{iG} - C_{iG,if}\right)} \rightarrow \frac{1}{K_{iG}} = \frac{1}{k_{iG}}\left(\frac{C_{iG} - {C_{iG}}^{eq}}{C_{iG} - C_{iG,if}}\right)$$
$$= \frac{1}{k_{iG}}\left[\frac{\left(C_{iG} - C_{iG,if}\right) + \left(C_{iG,if} - {C_{iG}}^{eq}\right)}{C_{iG} - C_{iG,if}}\right] = \frac{1}{k_{iG}} + \frac{1}{k_{iG}}\left(\frac{C_{iG} - {C_{iG}}^{eq}}{C_{iG} - C_{iG,if}}\right)$$

Now, using the ratio between k_{iG} and k_{iL} given by Equation 37:

$$\frac{1}{K_{iG}} = \frac{1}{k_{iG}} + \frac{1}{k_{iL}}\left(\frac{C_{iG,if} - {C_{iG}}^{eq}}{C_{iL,if} - C_{iL}}\right) \qquad [37]$$

In order to express the global mass transfer coefficient, it is obtained the well-known expression in terms of individual mass transfer coefficients of Equation 38.

$$\frac{1}{K_{iG}} = \frac{1}{k_{iG}} + \frac{1}{m_i\, k_{iL}} \qquad [38]$$

However, it is easier to interpret Equation 38 if we express every term as resistance to mass transfer, in order words, the inverse of the mass transfer coefficient. Assuming that global mass transfer coefficient in the gas phase as sum of the mass transfer resistances, it is obtained the following equation:

$$R_{iG,ov} = R_{iG} + R_{iL} \qquad [39]$$

3.3.4. Mass transfer in the liquid phase

On the one hand, mass transfer coefficient in the liquid phase is calculated by the well-known correlation presented in Equation 40 (Wang *et al.*, 2005) (Rode, 2019).

$$k_{iL}\left(\frac{\rho_L}{\mu_L\, g}\right)^{1/3} = 0{,}0051\left(\frac{\rho_L\, u_L}{a_{LG}\, \mu_L}\right)^{2/3}\left(\frac{\mu_L}{D_{iL}\, \rho_L}\right)^{-1/2}(a\, d_{nom})^{0{,}4} \qquad [40]$$

Where gas-liquid specific area, a_{LG}, is computed with equation 41, which depends on some dimensionless numbers like Reynolds (Re), Froude (Fr) and Webber (We).

$$a_{LG} = 1 - \exp\left[-1{,}45\left(\frac{\sigma_c}{\sigma}\right)^{0{,}75} {Re_L}^{0{,}1}\, {Fr_L}^{-0{,}05}\, {We_L}^{0{,}2}\right] \qquad [41]$$

$$Re_L = \frac{\rho_L\, u_L}{a\, \mu_L}; \qquad Fr_L = \frac{{u_L}^2\, a}{g}; \qquad We_L = \frac{\rho_L\, {u_L}^2}{a\, \sigma} \qquad [42\ ]$$

Therefore, the gas-liquid specific area is variable along the packed contactor since it depends on the velocity of the liquid and other properties.

Finally, as reported by Rode (2019) $\sigma/\sigma_c \approx 1$, because the material is generally contaminated and becomes wettable.

3.3.5. Mass transfer in the gas phase

On the other hand, mass transfer coefficient in the gas phase is calculated with the following correlation (Wang *et al.*, 2005) (Rode, 2019).

$$\frac{k_{iG}}{a\, D_{iG}} = 5.23\left(\frac{\rho_G\, u_G}{a\, \mu_G}\right)^{0{,}7}\left(\frac{\mu_G}{D_{iG}\, \rho_G}\right)^{1/3}(a\, d_{nom})^{-2} \qquad [43]$$

Equation 43 is multiplied by 5.23 due to the selected packing, metal Pall rings (Rode, 2019).

3.4. Hollow fiber membrane contactor technology

3.4.1. Geometrical parameters

Concerning the less known contactor, the hollow fiber membrane (HFMC), it involves a bundle of composite cylindrical hollow fibers. They can be porous, which are adequate when using non-aqueous physical solvents or they can contain a dense layer covered by a hydrophobic microporous support, which is more suitable for physical solvents in order to prevent flooding (Belaissaoui and Favre, 2018). The structure of the HFMC with a dense layer can be observed in Figure 22.

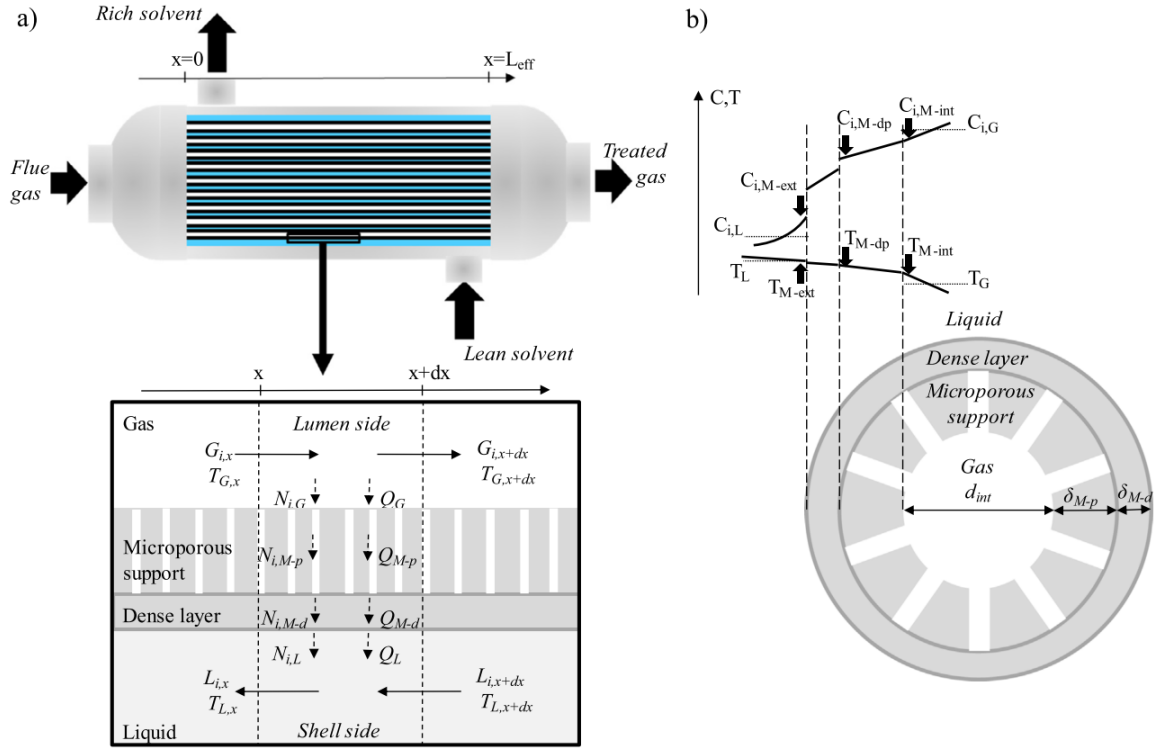

Figure 22. Representation of the hollow fiber membrane contactor (HFMC) used for absorption of CO2 in methanol (Villeneuve et al., 2018a)

Moreover, in the following table it is presented the hollow fiber membrane parameters related to geometry, for the baseline case, simulation 1. For HFMC, a commercial composite non-selective membrane (Oxyplus®) with dense polymethylpentene (PMP) skin and with polypropylene (PP) as support material was selected, therefore with this membrane flooding should not be an issue.

Table 10. Baseline geometrical parameters of simulations

HFMC (Nonselective membrane)[1]	Information	Units
Dense layer material	PMP (Oxyplus®)	-
Dense layer thickness, $\delta_{MC\text{-}d}$	1,00E-07	m
Microporous support material	PP (Oxyplus®)	-
Microporous mass transfer coefficient, $k_{CO2,\ M\text{-}p,\ 21deg}$	5,50E-4	m s^{-1}
External fiber diameter, $d_{MC\text{-}ext}$	3,80E-04	m
Microporous support thickness, $\delta_{MC\text{-}p}$	9,00E-05	m
Internal microporous support diameter, d_{int}	2,00E-04	m
Relative membrane thickness (RMT), δ_{MC}/ $r_{MC\text{-}ext}$	0,47	-
Specific interfacial area respect with the external fiber, a_{LG}	6311	m^{-1}
Packing factor, φ	0,60	-
Activation energy of the membrane, $E_{a,i}$	15,2	kJ $mole^{-1}$
Permeation activation energy of component i in the membrane, $P_{i,0}$	332 621	barrer

[1] Villeneuve *et al.* (2018a).

From geometrical data inputs from Table 9, some important geometrical parameters can be derived, they are presented in Table 10.

Table 11. Important geometrical features of the hollow fiber bundle (Rode et al., 2012)

	Equation		
Parameter	**External**	**Internal**	**Units**
Specific flow section	$\varepsilon_{ext} = 1 - \varphi$	$\varepsilon_{int} = \varphi\left(1 - \frac{\delta_{MC-p} + \delta_{MC-d}}{r_{MC-ext}}\right)$	-
Logarithmic fiber diameter	$d_{MC-lm-d} = \frac{\delta_{MC-d}}{\ln\left(\frac{d_{MC-int} + \delta_{MC-p} + \delta_{MC-d}}{d_{MC-int} + \delta_{MC-p}}\right)}$	$d_{MC-lm-p} = \frac{\delta_{MC-p}}{\ln\left(\frac{d_{MC-int} + \delta_{MC-p}}{d_{MC-int}}\right)}$	m
Relative membrane thickness (RMT)	$RMT = \frac{\delta_{MC}}{r_{MC-ext}} = \frac{2\,\delta_{MC}}{d_{MC-ext}} = \frac{2\,(\delta_{MC-p} + \delta_{MC-d})}{d_{MC-ext}}$		m
Hydraulic diameter	$d_{h,ext} = d_{MC-ext}\left(\frac{1-\varphi}{\varphi}\right)$	$d_{h,int} = d_{MC-int}$	m
Specific interfacial area	$a_{LG,ext} = \frac{2\varphi}{r_{MC-ext}}$	$a_{LG,int} = \frac{2\varphi\left(1 - \frac{\delta_{MC}}{r_{MC-ext}}\right)}{r_{MC-ext}}$	m^{-1}

Finally, it should be noted that the external parameters are those which are involved with calculations respect the liquid phase, since liquid it flows out of the fibers, and internal parameters are those which are related with the gas phase, since gas flows inside the fibers.

3.4.2. Global mass transfer in the membrane

Mass conservation law states that in a steady state process there is an equality of molar fluxes for the system considered (Villeneuve *et al*., 2018a), as it is stated in equation 44.

$$N_{i,G}\, d_{int} = N_{i,MC-p}\, d_{MC-lm-p} = N_{i,MC-d}\, d_{MC-lm-d} = N_{i,L}\, d_{ext} \qquad [44]$$

Where:

$$N_{i,G} = k_{iG}\left(C_{iG} - C_{i,MC-int}\right) \qquad [45]$$

$$N_{i,MC-p} = k_{i,MC-p}\left(C_{i,MC-int} - C_{i,MC-dp}\right) \qquad [46]$$

$$N_{i,MC-d} = k_{i,MC-d}\left(C_{i,MC-dp} - C_{i,MC-ext}\right) \qquad [47]$$

$$N_{i,L} = k_{iL}\left(m_i\, C_{i,MC-ext} - C_{iL}\right) \qquad [48]$$

Thus, molar flow of specie i can be expressed as follows:

$$N_i = K_{iG}\left(C_{iG} - \frac{C_{iL}}{m_i}\right) \qquad [49]$$

Where K_{iG} is the global mass transfer coefficient respect to the gas phase, expressed in cylindrical geometry:

$$\frac{1}{K_{iG}} = \frac{d_{MC-ext}}{d_{MC-lm-p}} \cdot \frac{1}{k_{i,MC-p}} + \frac{d_{MC-ext}}{d_{MC-lm-d}} \cdot \frac{1}{k_{i,MC-d}} + \frac{d_{MC-ext}}{d_{MC-int}} \cdot \frac{1}{k_{iG}} + \frac{1}{m_i\, k_{iL}} \qquad [50]$$

It is easier to express every term of Equation 50 as a resistance to mass transfer, in order words, the inverse of the mass transfer coefficient, as it has been done for the mass transfer coefficients in the packed contactor. Thus, assuming that global mass transfer coefficient in the gas phase as sum of the mass transfer resistances in the microporous support, the dense layer, the gas phase and in the liquid phase (Villeneuve *et al*., 2018a), it is obtained the following equation:

$$R_{iG,ov} = R_{i,MC-p} + R_{i,MC-d} + R_{iG} + R_{iL} \qquad [51]$$

3.4.3. Liquid side and gas side mass transfer

In both phases it is going to admit a laminar flow and a fully developed profile of CO_2 concentration, so the Sherwood number (Sh) is considered as 3.66 (Villeneuve *et al*., 2018a). The stated non dimensional number is defined by the following equation:

$$Sh_{ij} = \frac{k_{ij}\, d_h}{D_{ij}} \qquad [52]$$

Therefore, the mass transfer coefficient of the component i can be deduced from Equation 52 as follows for the liquid and gas phase:

$$k_{iL} = \frac{Sh_{iL}\, D_{iL}}{d_{h,ext}}; \qquad k_{iG} = \frac{Sh_{iG}\, D_{iG}}{d_{h,int}} \qquad [53]$$

Where, diffusion coefficients, D_{iL} and D_{iG}, are computed with correlations mentioned the following points.

3.4.4. Dense layer mass transfer

According to Villeneuve *et al*. (2018a), permeability of component i in the dense layer is expressed as Equation 54:

$$P_i = P_{i,0} \exp\left(\frac{-E_{a,i}}{R\, T}\right) \qquad [54]$$

Where, $P_{i,0}$ and $E_{a,i}$ depend on the type of membrane and the specie i.. Hence, the mass transfer coefficient of component i in the dense layer is expressed in equation 55 (Villeneuve *et al*., 2018a).

$$k_{i,MC-d} = P_i \left(\frac{RT}{\delta_{MC-d}}\right) \qquad [55]$$

3.4.5. Microporous support mass transfer

Mass transfer coefficient for a specie i in the microporous support $k_{i,MC\text{-}p}$ is a function of the porosity of the membrane ε, its tortuosity τ, the thickness of the microporous support $\delta_{MC\text{-}p}$ and the diffusion coefficient of i in the gas phase D_{iG} (equation 56) (Villeneuve *et al*., 2018a).

$$k_{i,MC-p} = \frac{\varepsilon\, D_{iG}}{\tau\ \delta_{MC-p}} \qquad [56]$$

However, for the same support ε, τ and $\delta_{M\text{-}p}$ are constant and $k_{i,M-p}$ only is a function of D_{iG}, which only depends on the specie i. Therefore, this mass transfer coefficient can be expressed as a function of the mass transfer coefficient and the diffusion coefficient of a reference, in this case CO_2 at 21 degC (Villeneuve *et al*., 2018a).

$$k_{i,MC-p} = k_{CO2,MC-p,21degC} \left(\frac{D_{iG}}{D_{CO2,G,21degC}}\right) \qquad [57]$$

$k_{CO2,MC-p,21degC}$ is given at Villeneuve *et al*. (2018a) and $D_{CO2,G,21degC}$ was calculated with the correlation of diffusion in the gas phase of equation 58.

3.5. Correlations of transport properties

In this section will be presented the correlations used in order to compute the transport properties since they are required in order to calculate the mass transfer coefficients in both contactors. All the correlations were validated with Aspen by Nanyonjo (2020) for the operating conditions of pressure and temperature and for the range of concentration of CO_2 of this report.

3.5.1. Diffusion coefficient in the gas phase

Initially, it is defined the diffusion coefficient of a component i on the gas phase, it has been applied the Fuller-Schettler-Giddings' (FSG) correlation for a binary diffusion, for components A and B the equation is the following (Fuller *et al.*, 1966) (Poling *et al.*, 2006).

$$D_{AB} = \frac{0{,}001T^{1.75}\left(\frac{1}{M_{mol-A}} + \frac{1}{M_{mol-B}}\right)^{0.5}}{P\left[v_A^{\frac{1}{3}} + v_B^{\frac{1}{3}}\right]^2} \qquad [58]$$

In our particular case, A: CO_2, B: H_2 and P must be introduced in atm.

Table 12. Parameters used in FSG correlation

Parameter	CO_2	H_2	Units
v_i	26,9	7,07	$cm^3\ mole^{-1}$
M_{mol-i}	44,0098	2,0159	$g\ mole^{-1}$

Despite this correlation of diffusion coefficient in the gas phase is for low pressures (<10 bar), it can be checked that it works with a suitable precision compared with experimental data at high pressures and in the temperature range along the contactor.

3.5.2. Diffusion coefficient in the liquid phase.

In the case of the diffusion coefficient of specie A, in our case CO_2, in a solvent B, methanol, Wilke-Chang correlation for a binary diffusion has been used, which is presented in equation 59 (Wilke and Chang., 1955) (Poling *et al.*, 2006).

$$\frac{D_{AB}\,\mu_B}{T} = 7.410^{-8}\frac{(\phi_B \cdot M_{mol-B})^{0.5}}{V^{0.6}{}_{mol-A(eb)}} \qquad [59]$$

$$V_{mol-A(eb)} = \frac{M_{mol-A}}{\rho_{A,eb}} \qquad [60]$$

In the following table is exposed the parameters used in order to calculate the diffusion coefficient in the liquid phase, for carbon dioxide and methanol.

Table 13. Parameters for CO_2 and methanol

CO_2 Parameters		
Parameter	**Value**	**Units**
$M_{\_CO2}$	44,01	g mole^{-1}
$\rho_{CO2\_éb}$	1178,40	kg m^{-3}
$V_{CO2\_éb}$	37,35	cm^3 mole^{-1}

Methanol parameters		
Parameter	**Value**	**Units**
$M_{\_MeOH}$	32,04	g mole^{-1}
φ_B	1,90	dimensionless

3.5.3. Surface tension

It is essential to calculate the surface tension at the liquid inlet because it is not included in the simulation results, there is no experimental data either, so it must be estimated by Aspen HYSYS®.

Thus, this transport property has been simulated using CPA property package and, according to Aspen Properties® Help, it was computed by the Hakim-Steinberg-Stiel submodel for pure component surface tension (Hakim *et al.*, 1971), that expression is presented in equation 61.

$$\sigma_j = 4{,}60104 \cdot 10^{-7} P_{crit,j}^{\frac{2}{3}} T_{crit,j}^{\frac{1}{3}} Q_{pj} \left(\frac{1 - T_{red,j}}{0{,}4}\right)^{m_j} \qquad [61]$$

Where:

$$Q_{pj} = 0{,}1574 + 0{,}359\omega_j - 1{,}769X_j - 13{,}69X_j^{\,2} - 0{,}510\omega_j^{\,2} + 1{,}29\omega_j X_j \qquad [62]$$

$$m_j = 1{,}210 + 0{,}5385\omega_j - 14{,}61X_j - 32{,}07X_j^{\,2} - 1{,}656\omega_j^{\,2} + 22{,}03\omega_j X_j \qquad [63]$$

$$T_{red,j} = \frac{T_j}{T_{crit,j}} \qquad [64]$$

Where, parameter X_j is the Stiel polar factor, its value is 0 by default.

Lastly, it is observed that the calculation of the surface tension for other conditions would be difficult as in the case of the partition coefficient, also it has been decided to use an extrapolation curve.

3.6. Partition coefficient

As it has been stated previously, partition coefficient is function of concentration in gas and liquid phase and the temperature, also it appears in the global mass transfer calculation. The value of this parameter is given by the simulations in Aspen HYSYS® for every equilibrium stage, but it is unknown for the liquid input stream. The reason is that, thermodynamically for the liquid input, it would represent the ratio of concentrations in the liquid phase and gas phase, but the concentration of CO_2 in the gas phase which would be in equilibrium with a known concentration of CO_2 in the liquid inlet, so in this case the concentration in the gas phase which would go out from stage 0, thus it would be hypothetic.

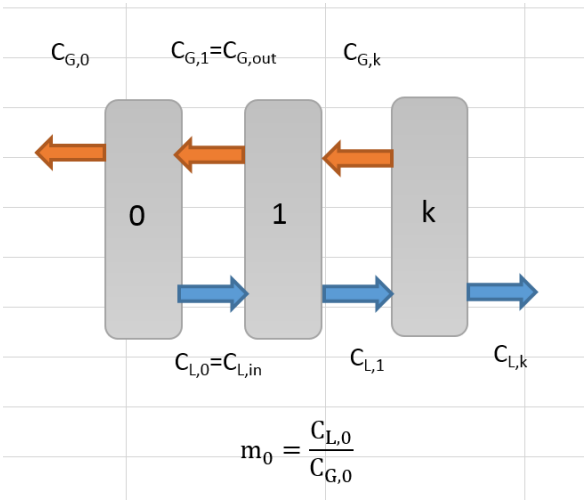

Figure 23. Scheme of the partition coefficient in stage 0

In order to calculate this coefficient, it has been simulated a ternary equilibrium in a flash drum with the software Aspen Plus® (Aspentech, 2020b), which provides a specific flash drum block (Figure 24).

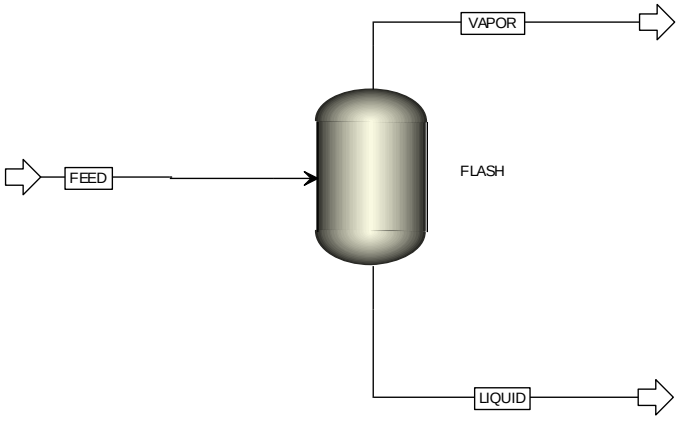

Figure 24. Flash drum simulation in Aspen Plus®

The procedure is as follows: the composition of the feed stream is changed until the liquid stream has a CO_2 fraction of 0,003 (composition of CO_2 in the liquid inlet), choosing the property package CPA in Aspen Plus®. In order to reach a CO_2 fraction of 0,003, the sensitivity analysis tool of Aspen Plus® has been used.

After that, it is obtained the CO_2 concentration in the vapour phase, so it is possible to calculate the partition coefficient.

Finally, it is important that this calculation is difficult to automatize, therefore, for a parametric analysis changing the operational conditions, an extrapolation curve will be applied.

4. STUDY OF THE PRESSURE IN THE HOLLOW FIBER MEMBRANE CONTACTOR

The design of the membrane contactor must include simultaneously the study of the mass transfer and the study of the pressure of the liquid and the gas phase along the membrane, both domains will determine the feasibility of the membrane contactor. The aim of the study of the pressure along is to have a design which leads to a good distribution of both phases in the contactor.

Indeed, as it will be shown in subsequent sections, the pressure drop in the contactor is a limiting factor in the design because it determines the flow distribution of the two phases. If the flow distribution is uniform it means that the gas and the liquid are in perfect plug flow, so maldistribution situation can be ignored (Rode *et al.*, 2012)

Moreover, the pressure drop is conditioned by the geometry of the membrane, its dimensions, the fluid flow and its properties. Therefore, it is a problem of optimization in which the geometry of the membrane and the dimensions of the contactor must be adjusted to obtain the desired pressure drop in both the gas and the liquid.

Finally, it is important to note that in the case of the packed contactor, this study was not carried out since the results in terms of mass transfer did not lead to a feasible tower design, so it is useless to perform a study of the pressure.

4.1. Pressure drop in the liquid phase

In order to calculate the pressure drop in the liquid phase per meter of contactor, it is applied a Kozeny-type equation for axial external flow of the liquid in the membrane contactor, with a Kozeny constant κ adjusted to the fiber geometry (Happel, 1959) (Rode *et al*. 2012).

$$-\frac{dP_L}{dz} = \frac{4\,\kappa\,\mu_L}{(r_{M-ext})^2}\,\frac{\varphi^2}{(1-\varphi)^3}\,u_L \qquad [65]$$

$$\kappa = 5{,}5\varphi^2 - 7{,}87\varphi + 7{,}43 \qquad [66]$$

4.2.Pressure drop in the gas phase

In the case of the axial internal flow, the gas phase, it has been used the Hagen-Poiseuille equation in order to calculate the pressure drop in the gas phase per meter, equation 67, for pipe flow (Rode *et al*. 2012), because the flow is assumed to be laminar.

$$-\frac{dP_G}{dz} = \frac{8\,\mu_G}{(r_{MC-ext} - \delta_M)^2}\,\frac{u_G}{\varepsilon_G} = \frac{8\,\mu_G}{(r_{MC-ext})^2\left(1-\frac{\delta_{MC}}{r_{MC-ext}}\right)^4\varphi}\,u_G \qquad [67]$$

Where:

$$\delta_{MC} = \delta_{MC-d} + \delta_{MC-p} \qquad [68]$$

4.3. Distribution considerations and pressure constraints

4.3.1. Pressure drop ratio

It is possible to compute the ratio of these two pressure drops directly without knowing the velocities in the liquid and in the gas phase, since, instead of velocities, it depends on the ratio of volumetric flows. That ratio is obtained dividing equation 67 and 65, it is expressed in the following expression (Rode *et al*. 2012):

$$\frac{dP_G}{dP_L} = \frac{2(1-\varphi)^3}{(5{,}5\varphi^2 - 7{,}87\varphi + 7{,}43)\varphi^3} \left(\frac{\mu_G}{\mu_L}\right) \frac{1}{\left(1 - \frac{\delta_{MC}}{r_{MC-ext}}\right)^4} \frac{\dot{V}_G}{\dot{V}_L} \qquad [69]$$

To know the value of this ratio is truly important in order to perform a preliminary analysis of the difference in terms of order of magnitude between the pressure drop in the gas and the liquid. In addition, this parameter is necessary to check if there is a similar distribution in both phases. Thus, the first constraint of this system is that this pressure drops ratio is one (in other words, the average value, since it is variable), in order to ensure the statement of similar distributions.

4.3.2. Relative pressure drop

Another significant indicator is the relative pressure drop. The inlet pressure in both phases is 40 bar in the baseline case, nevertheless in order to compare pressure drops at different inlet pressures it is defined the relative pressure drop as following, for the gas and the liquid, respectively:

$$\Delta P_{G,rel} = \frac{P_{G,in} - P_{G,out}}{P_{G,in}} \qquad \Delta P_{L,rel} = \frac{P_{L,in} - P_{L,out}}{P_{L,in}} \qquad [70]$$

This parameter is important because it must have a certain value in order to have an ideal distribution in the contactor, then it is the second restriction. Furthermore, since $P_{G,in} = P_{L,in}$, which is given usually in packed contactors, then the relative pressure drops in both phases will tend to be similar, which indicates that the pressure drop ratio will tend to one.

4.3.3. Inertial pressure drop

Regarding the design of membrane contactors, as it has been said, it is essential to have a minimum pressure drop in both phases so that there is a good distribution throughout the contactor, in other words, that minimum is a function of the inertial pressure drop.

Hence, it is required to calculate a reference pressure drop to get an idea of the minimum pressure necessary for an acceptable distribution, this minimum depends on the inertial pressure drop, which is defined with the following equation for the liquid and the gas phase, respectively:

$$\Delta P_{G,inertial} = \frac{\rho_G {v_G}^2}{2} \qquad \Delta P_{L,inertial} = \frac{\rho_L {v_L}^2}{2} \qquad [71]$$

Normally, the minimum pressure drop in the gas and the liquid phase for the contactor is around ten times the inertial pressure drop.

Consequently, there is another constraint in the system, which is that the pressure drop in both phases must be over a minimum. However, it is also necessary not to have an excessive pressure drop, since we would lose efficiency and also the operational costs that this would entail, so there is also a constraint of the maximum pressure drop.

4.3.4. Operational constraints for membrane contactor design

The overall constraints of the problem on the design of the contactor are reflected in the following table:

Table 14. Restrictions of the optimization problem

Restrictions
$\frac{\Delta P_G}{\Delta P_L} \cong 1$
$\Delta P_{G,min} \leq \Delta P_G \leq \Delta P_{G,max}$
$\Delta P_{L,min} \leq \Delta P_L \leq \Delta P_{L,max}$
$\Delta P_{G,rel} = x$
Z consistent with actual technology

Where x is a value between 0 and 1, a typical value for conventional packed contactors is 0.05 at atmospheric pressure (Villeneuve *et al.*, 2018a), but probably for HFMC is a little different, thus a research on pressure drop of commercial HFMC is required.

The final constraint of the problem is the technology available, certainly the membrane design must be consistent with dimensions of industrial membranes and scientific literature.

To conclude, in order to solve the optimization problem, the easiest way is to change geometrical parameters such as Z/A and relative membrane thickness, RMT. The objective function can be to minimize the volume of the hollow fiber membrane contactor or to increase the intensification factor.

4.3.5. Pressure profile calculation

Previously, it has been demonstrated that the length of the membrane contactor will not be known, since the volume is obtained directly. In order to obtain the pressure drop profile, it is essential to estimate the velocity profile, so cross section area A is required, but also A must be computed to calculate the length of the contactor Z and this last one is needed in order to have the pressure drop profile, consequently there is a degree of freedom in the equations, as it was commented before. Certainly, A is a constant and it is proportional to the pressure drop, so the curve shape of pressure drop will not change with A, just its magnitude.

Thus, it is observed that it is possible to make a rearrange of the terms and a change of variable of equations 65 and 67, then it is obtained the following expressions, equations 72 and 73, for the liquid and the gas, respectively.

$$\frac{A}{Z}\left(-\frac{dP_L}{dz^*}\right) = \frac{4\,\kappa\,\mu_L}{(r_{MC-ext})^2}\,\frac{\varphi^2}{(1-\varphi)^3}\,\dot{V}_L \qquad [72]$$

$$\frac{A}{Z}\left(-\frac{dP_G}{dz^*}\right) = \frac{8\,\mu_G}{(r_{MC-ext})^2\left(1-\frac{\delta_{MC}}{r_{MC-ext}}\right)^4\varphi}\,u_G \qquad [73]$$

Where z* is the normalized axial coordinate.

Now, all the values of this functions along coordinate z* are known, so it is possible to assign a fitting function and integrate it respect to z* and once we give a value of A/Z it can be obtained the pressure profile. This procedure is illustrated in the following equations for a pressure in the gas and in the liquid in a certain point along the axial coordinate of the contactor, it will be integrated locally, in order to obtain the profile, using the trapezoidal rule.

$$P_G(z_n) = P_G(z_{n-1}) + \left[\frac{1}{2}\left(\frac{A}{Z}\left(-\frac{dP_G}{dz^*}\right)\Big|_{z=z_n} + \frac{A}{Z}\left(-\frac{dP_G}{dz^*}\right)\Big|_{z=z_{n-1}}\right)\cdot(z_n - z_{n-1})\right]\cdot\left(\frac{Z}{A}\right) \qquad [72]$$

$$P_L(z_n) = P_L(z_{n+1}) + \left[\frac{1}{2}\left(\frac{A}{Z}\left(-\frac{dP_L}{dz^*}\right)\Big|_{z=z_n} + \frac{A}{Z}\left(-\frac{dP_L}{dz^*}\right)\Big|_{z=z_{n+1}}\right)\cdot(z_{n+1} - z_n)\right]\cdot\left(\frac{Z}{A}\right) \qquad [73]$$

The boundary conditions are: $P_G(z_0 = 0) = P_{G,in}$ and $P_L(z_N = Z) = P_{L,in}$, N is the number of intervals along the axial coordinate. Absolute axial coordinate z is obtained giving a value of Z/A, which implies that Z can be calculated and then $z = z^* \cdot Z$

In addition, it is important to remember that in the case of HFMC, there is not flooding restrictions, so it can be chosen the ratio Z/A in order to change the magnitude of the pressure drop, once that ratio is selected it is possible to get the Z and obtain pressure profile.

5. RESULTS AND DISCUSSION

5.1.Case study simulations

Figure 25 below shows an example of the preliminary case studies run to determine the inlet liquid molar flow for 95% of CO_2 recovery. For an absorption column within Aspen HYSYS®, the recovery could not be set as a fixed variable and hence the case study function allowed for a range of inlet liquid molar flowrates (Mckechnie, 2020).

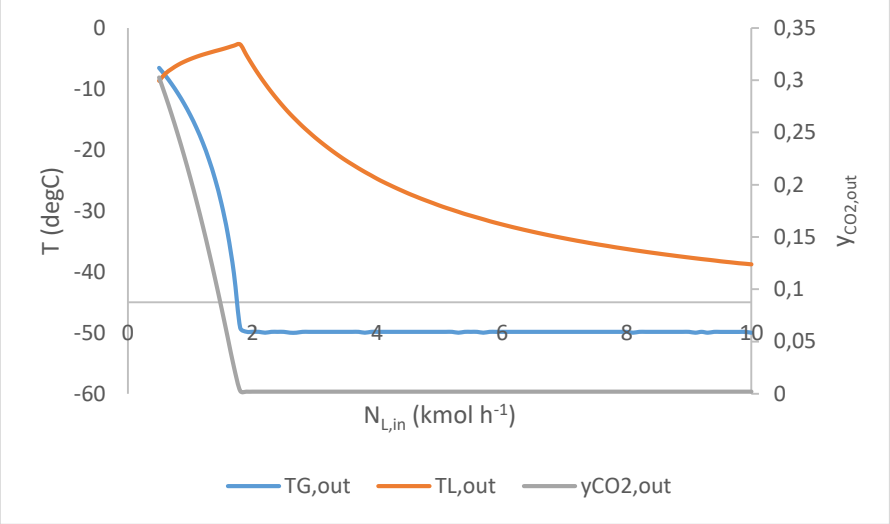

Figure 25. Variation of outlet CO_2 mole fraction, outlet temperature of gas and outlet temperature of liquid with varying inlet liquid molar flowrate (baseline case) (Mckechnie, 2020)

The change in carbon dioxide molar fraction is unsurprising as the increased liquid flow leads to reduced carbon dioxide outlet molar gas fraction as more carbon dioxide is absorbed. The trend shows a negative logarithmic curve until the molar fraction reaches approximately 0, after which increasing the liquid molar flow has no observable effect on the carbon dioxide removal from the syngas. The outlet gas temperature shows a similarly predictable curve, decreasing in a more pronounced negative logarithmic curve until the gas outlet temperature equates to the liquid inlet temperature, -50 degC. Finally, the liquid outlet temperature gradually increases until no more observable carbon dioxide is seen to be absorbed then proceeds to decrease as there is no more generation of heat from the carbon dioxide being absorbed and decreases towards the liquid inlet temperature as the entire column cools (Mckechnie, 2020).

A pinch point defines the point in the contactor which is limiting the absorption of carbon dioxide. This correlates to the warmest point within the contactor where the absorption of carbon dioxide into methanol is at its lowest. In fact, in some cases, the inlet gas temperature can be that much higher than the temperature within the contactor that there is a significant increase of temperature on the final stage that carbon dioxide can desorb.

To maximize the efficiency of the absorption process, the pinch point is ideally situated at the very bottom of the column on stage 10 and the temperature of the syngas entering should equate to the operating temperature of the final stage. This conclusion does not account for the energy expended to reduce the gas temperature before entering and the capital and operating cost of the additional heat exchanger. A separate economic evaluation would have to be undertaken to optimize and encompass surrounding process equipment for a given process (Mckechnie, 2020).

In Figure 26, it is shown two random cases (5 and 8, for example) in which the pinch point occurs at different stages of the contactor.

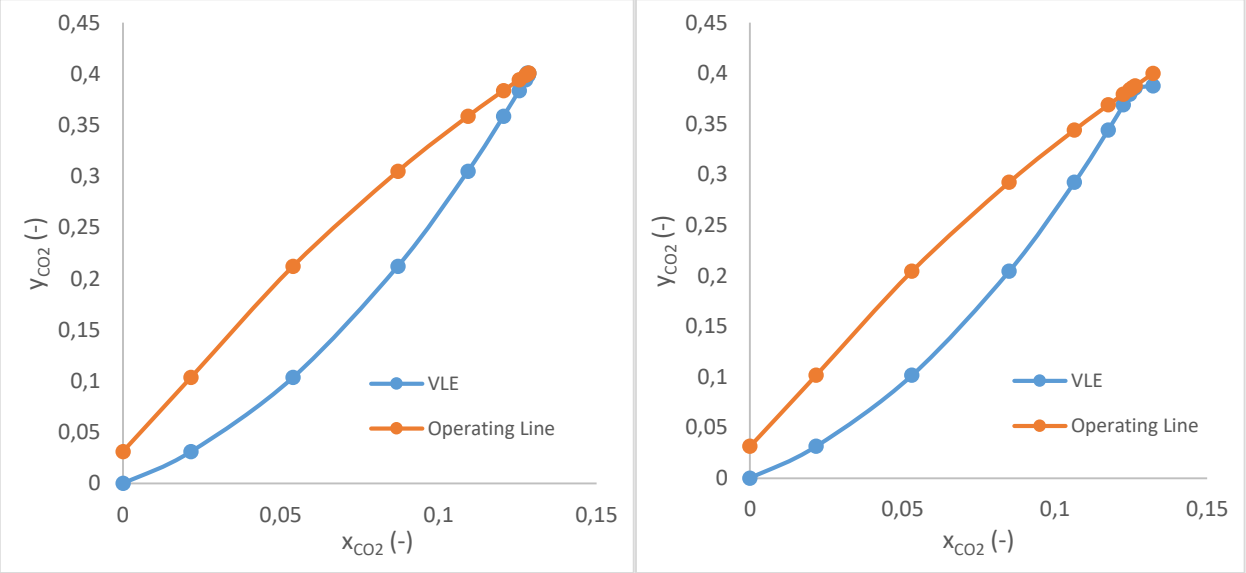

Figure 26. VLE of CO_2-methanol and operating line (for simulation 5 and 8, respectively) (Mckechnie, 2020)

5.2.Baseline case

It is important to highlight that to calculate the profiles in the baseline case, a relative membrane thickness (RMT) of 0.47 is taken. RMT influences the mass transfer coefficients of the membrane since the height of a transfer unit (HUT_{OG}) is a function of the mass transfer. As it has been mentioned, z* is a function of HUT_{OG}, consequently the profile depends on the mass transfer coefficients.

5.2.1. Axial profiles

In this section, the axial profiles (Concentration of specie i, Temperature vs z*) of baseline case are presented. In Figure 27 it can be seen how varies the concentration as a function of normalized axial coordinate z*. As it has been stated previously, z*=0 corresponds to the gas inlet and z*=1 to the liquid inlet.

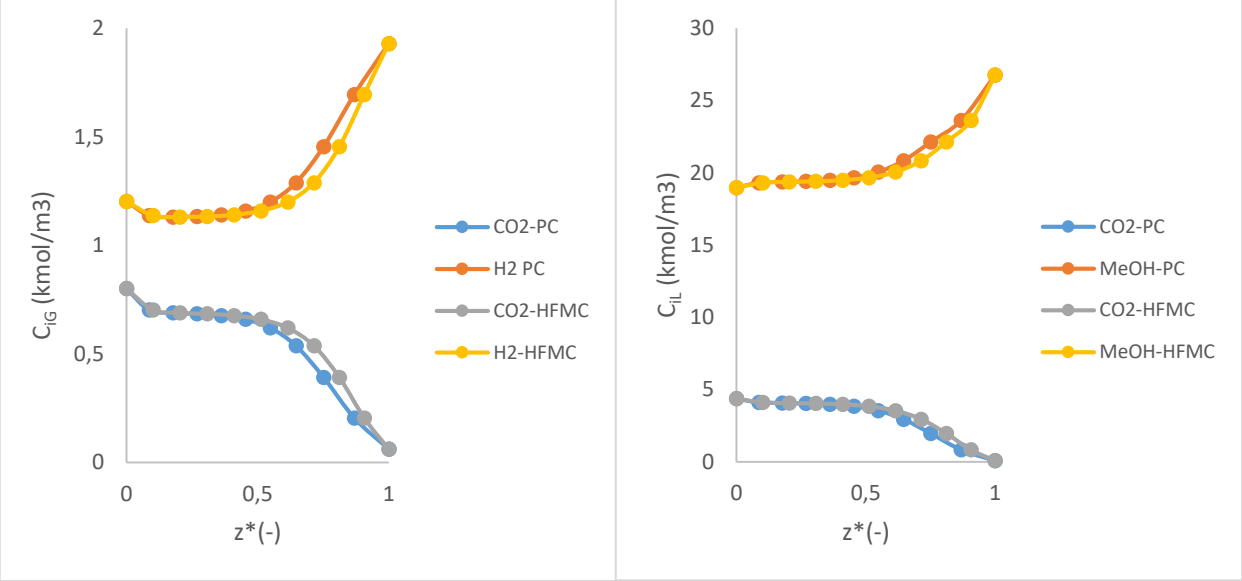

Figure 27. Concentration in the gas and in the liquid phase vs z in PC and HFMC (baseline case)*

Regarding the concentration profile, it is logic that at the gas inlet the concentration of CO_2 is maximum and after that it starts to decrease until reach a minimum at z*=1. In the case of the liquid profile of CO_2, is equivalent because at the liquid inlet it is obtained the minimum of the curve.

Concerning the temperature profile, it is confirmed the supposition of non-isothermal behaviour, since it can be observed that exists a temperature peak for both phases (Figure 28 and Figure 29).

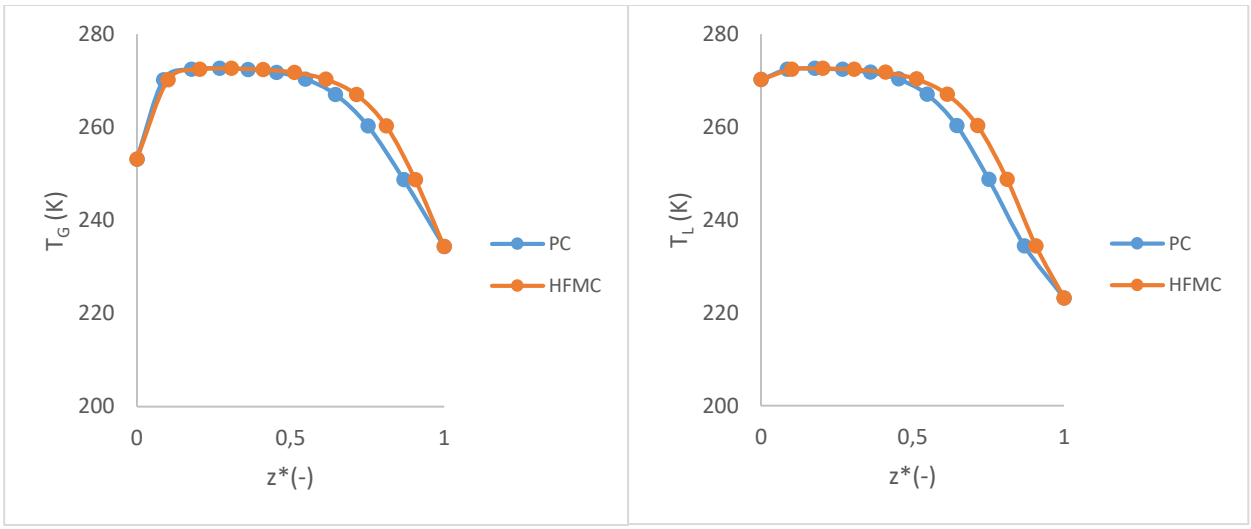

Figure 28. Temperature in the gas and in the liquid phase vs z for PC and HFMC (baseline case)*

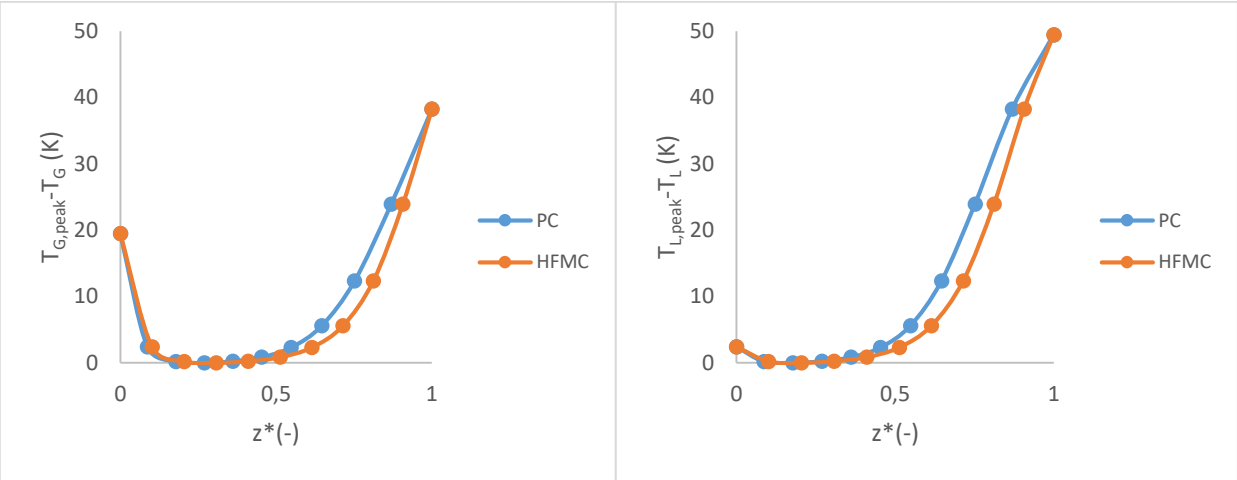

Figure 29. T-T_{peak} in the gas and in the liquid phase vs z for the PC (baseline case)*

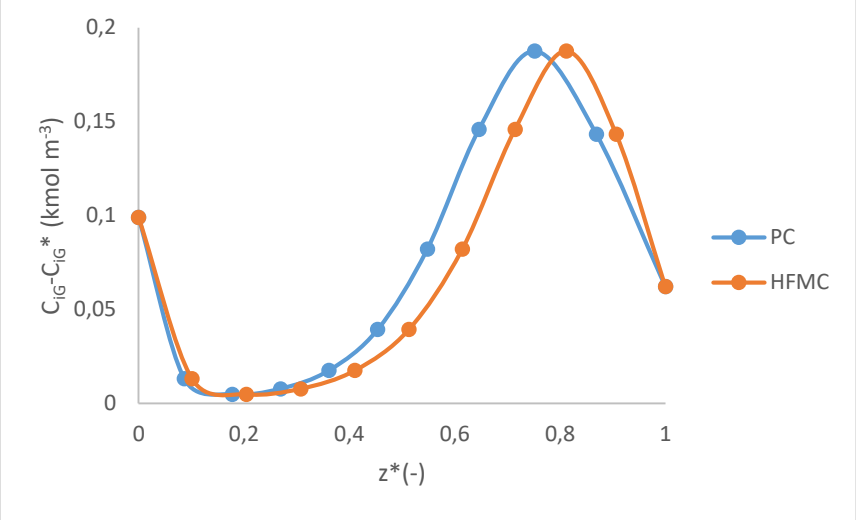

Figure 30. Driving force of mass transfer vs z for PC and HFMC (baseline case)*

In Figure 30, driving force vs z*, it can be observed the pinch point, which it is defined by the point of the contactor in the axial direction which limits the absorption of carbon dioxide in methanol. It corresponds to the warmest point of the contactor, where the driving force is minimum, therefore, the absorption is minimum.

Therefore, the perfect situation would be that the pinch point is on the gas inlet, not within the column.

Finally, the same analysis and discussion of the profiles carried out in the case of packed contactor can be performed for the case of HFMC, since the magnitude of the y coordinate does not change, only the normalized axial coordinate, since it depends on the mass transfer, which, as it has been proven, does not follow the same pattern in the two contactors.

5.2.2. Contactors volume calculation

As it was mentioned in point 3, it is necessary to integrate properly the function F in order to design a contactor. Thus, in this part it is going to show and discuss the curves of F function with the aim of decide a method of integration.

For example, in the case of the packed column, a representation function F is presented in Figure 31 for the baseline case. It is important to mention that for the membrane contactor and the rest of simulations, the curve shape will be similar, only depending on the pinch point (the maximum of the function F, which indicates the minimum driving force), so this analysis will be valid also for the HFMC.

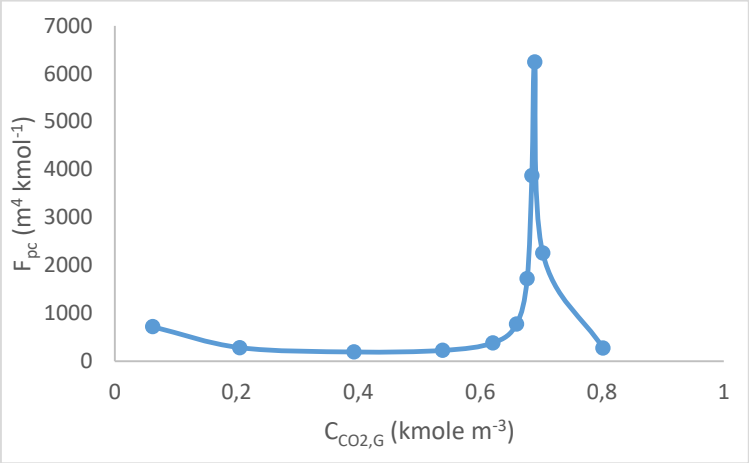

Figure 31. Graphic representation of F_{pc} vs concentration of CO_2 in the gas phase (baseline case)

In Figure 31. it should be noted that at higher concentrations it is obtained a stiff function, so it will be harder to integrate numerically, since it should be considered different fitting functions and its precision would not be appropriate. Consequently, the option selected is to evaluate the inverse of this function and integrate it by parts, the graphic illustration of this new function is in Figure 32.

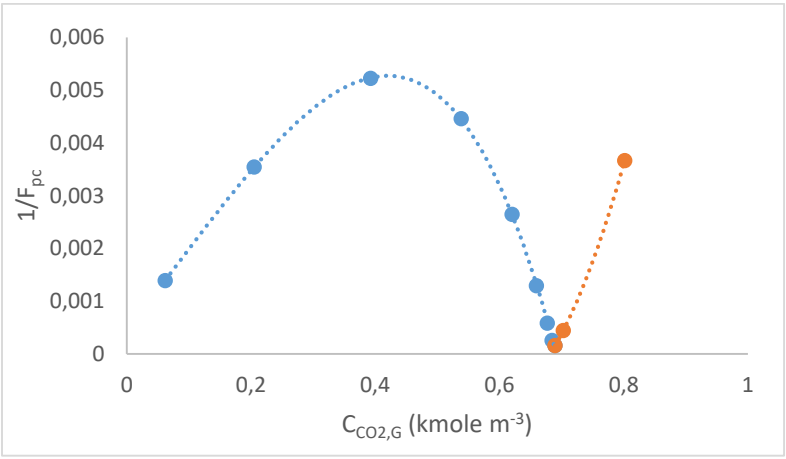

Figure 32. Graphic representation of $1/F_{PC}$ vs concentration of CO_2 in the gas phase for the baseline case.

Thus, on Figure 32 can be observed that the stiffness of the curve has disappeared with this function rearrange and it is possible to approximate the function with two simple polynomial expressions. Consequently, Tchevychev method seems ideal to integrate numerically this function.

Finally, it must be underlined that, for HFMC, the shape of the curve would be the same, but the result of the integration will give directly the volume of the contactor, not the length, as in the case of the packed contactor.

5.2.3. Dimensions of the contactors

5.2.3.1. Packed contactor

In the PC, the cross-section area will be given by the restriction of flooding, as it has been explained before. The length of this contactor has been calculated with the three methods in order to check their accuracy.

Table 15. Dimensions of the packed contactor for the baseline case (RMT=0,47)

Method	**Length** m	**Error[1]** %	**Area** m^2	**Volume** m^3
HUT_{OG}	325,00	9,63	1,06E-03	3,43E-01
Tchevychev	307,97	14,36		3,25E-01
Wolfram Alpha®	359,62	0,00		3,80E-01

In addition, the error has been computed taking as a reference the Wolfram Alpha® solution, since theoretically it is the most exact result because it makes an analytical integration of the fitting function, but it is harder to automatize. Consequently, it is clear that the best method is HUT_{OG}, provided that its condition of application is met, since it gives an equilibrium between good precision and ease of calculation.

As a conclusion, the length computed by the three methods is quite large if it is taken into account commercial packed beds, it seems not feasible to build a contactor with the obtained dimensions, since the HETP of absorption towers are 0.8 m (Sinnot *et al.*, 2005), so the tower height for 10 stages should be around 8 m. The reason can be the flooding constraint, which implies having low gas superficial velocity, therefore low global mass transfer coefficient, then a poor mass transfer in the packed contactor, so it would be required a longer tower.

5.2.3.2. Hollow fiber membrane contactor

In this case, the solution of the HFMC mass balance gives as a result directly the volume of the contactor without requiring its length or its cross-section area.

Table 16. Volume of the HFMC for the baseline case (RMT=0,47)

Method	**Volume** m^3	**Error[1]** %
HUT_{OG}	2,23E-03	9,61
Tchevychev	2,06E-03	16,21
Wolfram Alpha®	2,46E-03	0,00

Moreover, it is observed in Table 15 that it is obtained the same result than PC in terms of errors. However, it is unknown if the obtained volume would lead to a viable contactor dimensions, since this system has still one degree of freedom, then it is possible to assign dimensions provided that the volume calculated is reached.

In conclusion, as it can be seen in Table 15, the best method so far is the HUT_{OG} method, therefore its result will be applied in the following points of this report. Nevertheless, a validation of the method should be performed.

5.2.3.3.Validation of HUT_{OG} method

As it has been exposed, HUT_{OG} method only can be applied if the extraction ratio, λ, is between 0.8 and 1.25 (Rode, 2019). Therefore, this ratio has been calculated along the contactor, the result of its average value is 0.87, then it is reasonable to apply this method for this system.

In Figure 33 can be observed the extraction ratio as a function of z*. For z* close to 1, λ gets out of the required interval, however its average value meets the requirement.

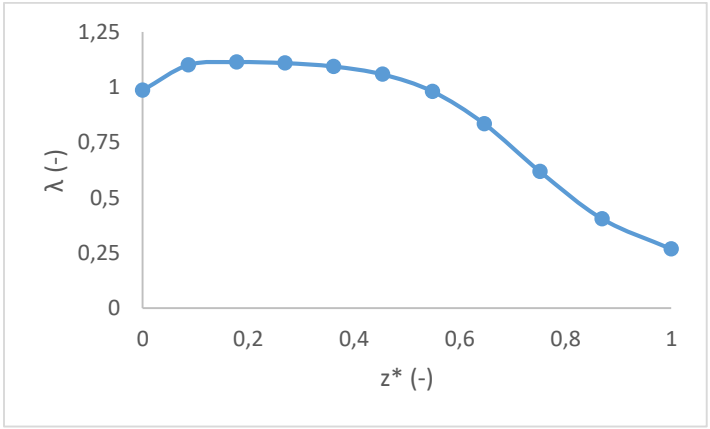

Figure 33. Extraction ratio, λ, as a function of the normalized axial coordinate

5.2.4. *Intensification potential as a function of the method*

The results in terms of the contactor volume reduction (i.e. intensification factor) that were for the baseline case are exposed in Table 16, as a function of the different methods implemented in this report.

Table 17. Overall intensification results

	Volume			
Method	**PC**	**HFMC**	**Units**	**Intensification factor**
HUT_{OG}	3,43E-01	2,23E-03	m^3	154,26
Tchevychev	3,25E-01	2,06E-03	m^3	157,70
Wolfram Alpha®	3,80E-01	2,46E-03	m^3	154,30

5.2.5. *Pressure in the contactors*

First, it is necessary to emphasize that the results obtained in terms of intensification potential are not complete without first carrying out an analysis of the pressure along the contactor, in addition to making a comparison with current industrial technology.

In Figure 34 is presented the ratio between pressure drop in the gas and in the liquid phase. As it can be observed, there is a high difference between the pressure drop in both phases along the contactor for the baseline case, the average value of this ratio must be one, as it has been shown in point 4.

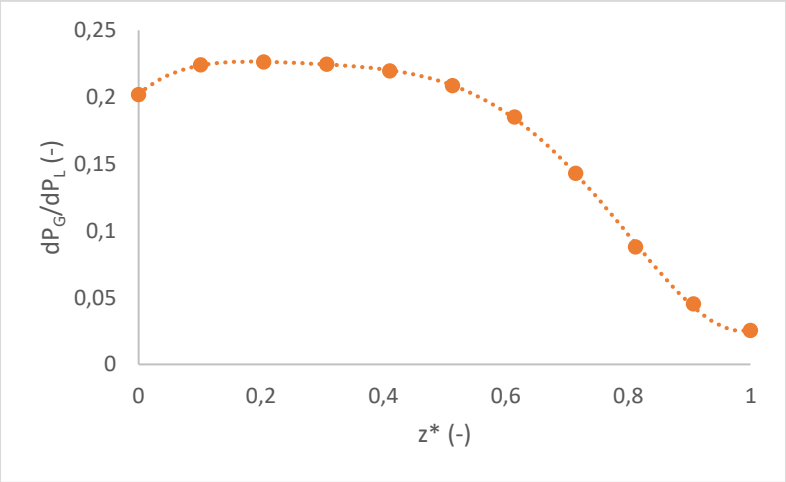

Figure 34. Pressure drop ratio among the gas and liquid vs z in the baseline case (RMT=0.47)*

On the other hand, as it has been presented in point 4, in order to obtain the absolute value of the pressure profile, the ratio A/Z must have a value because of the geometry degree of freedom. Furthermore, dP_G/dz and dP_L/dz must be integrated locally to obtain the profile, the method applied in this case was Trapezoidal method, since the curves are continuous, it is easy to implement it.

A common gas relative pressure drop in order to have a uniform distribution reducing compression costs in conventional packed columns, is 5% (Villeneuve *et al.*, 2018), however, according to Favre and Svendsen. (2012), it must not be far above 7%, whereas Chu *et al.* (2019) stated that 1% is sufficient for most of applications. Indeed, that value depends on whether the process is at high pressure or at atmospheric pressure.

In Figure 35 can be appreciated the pressure profile assuming A/Z such that a relative pressure drop ($\Delta P_{G,rel}$) is equal to 5%, for the baseline case. Moreover, it is important to remark that this pressure profile has the same shape, independently of A/Z, but the absolute value of the pressure profile is proportional to A/Z.

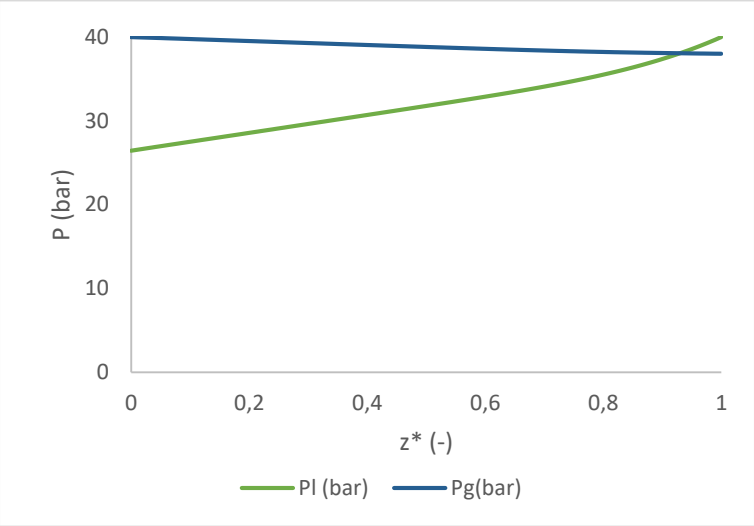

Figure 35. Pressure profile in the gas and in the liquid phase in the baseline case (RMT=0.47) with Z/A such that a relative pressure drop ($\Delta P_{G,rel}$) is equal to 5%

However, as it can be observed in Figure 35, an excessive pressure drop is perceived in the liquid phase, which would make the process unfeasible. However, that pressure drop was calculated assuming a relative pressure drop in the gas phase of 5% (200 kPa).

Then, if the inertial pressure drop in the gas phase is computed it is obtained a maximum of 0.153 kPa. As it has been commented previously, the minimum pressure drop is around 10 times the inertial pressure drop, which is 1.53 kPa, truly small value, since it would represent a relative pressure drop in the gas phase of 0,038%.

According to Lee *et al.* (2020a), for a long-term operating conditions, it is achieved a relative pressure drop in the gas phase of 4.49% for a pressure of the gas inlet of 1 bar and a fiber length of 13 cm, a result consistent with this study, but the process of this report is a high pressure process. In addition, Dalane *et al*. (2018) determines, for a fiber length of 1 m and a ceramic HFMC, around 0.06% of relative pressure drop in the gas phase, for a dehydration of natural gas at 80 bar. In the case of another high pressure process (Chu *et al.*, 2019), it was determined a $\Delta P_{G,rel}$ of less than

0.5% for a CO_2 removal from natural gas without solvent. Moreover, Belaissaoui and Favre (2018) achieved 1.75% of pressure drop at 36 bar. Those results are similar to an industrial HFMC (3M™ Liqui-Cel™ EXF-2.5×8) at 7.2 bar.

Nevertheless, as stated by Hoff *et al.* (2013), the result is 49.2% of pressure drop at 1 bar of gas inlet, truly very high pressure drop which could imply the unfeasibility of the contactor. Therefore, Hoff *et al.* (2013) will not be taken as reference in the discussion.

Table 17 summarizes the results in terms of pressure drop found in the literature and for a commercial HFMC. Apparently, the relative pressure drop in the gas phase must be less than 1% for high pressure processes.

Table 18. Results obtained by different sources in terms of pressure drop and contactor dimensions

Source	Process	$P_{G,in}$	$\Delta P_{G,rel}$	Z
		bar	%	m
3M™ Liqui-Cel™ EXF-2.5×8	General purpose. Liquid side	7,2	<1	0,28
Hoff *et al.* (2013)	CO_2 absorption in MEA[1] in post combustion	1,00	49,2	3
Villeneuve *et al.* (2018a)	CO_2 absorption in aqueous ammonia in post combustion	1,00	5,00	0,25
Belaissaoui and Favre (2018)	CO_2 absorption from syngas using Selexol®	36	1,75	1
Dalane *et al*. (2018)	Subsea natural gas dehydration by absorption in TEG[2]	80,00	0,06	1
Chu *et al.* (2019)	CO_2 removal from natural gas (without solvent). Outside fibers.	60,00	<0,5	1
Lee *et al.* (2020a)	CO_2 absorption in MEA[1] with ceramic HFMC	1,09	4,49	0,13

[1]Monoethanolamine.
[2]Triethylene glycol.

In terms of length of the contactor, the mentioned profile (Figure 35) implied a length of 7.80 m. Therefore, it is too large compared to contactors from the literature and commercial contactors. Since, as stated by McKeen (2012), hollow fiber membrane modules should have typically a fiber length from 1 to 1.6 m, which agrees with Rackley (2017b), who indicates that typical fiber lengths

are usually around 1 m. In the case of commercial HFMC, and their lengths goes from 50 to 140 cm (Lenntech, 2020).

As a conclusion, it is necessary to perform an optimization by changing geometric parameters. In that analysis it must be considered typical geometries and pressure drops of the literature and commercial membrane contactors, in order to have a design adjusted to reality.

5.2.6. Optimization problem

In the first place, it is important to do a sensitivity analysis before solving the optimization problem. The easiest way to do it is to modify the geometry of the membrane fibers (see equation 69), in other words, relative membrane thickness (RMT).

The reason why RMT has been chosen to be changed is because if φ, fiber volume fraction, was altered, for example, the volume of the contactor would be modified excessively, the aim is to optimize the pressure drop without interfere in the intensification result. Therefore, changing relative membrane thickness does imply only an unimportant change in the contactor volume.

Thus, in next figure it is presented the sensitivity analysis of the variable pressure drop ratio changing the relative membrane thickness, using equation 69.

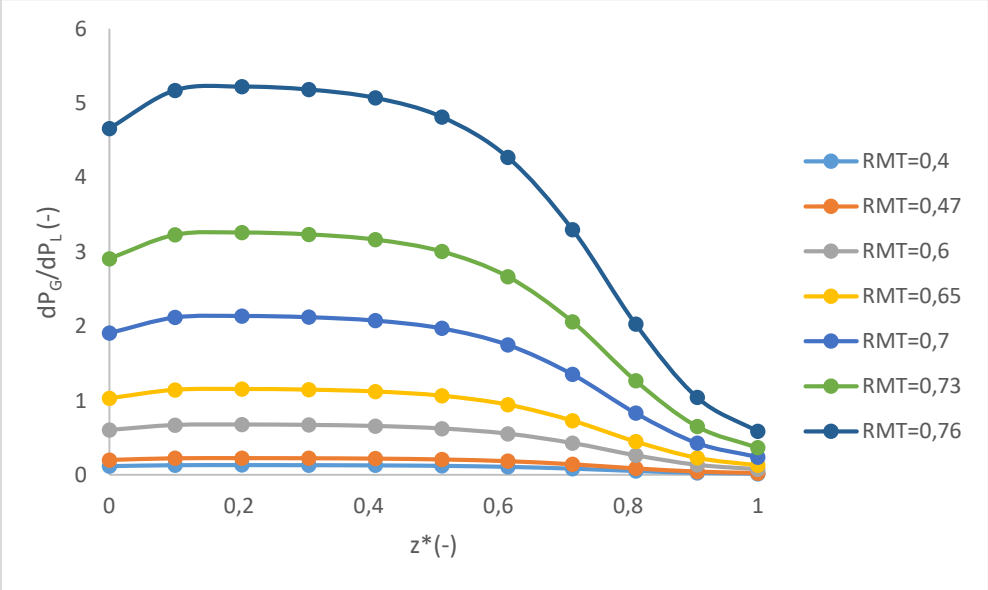

Figure 36. Sensitivity analysis of $\Delta P_G / \Delta P_L$ vs z, changing relative membrane thickness (RMT)*

In Figure 36 it can be observed that there is a large sensitivity of pressure drop ratio to positive changes in RMT, whereas there is a small sensitivity when this parameter is decreased. The range of variation was between 0.4 and 0.76, but it is useless to decrease this variable below 0.4, since there is not sensitivity in that range; also it does not make sense to increase above 0.76, since it is

not desirable that the value is far from one. Moreover, it is significant that this sensitivity obtained is consistent with a similar analysis taken out by Chu *et al.* (2019) in a simulation of CO_2 capture from natural gas.

Thus, the optimum point, pressure drop ratio one, is found for relative membrane thickness of 0.67, it is not necessary to perform more iterations in order to gain precision, since this work is based on simulations and approximations. The next step it to change Z/A ratio, maintaining the relative membrane thickness of 0.67.

On the other hand, concerning the relative pressure drop requirement, it must not be considered the value of 5%, since as it has been checked previously, it is too large for a high-pressure process. In addition, as stated by Lee *et al.* (2020a), it is expected that HFMC are a good alternative to PC because of its high performance, even at low pressure drops. Furthermore, according to typical values of shell and tubes heat exchangers and the values of the literature (Table 17), a pressure drop of 1 bar must be met as maximum in both phases, therefore it has been decided that this new constraint replace the restriction of 5% of pressure drop, as an upper limit to have a good distribution in the HFMC.

Consequently, in the following figure is presented the pressure drop results and the pressure profile meeting all restrictions, the optimized case.

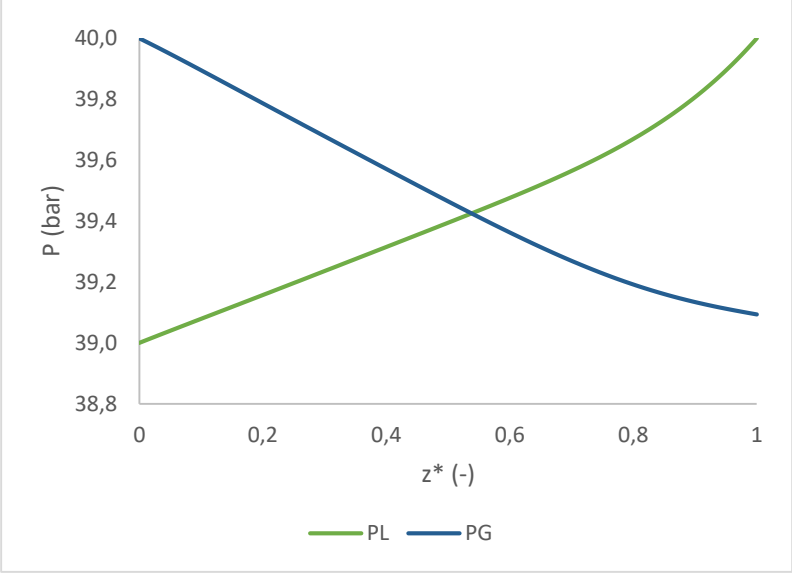

Figure 37. Pressure profile in the gas and in the liquid phase (optimized case), RMT=0.67, Z=2.18 m

Moreover, in the following table is exposed the overall results of the optimization of the hollow fiber membrane contactor compared to the baseline case.

Table 19. Global results of the optimization problem compared to the baseline case

	Inputs			Outputs		
Case	**Parameters**	**Value**	**Units**	**Parameters**	**Value**	**Units**
Baseline	RMT	0,47	-			
	Z	7,80	m	Volume[1]	2,23E-03	m^3
	$\Delta P_{G,rel}$	5,00	%			-
	$\Delta P_{L,rel}$	33,92	%	Intensification factor	154,26	
	ΔP_G	2,00	bar			
	ΔP_L	13,57	bar			
Optimized problem	RMT	0,67	-			
	Z	2,18	m	Volume[1]	2,36E-03	m^3
	$\Delta P_{G,rel}$	2,27	%			-
	$\Delta P_{L,rel}$	2,50	%	Intensification factor	145,60	
	ΔP_G	0,90	bar			
	ΔP_L	1,00	bar			

[1]Volume calculated by HUT_{OG} method.

As it can be appreciated in Table 18, the volume barely changes if we compare the optimized result with the baseline case; besides the intensification factor it is still very high (the volume of the hollow fiber membrane contactor would be 145.60 times smaller compared to the packed contactor at the same conditions), which represents a huge intensification potential. This intensification result is certainly optimistic if it is taken into account results obtained by Hoff *et al.* (2013), in a CO_2 capture in post combustion process, who obtained only a 75% of volume reduction compared to a conventional packed column at 1 bar.

Finally, a sensitivity analysis was performed varying the length Z in order to see how important it is relating to the variation of the length in the relative pressure drop for different values of RMT. It is observed also a large sensitivity to higher RMT, it makes sense since the pressure drop in the gas phase is a function of RMT to the fourth power, as it has been shown in the pressure drop equations.

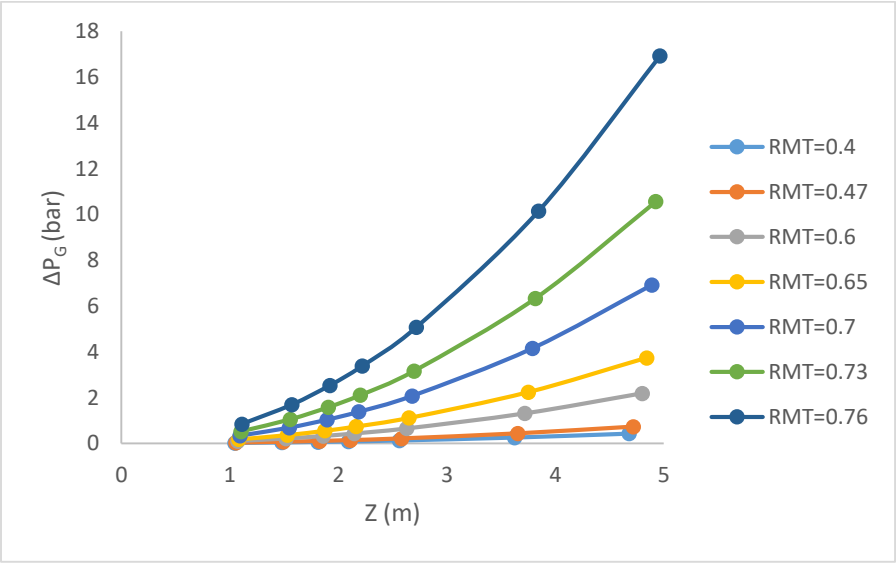

Figure 38. Sensitivity analysis of $\Delta P_{G,rel}$ vs Z changing RMT for baseline case

5.3. Parametric analysis: effect of liquid inlet temperature, inlet pressure and CO_2 gas inlet concentration

It is necessary to underline that in previous steps it has been optimized only the baseline case, which is one of the 90 simulations taken out originally by Mckechnie (2020), and 18 additional simulations performed by the author of this report, with Aspen HYSYS®, varying operational parameters. Therefore, it is essential to check how the optimization results are affected by the change of some parameters as liquid inlet temperature, inlet pressure and gas inlet CO_2 concentration.

Regarding the flow factor (F_{LG}) at the liquid inlet, which will be affected since, since it varies with the liquid inlet temperature, $T_{L,in}$, The flow factor fluctuates from 1.94 to 7.35 along the simulations and the inlet liquid temperature varies from -50 to 20 degC, in function of the 95% of CO_2 recovery requirement in every simulation. In the baseline case F_{LG} is equal to 2.33.

In Figure 39 it is shown a comparison of the flow factor at the inlet. The flow factor is slightly affected by the inlet molar fraction of CO_2, but there is a significant variation of it with the change of temperature of the liquid inlet, $T_{L,in}$

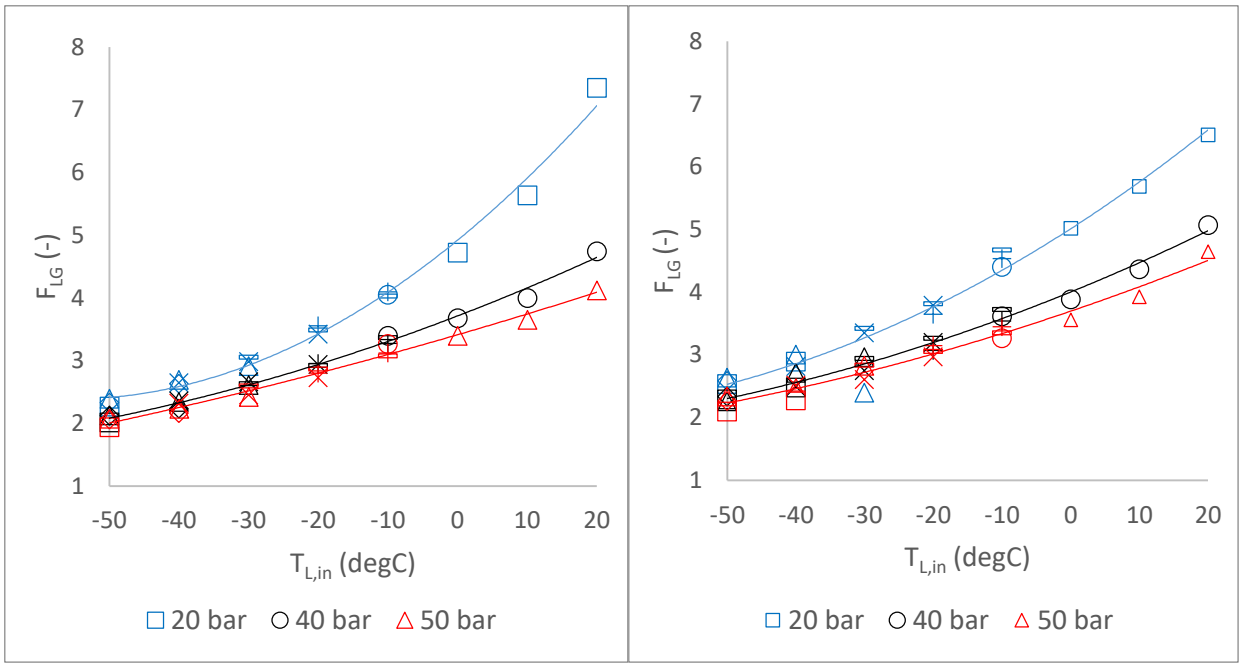

Figure 39. F_{LG} vs temperature of the liquid inlet and for different pressures, and for y_{co2}=0,3 and 0,4, respectively (Mckechnie, 2020)

Table 20. F_{LG} vs temperature of the liquid inlet and for different pressures legend: shapes

$T_{G,in}$ (degC)	**Shape**
-30	Square
-20	Square rotated 45°
-10	Triangle
0	Cross (x)
10	Dash
20	Cross (+)
30	Circle

Certainly, the higher temperature of methanol absorbent at the inlet, it implies an increase in the methanol flowrate required to meet the 95% of CO_2 recovery. Moreover, it is favorable to work at a higher temperature of the liquid, since we will be closer to the isothermal behavior (it maximizes the absorption capacity), but this would involve that it will be necessary a higher methanol flow.

The main interrogation is whether the observed variation of the flow factor with temperature of the liquid inlet would involve a substantial change in the volume of the contactors, thus in the intensification factor. The volume for other simulations will be computed by HUT_{OG} method, since it is the easiest and most accurate among the methods exposed in this report, moreover its requirement is met for all the simulations.

Thus, a sensitivity analysis changing inlet liquid temperature, inlet pressure and inlet gas CO_2 concentration (which implies that F_{LG} would change) is necessary in order to figure out how the volume of the contactors would be affected, and therefore the intensification factor. This analysis has been carried out for a gas inlet temperature of 10 degC, although the aim was to perform it for the least favorable temperature for the system, in other words, the most restrictive (30 degC), however, there are not enough available simulations to perform a parametric analysis under these conditions, not even at 20 degC.

Table 21. Variation range of the variables and the value of fixed parameters for the pressure drop optimization

Variable parameters			**Fixed parameters**	**Optimization parameters**	
$T_{L,in}$	**$P_{G,in}=P_{L,in}$**	**$y_{CO2,\ in}$**	**$T_{G,in}$**	**RMT**	**Z**
degC	**bar**	**(-)**	**degC**	**(-)**	**m**
-50					
-40					
-30	20	0.3			
-20	40	0.4	10	*	*
-10	50				
0					
10					
20					

* The value which must verify the pressure drop constraints of Table 13.

Therefore, the results in terms of volume of the contactors and intensification factor are presented in Figures 40 and 41 for the pressures of 20, 40 and 50 bar, for the molar fraction of CO_2 in the inlet gas of 0.3 and 0.4, also varying the temperature of the inlet liquid ($T_{L,in}$). Furthermore, it should be noted that these results have been calculated solving simultaneously the pressure optimization problem.

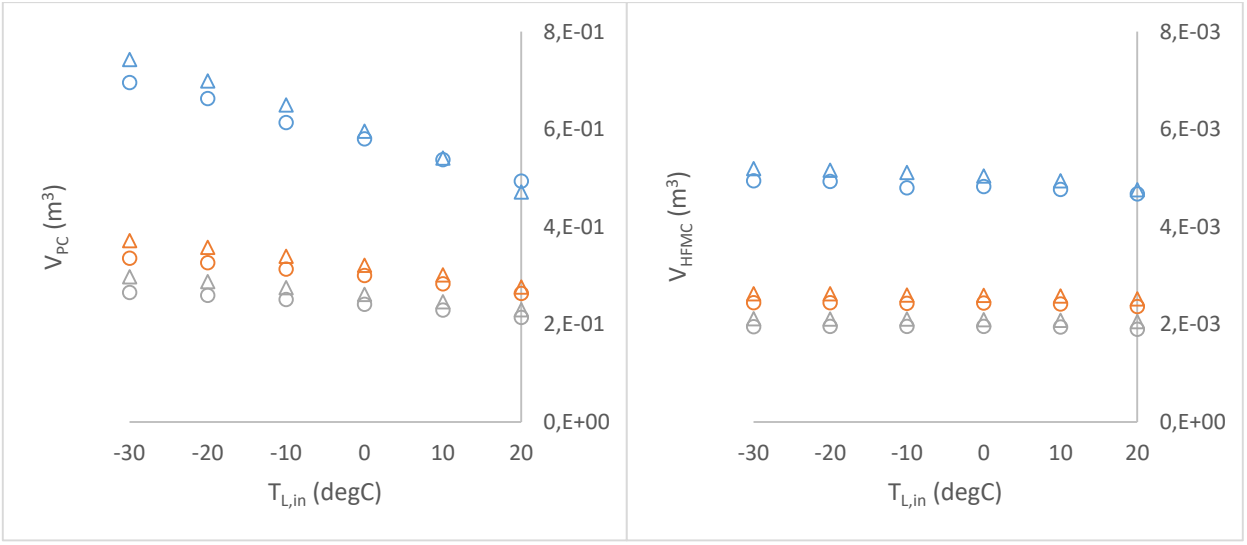

Figure 40. Parametrical analysis of the volume of the contactors for $T_{G,in}$=10 degC

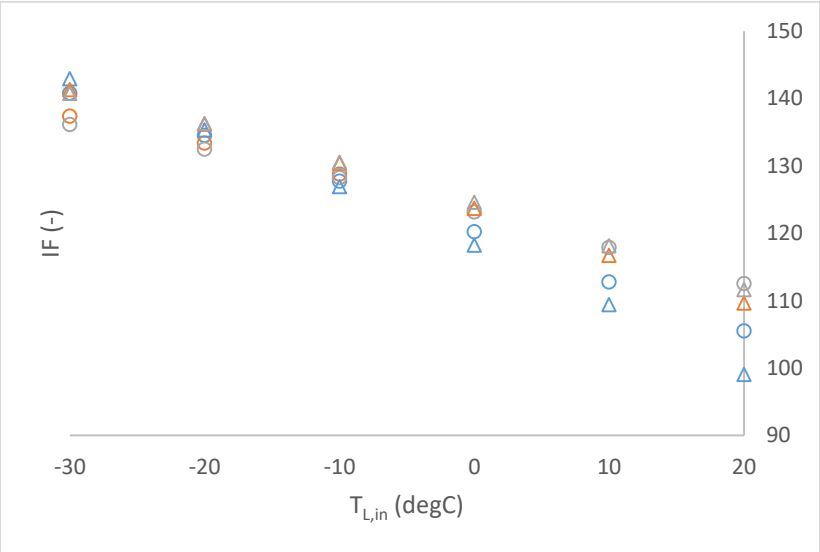

Figure 41. Parametric analysis intensification factor for $T_{G,in}$=10 degC

Table 22. Parametric analysis graphical representation legend

Legend	$y_{CO2,in}$
Triangle	0,3
Circle	0,4

Legend	P_{in} (bar)
blue	20
orange	40
grey	50

Table 23. Numerical values of the parametrical analysis for $T_{G,in}$=10 degC

$y_{CO2,in}$ mole mole^{-1}	P_{in} bar	$T_{L,in}$ degC	Sim -	V_{HFMC} m^3	V_{PC} m^3	F_{LG} -	IF -	$\bar{\lambda}$ -	RMT -	L m	ΔP_G bar	ΔP_L bar
0,3	20	-30	52	5,19E-03	7,43E-01	3,053	142,980	0,838	0,6896	2,194	0,965	1,000
		-20	56	5,16E-03	6,99E-01	3,484	135,361	0,822	0,6945	2,137	0,982	1,000
		-10	60	5,11E-03	6,49E-01	4,027	126,987	0,801	0,6991	2,070	0,994	1,000
		0	91	5,04E-03	5,96E-01	4,724	118,284	0,770	0,6991	1,991	1,001	1,000
		10	92	4,94E-03	5,41E-01	5,636	109,446	0,722	0,6991	1,891	1,005	1,000
		20	93	4,76E-03	4,72E-01	7,353	99,095	0,605	0,6991	1,700	1,000	1,000
	40	-30	67	2,63E-03	3,72E-01	2,631	141,348	0,857	0,6850	2,145	0,942	1,000
		-20	71	2,63E-03	3,58E-01	2,919	136,211	0,846	0,6892	2,111	0,963	1,000
		-10	75	2,60E-03	3,40E-01	3,363	130,456	0,814	0,6954	2,047	0,978	1,000
		0	94	2,59E-03	3,21E-01	3,677	123,757	0,819	0,6954	2,022	0,993	1,000
		10	95	2,58E-03	3,01E-01	3,998	116,780	0,827	0,6954	1,998	1,005	1,000

		20	96	2,52E-03	2,77E-01	4,746	109,666	0,778	0,6954	1,909	1,010	1,000
	50	-30	82	2,11E-03	2,98E-01	2,594	140,795	0,846	0,6860	2,105	0,929	1,000
		-20	86	2,11E-03	2,88E-01	2,866	136,325	0,832	0,6905	2,073	0,951	1,000
		-10	90	2,11E-03	2,75E-01	3,074	130,587	0,840	0,6915	2,062	0,974	1,000
		0	97	2,10E-03	2,61E-01	3,399	124,659	0,834	0,6915	2,027	0,989	1,000
		10	98	2,08E-03	2,46E-01	3,650	118,179	0,844	0,6915	2,010	1,002	1,000
		20	99	2,06E-03	2,30E-01	4,122	111,686	0,825	0,6915	1,958	1,010	1,000
0,4	20	-30	26	4,94E-03	6,96E-01	3,420	140,851	0,856	0,6742	2,190	0,979	1,000
		-20	32	4,93E-03	6,63E-01	3,813	134,553	0,848	0,6783	2,147	0,998	1,000
		-10	38	4,80E-03	6,14E-01	4,671	127,770	0,788	0,6885	2,038	1,009	1,000
		0	100	4,82E-03	5,80E-01	5,020	120,289	0,804	0,6885	2,020	1,022	1,000
		10	101	4,77E-03	5,38E-01	5,687	112,826	0,787	0,6885	1,961	1,031	1,000
		20	102	4,67E-03	4,93E-01	6,507	105,526	0,757	0,6885	1,891	1,036	1,000
	40	-30	25	2,44E-03	3,36E-01	2,942	137,427	0,864	0,6697	2,127	0,952	1,000
		-20	31	2,45E-03	3,26E-01	3,264	133,439	0,852	0,6743	2,093	0,972	1,000
		-10	37	2,43E-03	3,13E-01	3,723	128,824	0,826	0,6802	2,039	0,987	1,000
		0	103	2,44E-03	3,00E-01	3,888	123,027	0,843	0,6802	2,033	1,006	1,000
		10	104	2,41E-03	2,83E-01	4,365	117,262	0,827	0,6802	1,985	1,018	1,000
		20	105	2,37E-03	2,63E-01	5,069	111,312	0,791	0,6802	1,915	1,026	1,000
	50	-30	27	1,95E-03	2,66E-01	2,831	136,184	0,863	0,6690	2,100	0,941	1,000
		-20	33	1,96E-03	2,59E-01	3,051	132,544	0,860	0,6723	2,083	0,963	1,000
		-10	39	1,96E-03	2,51E-01	3,350	128,317	0,851	0,6759	2,052	0,982	1,000
		0	106	1,96E-03	2,41E-01	3,562	123,196	0,856	0,6759	2,036	1,000	1,000
		10	107	1,94E-03	2,29E-01	3,928	117,958	0,847	0,6759	1,999	1,013	1,000
		20	108	1,90E-03	2,14E-01	4,648	112,590	0,803	0,6759	1,921	1,022	1,000

In view of the results (Figure 40 and Table 22), on the one hand is detected that the volume of the packed contactor is decreased (in other words, the absorption capacity is improved) if $T_{L,in}$ is increased. However, in industrial packed contactors is not common to work at high inlet liquid temperatures since it would make the process less feasible in terms of flooding since F_{LG} would grow up and consequently the length of the packed contactor.

On the other hand, the volume of the HFMC is not notably affected with the variation of liquid inlet temperature, which is a good result since it implies that the process can work at higher temperatures, therefore the cooling costs would be reduced. The same result for the HFMC was obtained by Yan *et al*. (2007) and Lee *et al*. (2020b), who found that the absorption capacity does not varies significantly with the solvent temperature for a CO_2 absorption in MEA within the interval of 20-50 degC

Nevertheless, Ghobadi *et al.* (2018) achieved a growth in the absorption capacity with the increase of the temperature using distilled water as physical solvent. In addition, Cao *et al*. (2019) stated that the increase in inlet liquid temperature can make a positive influence on the diffusion coefficient in the liquid phase, thus the mass transfer would be improved at higher temperatures.

Moreover, the volume of the two contactors is reduced at high pressures, therefore is better to work at 50 bar; it is a consistent result, since the absorption capacity of the solvent will be improved with the increment of pressure. The reason is that the partial pressure of CO_2 also will be increased, therefore the driving force will also be amplified.

Concerning the inlet molar fraction of CO_2 in the gas phase, at identical conditions of $T_{L,in}$ and pressure, the volume of both contactors is reduced at higher $y_{CO2,in}$, it makes sense since the driving force will be also incremented.

Furthermore, it is noteworthy that in some simulations have the extraction ratio λ been outside the interval of application of Colburn's equation. Therefore, the hypothesis which has been considered for the baseline case is not valid for all the simulations, however, even for simulations out of the Colburn interval the results gotten are similar to the ones obtained by Tchebychev method, thus HUT_{OG} method has been applied to obtain all the volumes. In addition, in the following figure can be observed that is less probable to meet Colburn's equation conditions at higher liquid inlet temperatures:

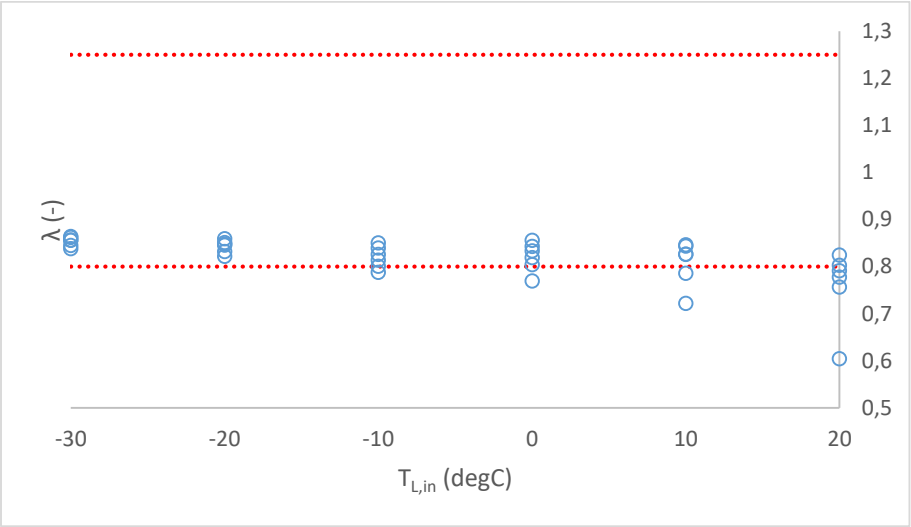

Figure 42. Extraction ratio λ vs $T_{L,in}$

As a conclusion, in relation to the intensification factor (Figure 41 and Table 22), indeed the best conditions to optimize it are higher pressures, lower inlet liquid temperatures and $y_{CO2,in}$=0.3.

6. CONCLUDING REMARKS AND OUTLOOK

In this work, the intensification potential of hollow fiber membrane contactors for CO_2 capture by physical absorption using methanol as solvent have been evaluated by simulation and modeling.

Concerning design and axial profiles, the main following conclusions can be extracted:

- The simulations have demonstrated that there is a similar behavior regarding the axial profiles of both contactors.
- The assumed operational conditions have led to an unfeasible height of the packed contactor, however, for the HFMC the dimensions obtained are consistent with current industrial membrane contactors and the literature.

In relation with the study of the pressure and the intensification potential:

- According to literature and industrial suppliers, the pressure drop in a membrane contactor must be as maximum 1 bar in order to have a good distribution of the fluid.
- The volume of the HFMC is not affected notably by the pressure drop constraints.
- It was obtained an intensification potential of the HFMC technology such that the volume of the contactor could be reduced as minimum 100 times if packed contactors are substituted by hollow fiber membrane contactors.
- For PC it is observed that the volume is reduced at higher liquid inlet temperatures, whereas for the HFMC, the volume does not change notably with the variation of liquid inlet temperature.
- The volume of the two contactors is reduced at high pressures, therefore, for the operation conditions of this report, it is better to work at 50 bar.
- The volume of both contactors is reduced at higher concentration of CO_2 in the gas inlet, so the best operating condition is the inlet molar fraction of CO_2 of 0.4.

7. REFERENCES

Albarracin Zaidiza, D., Belaissaoui, B., Rode, S., Neveux, T., Makhloufi, C., Castel, C., Roizard, D. and Favre, E., 2015. Adiabatic Modelling of CO_2 Capture by Amine Solvents Using Membrane Contactors. *Journal of Membrane Science*, vol. 493, pp. 106–119, 10.1016/j.memsci.2015.06.015. Accessed 22 Oct 2020.

Albarracin Zaidiza, D., Wilson, S.G., Belaissaoui, B., Rode, S., Castel, C., Roizard, D., and Favre, E., 2016. Rigorous modelling of adiabatic multicomponent CO_2 post-combustion capture using hollow fibre membrane contactors. *Chemical Engineering Science*, vol. 145, pp. 45-58, 10.1016/j.ces.2016.01.053. Accessed 10 Nov 2020.

Allen, M.R., O.P. Dube, W. Solecki, F. Aragón-Durand, W. Cramer, S. Humphreys, M. Kainuma, J. Kala, N. Mahowald, Y. Mulugetta, R. Perez, M. Wairiu, and K. Zickfeld, 2018: Framing and Context. In: *Global Warming of 1.5°C. An IPCC Special Report on the impacts of global warming of 1.5°C above pre-industrial levels and related global greenhouse gas emission pathways, in the context of strengthening the global response to the threat of climate change, sustainable development, and efforts to eradicate poverty* [Masson-Delmotte, V., P. Zhai, H.-O. Pörtner, D. Roberts, J. Skea, P.R. Shukla, A. Pirani, W. Moufouma-Okia, C. Péan, R. Pidcock, S. Connors, J.B.R. Matthews, Y. Chen, X. Zhou, M.I. Gomis, E. Lonnoy, T. Maycock, M. Tignor, and T. Waterfield (eds.)]. In Press.

Asendrych, D., Niegodajew, P., and Drobniak, S., 2013. CFD modelling of CO_2 capture in a packed bed by chemical absorption. *Chemical and Process Engineering - Inzynieria Chemiczna i Procesowa*, *34*(2), 269–282. https://doi.org/10.2478/cpe-2013-0022

Aspentech, 2020a. *Aspen HYSYS®* [online] Available at <https://www.aspentech.com/en/products/engineering/aspen-hysys> [Accessed 10 November 2020].

Aspentech, 2020b. *Aspen Plus®* [online] Available at < https://www.aspentech.com/en/products/engineering/aspen-plus> [Accessed 10 November 2020]

Belaissaoui, B., Claveria-Baro, J., Lorenzo-Hernando, A., Albarracin Zaidiza, D., Chabanon, E., Castel, C. and Favre, E., 2016. Potentialities of a dense skin hollow fiber membrane contactor for biogas purification by pressurized water absorption. *Journal of Membrane Science*, *513*, 236–249. https://doi.org/10.1016/j.memsci.2016.04.037

Belaissaoui, B., and Favre, E., 2018. Evaluation of a dense skin hollow fiber gas-liquid membrane contactor for high pressure removal of CO_2 from syngas using Selexol as the absorbent. *Chemical Engineering Science*, *184*, 186–199. https://doi.org/10.1016/j.ces.2018.02.028

Carpenter, S. M. and Long, A. H., 2017. Integration of Carbon Capture in IGCC Systems. *Integrated Gasification Combined Cycle (IGCC) Technologies*, pp. 445–463, 10.1016/b978-0-08-100167-7.00036-6. Accessed 29 Oct. 2020.

Cao, F., Gao, H., Xiong, Q., and Liang, Z., 2019. Experimental studies on mass transfer performance for CO_2 absorption into aqueous N,N-dimethylethanolamine (DMEA) based solutions in a PTFE hollow fiber membrane contactor. *International Journal of Greenhouse Gas Control*, *82*, 210–217. https://doi.org/10.1016/j.ijggc.2018.12.011

Chabanon, E., Belaissaoui, B., and Favre, E., 2014. Gas-liquid separation processes based on physical solvents: Opportunities for membranes. *Journal of Membrane Science*, 459, 52–61. https://doi.org/10.1016/j.memsci.2014.02.010

Chu, Y., Lindbråthen, A., Lei, L., He, X., and Hillestad, M., 2019. Mathematical modeling and process parametric study of CO_2 removal from natural gas by hollow fiber membranes. *Chemical Engineering Research and Design*, *148*, 45–55. https://doi.org/10.1016/j.cherd.2019.05.054

Dalane, K., Svendsen, H. F., Hillestad, M., and Deng, L., 2018. Membrane contactor for subsea natural gas dehydration: Model development and sensitivity study. *Journal of Membrane Science*, *556*(March), 263–276. https://doi.org/10.1016/j.memsci.2018.03.033

Favre, E., and Svendsen, H. F., 2012. Membrane contactors for intensified post-combustion carbon dioxide capture by gas-liquid absorption processes. *Journal of Membrane Science*, *407–408*, 1–7. https://doi.org/10.1016/j.memsci.2012.03.019

Fuller, E. N., Schettler, P. D. and Giddings J. C., 1966. New method for prediction of binary gas-phase diffusion coefficients. *Industrial Engineering Chem*istry, 58(5): 18 (1966). https://doi.org/10.1021/ie50677a007

Ghobadi, J., Ramirez, D., Jerman, R., Crane, M., and Khoramfar, S., 2018. CO_2 separation performance of different diameter polytetrafluoroethylene hollow fiber membranes using gas-liquid membrane contacting system. *Journal of Membrane Science*, *549*, 75–83. https://doi.org/10.1016/j.memsci.2017.11.060

Hakim, D. I., Steinberg, D. and Stiel, L. I., 1971. Generalized Relationship for the Surface Tension of Polar Fluids. *Industrial & Engineering Chemistry Fundamentals*, vol. 10, no. 1, pp. 174–175, 10.1021/i160037a032.

Happel, J., 1959. Viscous flow relative to array of cylinders, AIChE J. 5, 174–177. https://doi.org/10.1002/aic.690050211

Henley, E. J., and Seader, J.D., 2000. *Equilibrium-Stage Operations in Chemical Engineering*. John Wiley & Sons, Inc.

Hoek, E.M. and Tarabara, V. eds., 2013. *Encyclopedia of Membrane Science and Technology, Volume 3*. Wiley.

Hoff, K. A., and Svendsen, H. F., 2013. CO_2 absorption with membrane contactors vs. packed absorbers- Challenges and opportunities in post combustion capture and natural gas sweetening. *Energy Procedia*, *37*(1876), 952–960. https://doi.org/10.1016/j.egypro.2013.05.190

Intergovernmental Panel on Climate Change (IPCC), 2005. *Special report on carbon dioxide capture and storage*. In: Metz B., Davidson O., de Coninck HC., Loos M., Meyer LJ., (eds) Prepared by Working Group III of the Intergovernmental Panel on Climate Change. Cambridge University Press, Cambridge, United Kingdom/New York, NY, USA, p 442

Intergovernmental Panel on Climate Change (IPCC), 2014. *Climate Change 2014: Mitigation of Climate Change. Contribution of Working Group III to the Fifth Assessment Report of the Intergovernmental Panel on Climate Change* [Edenhofer, O., R. Pichs-Madruga, Y. Sokona, E. Farahani, S. Kadner, K. Seyboth, A. Adler, I. Baum, S. Brunner, P. Eickemeier, B. Kriemann, J. Savolainen, S. Schlömer, C. von Stechow, T. Zwickel and J.C. Minx (eds.)]. Cambridge University Press, Cambridge, United Kingdom and New York, NY, USA.

Jonassen, Ø., Kim, I., and Svendsen, H. F., 2014. Heat of absorption of carbon dioxide (CO2) into aqueous Nmethyldiethanolamine (MDEA) and N,Ndimethylmonoethanolamine (DMMEA). *Energy Procedia*, 63(1876), 1890–1902. https://doi.org/10.1016/j.egypro.2014.11.198

Kartohardjono, S., Paramitha, A., Putri, A. A., and Andriant, R., 2017. Effects of Absorbent Flow Rate on CO_2 Absorption through a Super Hydrophobic Hollow Fiber Membrane Contactor. *International Journal of Technology*, *8*, 1429–1435. https://doi.org/10.14716/ijtech.v8i8.679

Khaisri, S., deMontigny, D., Tontiwachwuthikul, P., & Jiraratananon, R., 2011. CO_2 stripping from monoethanolamine using a membrane contactor. *Journal of Membrane Science*, *376*(1–2), 110–118. https://doi.org/10.1016/j.memsci.2011.04.005

Kontogeorgis, G.M., Michelsen, M.L., Folas, G.K., Derawi, N.S., and Stenby, H., 2006. Ten Years with the CPA (Cubic-Plus-Association) equation of state. Part 1. Pure compounds and self-associating systems. *Industrial and Engineering Chemistry Research*, 45(14), 4855-4868. https://doi.org/10.1021/ie051305v

Kumar-Pabby, A., Rizvi, S.S.H. and Sastre-Requena, A. M. eds., 2015. *Handbook of Membrane Separations. Chemical, Pharmaceutical, Food, and Biotechnological Applications.* 2th ed. CRC Press. Taylor & Francis Group.

Lallanila, M., 2018. What is the Greenhouse Effect? Live Science. [Online]. https://www.livescience.com/37743-greenhouse-effect.html.

Lee, H. J., Kim, M. K., Lee, S. H., Park, T. S., Park, S. Do, and Park, J. H., 2020a. Integrated membrane contactor absorber/regeneration column process for CO2 capture with large scale module at various operating conditions. *Catalysis Today*, (February 2019), 0–1. https://doi.org/10.1016/j.cattod.2020.03.008

Lee, H. J., Kim, M. K., Park, J. H., and Magnone, E., 2020b. Temperature and pressure dependence of the CO2 absorption through a ceramic hollow fiber membrane contactor module. *Chemical Engineering and Processing - Process Intensification*, *150*(May 2019), 107871. https://doi.org/10.1016/j.cep.2020.107871

Lenntech, 2020. *Hollow fiber membranes. Cartridge Information* [online] Available at: <https://www.lenntech.com/Data-sheets/GE-Osmonics-Hollow-Fiber-Membranes-L%20backup.pdf> [Accessed 11 November 2020].

Li, S., Rocha, D. J., James Zhou, S., Meyer, H. S., Bikson, B., & Ding, Y., 2013. Post-combustion CO_2 capture using super-hydrophobic, polyether ether ketone, hollow fiber membrane contactors. *Journal of Membrane Science*, *430*, 79–86. https://doi.org/10.1016/j.memsci.2012.12.001

Lockwood, T., 2017. A comparative review of next-generation carbon capture technologies for coal-fired power plant. *Energy Procedia*, pp. 2658-2670. https://doi.org/10.1016/j.egypro.2017.03.1850

Mahdavian, M., Atashi, H., Zivdar, M., and Mousavi, S. M., 2011. Application of methanol absorbent for CO_2 removal in gas- liquid hollow fiber membrane contactors. *The 7th International Chemical Engineering Congress & Exhibition (IChEC 2011).*

McCabe, W.L., Smith, J.C., and Harriot, P., 2007. *Units Operations in Chemical Engineering*. 7th edition. McGraw-Hill

McKeen, L.W., 2012. Market and applications for films, containers and membranes. *Permeability Properties of Plastics and Elastomers (Third Edition)*. https://doi.org/10.1016/B978-1-4377-3469-0.10004-9

Mckechnie, E., 2020. Evaluation of membrane contactors for CO_2 capture from syngas mixtures using physical absorbents: simulation study (Unpublished Results). ENSIC, Université de Lorraine.

Nanyonjo, A., 2020. Physical, transfer and thermodynamic properties of gas and liquid mixtures of hydrogen, carbon dioxide and methanol in view of the modelling of physical absorption processes (Unpublished Results). ENSIC, Université de Lorraine

National Aeronautics and Space Administration (NASA), 2020. *Climate Change: How Do We Know?* [online] Available at: <https://climate.nasa.gov/evidence/> [Accessed 27 October 2020]

Nguyen, P. T., Lasseuguette, E., Medina-Gonzalez, Y., Remigy, J. C., Roizard, D., and Favre, E., 2011. A dense membrane contactor for intensified CO_2 gas/liquid absorption in post-combustion capture. *Journal of Membrane Science*, *377*(1–2), 261–272. https://doi.org/10.1016/j.memsci.2011.05.003

Pahlavanzadeh, H., Darabi, M., Ghaleh, V. R., & Bakhtiari, O., 2020. CFD modeling of CO_2 absorption in membrane contactors using aqueous solutions of monoethanolamine-ionic liquids. *Industrial and Engineering Chemistry Research*, *59*(41), 18629–18639. https://doi.org/10.1021/acs.iecr.0c02242

Perry, R.H., 2008. *Perry's chemical engineers' handbook*. 6th ed. McGraw-Hill

Poling, B. E., Prausnitz, J. M. and O'Connell, J. P., 2006. *The Properties of Gases and Liquids*. Fifth Edition.

Rackley, S. A., 2017a. Absorption capture systems. In *Carbon Capture and Storage*. https://doi.org/10.1016/b978-0-12-812041-5.00006-4

Rackley, S. A., 2017b. Membrane separation systems. In *Carbon Capture and Storage*. https://doi.org/10.1016/B978-0-12-812041-5.00008-8

Rode, S., Nguyen, P. T., Roizard, D., Bounaceur, R., Castel, C., and Favre, E., 2012. Evaluating the intensification potential of membrane contactors for gas absorption in a chemical solvent: A generic one-dimensional methodology and its application to CO_2 absorption in monoethanolamine. *Journal of Membrane Science*, 389, 1–16. https://doi.org/10.1016/j.memsci.2011.09.042

Rode, S., 2019. *Opérations polyphasiques en génie des procédés - Hydrodynamique, transferts, réactions, séparations mécaniques*. Ellipses

Rode, S., 2020. *Séparations thermiques en génie de procédés. Destillation, air humide, séchage*. ENSIC, Université de Lorraine.

Scholes, C.A., Smith, K.H., Kentish, S.E. and Stevens, G.W., 2010. CO_2 Capture from Pre-combustion processes-strategies for Membrane Gas Separation. *International Journal of Greenhouse Gas Control*, pp. 739- 755. https://doi.org/10.1016/j.ijggc.2010.04.001

Scholes, C. A., Anderson, C. J., Stevens, G. W., and Kentish, S. E. (2013). Membrane gas separation physical solvent absorption combined plant simulations for pre-combustion capture. *Energy Procedia*, *37*, 1039–1049. https://doi.org/10.1016/j.egypro.2013.05.200

Scholes, C. A., Qader, A., Stevens, G. W., & Kentish, S. E., 2014. Membrane Gas-Solvent Contactor Pilot Plant Trials of CO2 Absorption from Flue Gas. *Separation Science and Technology (Philadelphia)*, *49*(16), 2449–2458. https://doi.org/10.1080/01496395.2014.937499

Sinnott, R. K., Coulson, J. M., and Richardson, J. F., 2005. *Coulson & Richardson's chemical engineering. Vol. 6*. Oxford, Elsevier Butterworth-Heinemann

Smith, J.M., Van Ness, H. C., and Abbott, M. M., 2001. *Introduction to Chemical Engineering Thermodynamics*. 6th ed. McGraw-Hill

Theo, W.L., Lim, J.S., Hashim, H., Mustaffa, A. A., Ho, W. S., 2016. Review of pre-combustion capture and ionic liquid in carbon capture and storage, *Applied Energy*, Elsevier, vol. 183(C), pages 1633-1663. https://doi.org/10.1016/j.apenergy.2016.09.103

Sun, L., and Smith, R., 2013. Rectisol wash process simulation and analysis. *Journal of Cleaner Production*, 39, 321–328. https://doi.org/10.1016/j.jclepro.2012.05.049

Usman, M., Hillestad, M., and Deng, L., 2018. Assessment of a membrane contactor process for pre-combustion CO2 capture by modelling and integrated process simulation. *International Journal of Greenhouse Gas Control*, *71*(July 2017), 95–103. https://doi.org/10.1016/j.ijggc.2018.02.012

Villeneuve, K., Albarracin Zaidiza D., Roizard, D. and Rode, S., 2018a. Modeling and Simulation of CO_2 Capture in Aqueous Ammonia with Hollow Fiber Composite Membrane Contactors Using a Selective Dense Layer. *Chemical Engineering Science*, vol. 190, pp. 345–360, 10.1016/j.ces.2018.06.01

Villeneuve, K., Torres Hernandez, A.A., Albarracin Zaidiza, D., Roizard, D., and Rode, S., 2018b. Effects of water condensation on hollow fiber membrane contactor performance for CO_2

capture by absorption into a chemical solvent, *Journal of Membrane Science*, pp. 365-373. https://doi.org/10.1016/j.memsci.2018.04.005

Wang, G. Q., Yuan, X. G., & Yu, K. T., 2005. Review of mass-transfer correlations for packed columns. *Industrial and Engineering Chemistry Research*, *44*(23), 8715–8729. https://doi.org/10.1021/ie050017w

Wilke, C. R and Chang, P., 1955. Correlation of diffusion coefficients in dilute solutions. *AIChE J.*, 1: 264. https://doi.org/10.1002/aic.690010222

Wolfram Research, Inc., 2020. *Wolfram Alpha* [online] Available at: <https://www.wolframalpha.com> [Accessed 11 November 2020].

Yan, S. ping, Fang, M. X., Zhang, W. F., Wang, S. Y., Xu, Z. K., Luo, Z. Y., & Cen, K. F., 2007. Experimental study on the separation of CO_2 from flue gas using hollow fiber membrane contactors without wetting. *Fuel Processing Technology*, *88*(5), 501–511. https://doi.org/10.1016/j.fuproc.2006.12.007

Zhao, S., Feron, P. H. M., Deng, L., Favre, E., Chabanon, E., Yan, S., Hou, J., Chen, V and Qi, H., 2016. Status and progress of membrane contactors in post-combustion carbon capture: A state-of-the-art review of new developments. *Journal of Membrane Science*, vol. 511, pp. 180-206, http://dx.doi.org/10.1016/j.memsci.2016.03.051

3M™, 2018. *Data sheet of 3M™ Liqui-Cel™ membrane contactors* [online] Available at: <www.3M.com/Liqui-Cel> [Accessed 16 November 2020].

3M™, 2019. *Data sheet of 3M™ Membrana™ OXYPLUS™, Capillary Membrane, PMP 90/200* [online] Available at: <www.3m.com/membrana> [Accessed 11 November 2020].

8. ANNEXES

8.1. Commercial tower packings

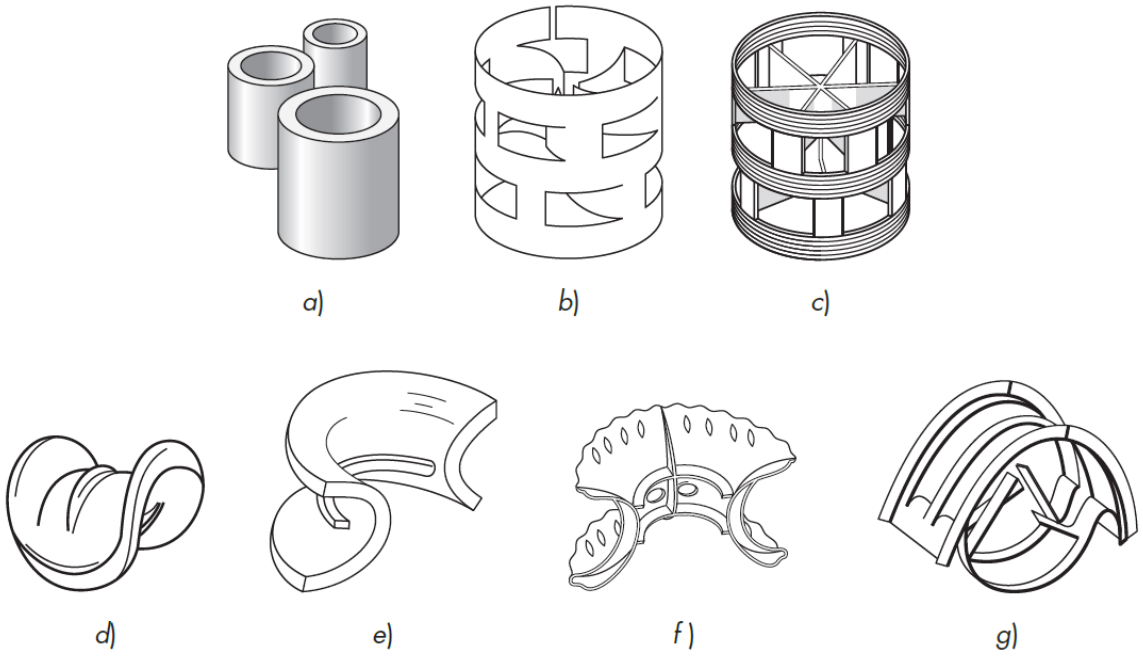

Figure 43. Common tower packings. (a) Rashig rings; (b) metal Pall ring; (c) plastic Pall ring; (d) Berl saddle; (e) ceramic Intalox saddle; (f) plastic Super Intalox saddle; (g) metal Intalox saddle (McCabe, 2007)

Table 24. Features of different packings (Rode, 2019)

Diamètre nominal	Caracté-ristiques *	Anneaux Raschig			Anneaux Pall			Anneaux Hiflow			Selles Intalox		
d_{nom}, m		C **	P **	M **	C **	P **	M **	C **	P **	M **	C **	P **	M **
0,0254	a, m^{-1}	190	-	185	220	206	205	-	192	203	256	207	207
	ε ,-	0,74	-	0,86	0,75	0,9	0,94	-	0,92	0,96	0,73	0,9	0,97
	ρ_{app} , kg m^{-3}	670	-	1140	620	71	325	-	63	298	672	83	224
	F_P, m^{-1}	587	-	472	350	180	183	-	138	-	302	131	134
0,0508	a, m^{-1}	92	-	95	121	102	105	89	110	92	118	108	98
	ε ,-	0,74	-	0,92	0,78	0,92	0,96	0,82	0,93	0,98	0,76	0,93	0,98
	ρ_{app} , kg m^{-3}	660	-	590	550	60	198	405	59	175	608	60	166
	F_P, m^{-1}	213	-	187	142	85	89	95	66	52	131	92	59

* a en $m^2_{solide} m^{-3}_{col}$; ε en $m^3_{vide} m^{-3}_{col}$; $\rho_{app} = \rho_S(1-\varepsilon)$ en kg m^{-3}_{col} ; $F_P \propto a/\varepsilon^3$

** C : céramique, P : plastique, M : métal

8.2.*Specification data sheet of 3M™ Membrana™ OXYPLUS™*

Chemical Composition	
Polymer	Polymethylpentene
Solvent residues	≤100 ppm

Physical Properties	
Wall Thickness	90 ±10 µm
Outer diameter	380 ±30 µm
Inner diameter	200 ±50 µm
Tensile strength	≥ 60 cN
Elongation at break	≥ 60%
Porosity	≥ 50 %
Explosion pressure	≥ 2.0 bar
Implosion pressure	≥ 3.5 bar

All specifications are based on 3M internal test procedures and represent average lot performance.

Membrane performance characteristics	
Nitrogen flux	0.2 - 2 ml/[min x cm^2 x bar]

Available Make-up Configuration
Single-thread spools Single layer mats or cross-wound mats

Figure 44. Data sheet of 3M™ Membrana™ OXYPLUS™, Capillary Membrane, PMP 90/200 (3M, 2019)

8.2. Specification data sheet of other membranes

Table 25. HFMC parameters as a function of different articles.

		Value		Units
Specification	Chu *et al.* (2020)	Dalane *et al.* (2018)	Lee *et al.* (2020a)	
Number of fibers	6,00E+04	9,20E+06	200	-
Fiber external diameter, d_{MC-ext}	250	704	208	µm
Fiber internal diameter, d_{MC-int}	200	600	127	µm
Packing density	6000	1500	na	m^{-1}

8.3.Commercial hollow fiber membrane contactors

Table 26. Lenntech® hollow fiber membrane contactors (Lenntech, 2020).

Hollow fiber membrane	Length	Diameter	Units
Housing 45	50,3	10,8	cm
Housing 65	73,2	10,8	cm
Housing 85	131	10,8	cm
Housing 152M	81,3	16,8	cm
Housing 154M	139	16,8	cm

Table 27. 3M™ Liqui-Cel™ hollow fiber membrane contactors on countercurrent flow (3M, 2020)

Hollow fiber membrane contactor	Length	Diameter	Units
EXF-2.5x8 Series	277	77	mm
EXF-4x28 Series	889	85	mm
EXF-8x40 Series	1502	255	mm
EXF-8x80 Series	2518	255	mm

8.4. Raw simulation data

Table 28. Raw simulation data from Aspen HYSYS (Mckechnie, 2020)

Case study	$Y_{CO2,G,in}$	P_{in}	Stages	$T_{L,in}$	$T_{G,in}$	$N_{L,in}$	T_{peak}	Stage T_{peak}	F_{LG}	η_{CO2}	T_{dif}
(-)	mole mole^{-1}	bar	-	degC	degC	kmole h^{-1}	degC	(-)	(-)	(-)	degC
1	0,4	40	10	-50	-20	1,68	-0,52	8	2,33	95,26%	49,48
2	0,4	20	10	-50	-20	2,60	-13,70	9	2,58	95,20%	36,30
3	0,4	50	10	-50	-20	1,46	3,88	8	2,26	95,32%	53,88
4	0,4	40	10	-50	-10	1,70	0,07	8	2,26	94,31%	50,07
5	0,4	20	10	-50	-10	2,65	-13,04	10	2,64	95,22%	36,96
6	0,4	50	10	-50	-10	1,50	4,59	8	2,33	95,38%	54,59
7	0,4	40	10	-50	-30	1,64	-1,15	8	2,29	95,35%	48,85
8	0,4	20	10	-50	-30	2,55	-14,09	8	2,53	95,19%	35,91
9	0,4	50	10	-50	-30	1,35	1,68	8	2,09	95,32%	51,68
10	0,4	40	10	-40	-30	1,80	2,06	8	2,47	95,24%	42,06
11	0,4	20	10	-40	-30	2,90	-10,11	8	2,89	95,52%	29,89
12	0,4	50	10	-40	-30	1,48	4,82	8	2,27	95,33%	44,82
13	0,4	40	10	-40	-10	1,90	3,16	8	2,71	95,94%	43,16
14	0,4	20	10	-40	-10	3,00	-9,34	9	3,00	95,60%	30,66
15	0,4	50	10	-40	-10	1,63	7,49	8	2,51	95,37%	47,49
16	0,4	40	10	-40	0	1,90	3,73	9	2,49	94,25%	43,73
17	0,4	20	10	-40	0	3,00	-8,31	10	2,81	94,18%	31,69
18	0,4	50	10	-40	0	1,66	8,10	8	2,51	95,00%	48,10
19	0,4	40	10	-30	-10	2,10	6,79	8	2,96	95,92%	36,79
20	0,4	20	10	-30	-10	3,40	-4,78	9	2,39	95,14%	25,22
21	0,4	50	10	-30	-10	1,80	10,87	8	2,82	95,91%	40,87
22	0,4	40	10	-30	0	2,10	7,36	9	2,75	94,39%	37,36
23	0,4	20	10	-30	0	3,45	-4,20	10	3,35	95,22%	25,80

Table 29. Raw simulation data from Aspen HYSYS (Mckechnie, 2020) (cont.)

Case study	$Y_{CO2,G,in}$	P_{in}	Stages	$T_{L,in}$	$T_{G,in}$	$N_{L,in}$	T_{peak}	Stage T_{peak}	F_{LG}	η_{CO2}	T_{dif}
(-)	mole mole^{-1}	bar	-	degC	degC	kmole h^{-1}	degC	(-)	(-)	(-)	degC
24	0,4	50	10	-30	0	1,80	11,50	8	2,61	94,28%	41,50
25	0,4	40	10	-30	10	2,16	7,98	10	2,94	95,24%	37,98
26	0,4	20	10	-30	10	3,50	-3,14	10	3,42	95,35%	26,86
27	0,4	50	10	-30	10	1,86	12,12	9	2,83	95,32%	42,12
28	0,4	40	10	-20	0	2,36	11,48	9	3,19	95,32%	31,48
29	0,4	20	10	-20	0	3,96	0,71	9	3,79	95,18%	20,71
30	0,4	50	10	-20	0	2,00	15,33	8	2,96	94,98%	35,33
31	0,4	40	10	-20	10	2,40	11,99	9	3,26	95,43%	31,99
32	0,4	20	10	-20	10	4,00	1,55	10	3,81	95,10%	21,55
33	0,4	50	10	-20	10	2,04	15,90	9	3,05	95,15%	35,90
34	0,4	40	10	-20	20	2,40	13,04	10	3,07	94,12%	33,04
35	0,4	20	10	-20	20	4,00	2,52	10	3,65	94,15%	22,52
36	0,4	50	10	-20	20	2,08	16,66	10	3,15	95,36%	36,66
37	0,4	40	10	-10	10	2,70	16,62	9	3,72	95,95%	26,62
38	0,4	20	10	-10	10	4,70	6,89	10	4,67	94,69%	16,89
39	0,4	50	10	-10	10	2,26	20,25	9	3,35	95,20%	30,25
40	0,4	40	10	-10	20	2,70	17,18	10	3,54	94,90%	27,18
41	0,4	20	10	-10	20	4,70	7,77	10	4,53	95,67%	17,77
42	0,4	50	10	-10	20	2,30	20,76	9	3,45	95,44%	30,76
43	0,4	40	10	-10	30	2,74	18,47	10	3,62	95,05%	28,47
44	0,4	20	10	-10	30	4,70	8,64	10	4,40	95,00%	18,64
45	0,4	50	10	-10	30	2,30	21,96	10	3,26	94,24%	31,96
46	0,3	20	10	-50	-10	2,50	-17,35	10	2,39	95,94%	32,65
47	0,3	20	10	-50	-20	2,45	-18,69	9	2,33	95,78%	31,31
48	0,3	20	10	-50	-30	2,40	-19,24	9	2,27	95,66%	30,76
49	0,3	20	10	-40	0	2,87	-12,33	10	2,65	95,28%	27,67
50	0,3	20	10	-40	-10	2,85	-13,65	10	2,69	95,96%	26,35
51	0,3	20	10	-40	-20	2,80	-14,56	9	2,63	95,78%	25,44
52	0,3	20	10	-30	10	3,35	-6,90	10	3,05	95,35%	23,10
53	0,3	20	10	-30	0	3,30	-8,05	10	2,98	95,11%	21,95
54	0,3	20	10	-30	-10	3,25	-9,24	10	2,91	94,89%	20,76
55	0,3	20	10	-20	20	3,95	-1,02	10	3,56	95,40%	18,98
56	0,3	20	10	-20	10	3,90	-2,02	10	3,48	95,20%	17,98
57	0,3	20	10	-20	0	3,85	-3,04	10	3,42	95,00%	16,96
58	0,3	20	10	-10	30	4,65	5,42	10	4,05	94,88%	15,42
59	0,3	20	10	-10	20	4,65	4,48	10	4,10	95,22%	14,48
60	0,3	20	10	-10	10	4,60	3,62	10	4,03	95,04%	13,62
61	0,3	40	10	-50	-10	1,63	-5,93	9	2,13	95,31%	44,07
62	0,3	40	10	-50	-20	1,60	-6,78	8	2,12	95,70%	43,22
63	0,3	40	10	-50	-30	1,55	-7,50	8	2,01	95,23%	42,50
64	0,3	40	10	-40	0	1,83	-1,76	10	2,35	95,21%	38,24
65	0,3	40	10	-40	-10	1,80	-2,73	9	2,34	95,49%	37,27
66	0,3	40	10	-40	-20	1,75	-3,50	8	2,23	94,98%	36,50
67	0,3	40	10	-30	10	2,07	3,28	10	2,63	95,20%	33,28
68	0,3	40	10	-30	0	2,05	1,74	9	2,66	95,77%	31,74
69	0,3	40	10	-30	-10	2,00	1,12	9	2,61	95,22%	31,12
70	0,3	40	10	-20	20	2,35	8,62	10	2,95	95,18%	28,62
71	0,3	40	10	-20	10	2,32	7,08	10	2,92	95,26%	27,08
72	0,3	40	10	-20	0	2,30	6,05	9	2,94	95,66%	26,05
73	0,3	40	10	-10	30	2,70	14,29	10	3,40	95,60%	24,29
74	0,3	40	10	-10	20	2,65	12,94	10	3,27	95,09%	22,94

Table 30. Raw simulation data from Aspen HYSYS (Mckechnie, 2020) (cont.)

Case study	**$Y_{CO2,G,in}$**	**P_{in}**	**Stages**	**$T_{L,in}$**	**$T_{G,in}$**	**$N_{L,in}$**	**T_{peak}**	**Stage T_{peak}**	**F_{LG}**	**η_{CO2}**	**T_{dif}**
(-)	mole $mole^{-1}$	bar	-	degC	degC	kmole h^{-1}	degC	(-)	(-)	(-)	degC
75	0,3	40	10	-10	10	2,65	11,47	9	3,36	95,83%	21,47
76	0,3	50	10	-50	-10	1,43	-1,86	9	2,08	95,36%	48,14
77	0,3	50	10	-50	-20	1,40	-2,77	8	2,06	95,66%	47,23
78	0,3	50	10	-50	-30	1,35	-3,62	8	1,94	95,06%	46,38
79	0,3	50	10	-40	0	1,60	2,02	9	2,32	95,52%	42,02
80	0,3	50	10	-40	-10	1,56	1,14	9	2,24	95,25%	41,14
81	0,3	50	10	-40	-20	1,52	0,31	8	2,16	95,07%	40,31
82	0,3	50	10	-30	10	1,80	6,71	10	2,59	95,69%	36,71
83	0,3	50	10	-30	0	1,75	5,52	9	2,45	94,93%	35,52
84	0,3	50	10	-30	-10	1,72	4,70	9	2,42	95,12%	34,70
85	0,3	50	10	-20	20	2,01	11,94	10	2,80	95,05%	31,94
86	0,3	50	10	-20	10	2,00	10,18	10	2,87	95,84%	30,18
87	0,3	50	10	-20	0	1,95	9,55	9	2,72	95,16%	29,55
88	0,3	50	10	-10	30	2,30	17,45	10	3,26	95,89%	27,45
89	0,3	50	10	-10	20	2,25	15,91	10	3,12	95,27%	25,91
90	0,3	50	10	-10	10	2,22	14,81	9	3,07	95,24%	24,81
91	0,3	20	10	0	10	5,50	9,99	10	4,72	94,94%	9,99
92	0,3	20	10	10	10	6,70	17,04	10	5,64	94,90%	7,04
93	0,3	20	10	20	10	8,90	24,41	10	7,35	95,01%	4,41
94	0,3	40	10	0	10	3,00	17,24	9	3,68	95,25%	17,24
95	0,3	40	10	10	10	3,40	23,82	9	4,00	94,46%	13,82
96	0,3	40	10	20	10	4,00	30,66	9	4,75	95,21%	10,66
97	0,3	50	10	0	10	2,50	20,11	9	3,40	95,06%	20,11
98	0,3	50	10	10	10	2,80	26,30	9	3,65	94,23%	16,30
99	0,3	50	10	20	10	3,20	33,02	9	4,12	94,35%	13,02
100	0,4	20	10	0	10	5,40	13,35	9	5,02	95,25%	13,35
101	0,4	20	10	10	10	6,30	20,56	9	5,69	95,01%	10,56
102	0,4	20	10	20	10	7,40	28,29	9	6,51	94,96%	8,29
103	0,4	40	10	0	10	3,00	22,05	9	3,89	94,93%	22,05
104	0,4	40	10	10	10	3,40	28,07	9	4,36	95,06%	18,07
105	0,4	40	10	20	10	3,90	34,64	9	5,07	95,66%	14,64
106	0,4	50	10	0	10	2,50	25,28	9	3,56	94,61%	25,28
107	0,4	50	10	10	10	2,80	30,96	9	3,93	94,58%	20,96
108	0,4	50	10	20	10	3,20	37,14	9	4,65	95,62%	17,14